

# Modeling and Analyzing the Thalamocortical System

Kumulative Dissertation  
zur Erlangung des Doktorgrades  
der Mathematisch-Naturwissenschaftlichen Fakultät  
der Christian-Albrechts-Universität  
zu Kiel

vorgelegt von

**Jörg Mayer**

Kiel

2008

Referent: Prof. Dr. H.G. Schuster

Korreferent(en): .....

.....

Tag der mündlichen Prüfung: .....

Zum Druck genehmigt: Kiel, den .....

Der Dekan

# Contents

<b>Abstract</b>	<b>1</b>
<b>Kurzfassung</b>	<b>2</b>
<b>1 Introduction</b>	<b>3</b>
1.1 Motivation . . . . .	3
1.1.1 Sleep . . . . .	3
1.1.2 Sleep and the thalamocortical system . . . . .	6
1.2 Thalamic oscillations and spike transfer . . . . .	9
1.2.1 Experimental motivation . . . . .	9
1.2.2 Modeling the thalamic circuit . . . . .	12
1.2.3 Dynamical behavior of thalamic circuits . . . . .	15
1.3 Synchronization of thalamic spindles in the thalamocortical system . . . . .	17
1.3.1 Experimental motivation . . . . .	17
1.3.2 Modeling cortical control of synchrony in the thalamus . . . . .	20
1.4 Emergence of slow-wave sleep and spike-timing dependent plasticity . . . . .	23
1.4.1 The hypothesis of synaptic homeostasis . . . . .	23
1.4.2 Synaptic potentiation by spike-timing dependent plasticity . . . . .	25
1.5 Survey of the publications . . . . .	27
1.5.1 Role of inhibitory feedback for information processing in thalamo-cortical circuits . . . . .	27
1.5.2 Corticothalamic projections control synchrony in locally coupled bistable elements . . . . .	28
1.5.3 Excitation of coherent oscillations in a noisy medium . . . . .	29
1.5.4 Dynamical mean-field equations for synaptic plasticity . . . . .	30
<b>2 Methods</b>	<b>31</b>
2.1 Modeling the electrophysiology of the neuron . . . . .	31
2.1.1 Conductance based neuron models . . . . .	31
2.1.2 The Hodgkin-Huxley model for action potentials . . . . .	32
2.2 Mathematical tools . . . . .	37
2.2.1 Linear stability analysis . . . . .	37
2.2.2 Bifurcations of equilibrium points . . . . .	39
2.2.3 Bifurcations of limit cycles . . . . .	45
2.2.4 Singular approximation . . . . .	47

2.2.5	Noisy dynamical systems . . . . .	47
2.2.6	Dynamic mean-field equations for spike-timing dependent plasticity	49
<b>3</b>	<b>Publications</b>	<b>53</b>
3.1	Role of inhibitory feedback for information processing in thalamocortical circuits . . . . .	54
3.2	Corticothalamic projections control synchronization in locally coupled bistable thalamic oscillators . . . . .	70
3.3	Excitation of coherent oscillations in a noisy medium . . . . .	75
3.4	Dynamical mean-field equations for a neural network with spike-timing dependent plasticity . . . . .	82
<b>4</b>	<b>Discussion</b>	<b>87</b>
4.1	Conclusions . . . . .	87
4.2	Outlook . . . . .	89
	<b>Bibliography</b>	<b>91</b>
	<b>Acknowledgements</b>	<b>101</b>
	<b>Curriculum Vitae</b>	<b>103</b>
	<b>Selbstständigkeitserklärung</b>	<b>105</b>

## Abstract

Major progress has been made in the study of fundamental neural processes over the last ten years. However, the thorough analysis of brain functions continues to be a challenge which, due to the complexity of the dynamic processes involved, is considered even more difficult than the study of structural and functional relations of the human genome. One of the most interesting questions in this context can be stated as follows: “Why do we not perceive sensory information consciously during sleep?”

Physiological evidence localizes the thalamocortical system as the functional unit being responsible for the perception of sensory input. In this thesis the dynamical processes in the thalamus during sleep are reduced to their bare bones. For this purpose the dynamical behavior of conductance based neuron models, which describe biophysical details with high accuracy, is investigated and reduced models of this behavior are derived. The simplified models derived in this thesis allow an explanation of how sensory perception is strongly decreased during sleep within the framework of nonlinear dynamics. A minimal model for such a mechanism is derived, coarse graining out details but preserving most salient dynamical features. If several of these models are coupled in a network the experimental observed influence of cortical slow-wave oscillations on thalamic spindle oscillations during deep sleep can be reproduced. In particular the influence of cortical oscillations on the synchrony in a thalamic network is studied and the underlying control mechanism is uncovered, leading to a control method which might be applicable for several types of oscillations in the central nervous system.

Further mechanisms how to influence the cortical activity by external stimulation are discussed. Experimental results indicate that electric fields allow to influence cortical activity. Again a simplified model of an experimental verified model is used to study several types of stimulation signals. As a surprising result, stimulation by noise allows a precise tuning between different types of cortical activity in the computational model for cortical activity. In previous studies in this direction mainly constant or periodic stimulation signals were used.

Another basic questions concerning sleep is what mechanism makes us falling a sleep. The determination of the relevant mechanism is still subject of research. It is a daily live experience that the need for sleep increases with the time being awake. One hypothesis posts that sleep emerges due to an increase of the total synaptic strength in the cortical network during waking, whilst during sleep the total synaptic strength is decreased back to its base line. We suggest a minimal model for cortical synaptic growth and derive the equation of motion for the total synaptic strength analytically. Previous models in this direction have mainly been treated by numerical simulations. We show that this mechanism can end up in a stable state of the network, which is robust against external disturbances. Further the model is able to detect correlations, a basic feature of synaptic learning.

The simplified models introduced in this thesis allow large scale simulations of the thalamocortical system. An assembly of the model for thalamic activity, cortical activity and spike-timing dependent plasticity, might allow simulations of the thalamocortical system, which lead to in vivo verifiable forecasts.

## Kurzfassung

Die Erforschung von wichtigen neuronalen Prozessen hat in den letzten Jahrzehnten bemerkenswerte Fortschritte gemacht. Dennoch bleibt die Klärung der unterschiedlichen Funktionen des Gehirns eine Herausforderung, die wegen der komplexen involvierten, dynamischen Prozesse oft, für schwieriger als die Erforschung des menschlichen Genoms angesehen wird. Eine der interessantesten Fragestellungen in diesem Zusammenhang kann folgendermaßen formuliert werden: „Warum wird während des Schlafes die sensorische Wahrnehmung stark eingeschränkt?“

Physiologisch betrachtet ist das thalamokortische System für die Verarbeitung und Wahrnehmung von sensorischen Reizen zuständig. In dieser Arbeit werden die dynamischen Vorgänge im Thalamus während des Schlafes auf ihre grundlegenden Eigenschaften reduziert. Dazu wird das dynamische Verhalten von komplexen Neuronenmodellen untersucht, die biophysikalische Details mit hoher Genauigkeit wiedergeben und vereinfachte Modelle dieses Verhaltens eingeführt.

Diese vereinfachten Modelle erlauben es, mit Hilfe der nichtlinearen Dynamik den Rückgang der sensorischen Wahrnehmung im Schlaf zu erklären. Dazu wird ein minimales Modell für den zugrunde liegenden Mechanismus abgeleitet, in dem Details vernachlässigt werden, ohne dass jedoch die wichtigsten dynamischen Eigenschaften verloren gehen. Kopelt man viele dieser Modelle in einem Netzwerk, so lässt sich der experimentell beobachtete Einfluss kortikaler Oszillationen auf thalamische Oszillationen reproduzieren. Ein besonderes Augenmerk liegt dabei auf der Synchronisation der thalamischen Oszillationen und dem zugrunde liegenden Mechanismus, welcher möglicherweise auch in anderen neuronalen Systemen anwendbar ist.

Des Weiteren werden Möglichkeiten untersucht, wie die kortikale Aktivität während des Schlafes durch externe elektrische Felder beeinflusst werden kann. Unter Benutzung eines vereinfachten Modells der kortikalen Aktivität werden unterschiedliche Stimulationsformen untersucht. Überraschend ermöglicht eine Stimulation durch weißes Rauschen eine präzise Regulierung des Aktivitätsmusters des Kortex-Modells. Bisher wurden zumeist konstante oder periodische stimulations Signale benutzt.

Von großem allgemeinen Interesse sind seit langer Zeit die Vorgänge die uns einschlafen lassen. Mögliche zugrundeliegende Mechanismen sind Gegenstand aktueller Forschung. Das Verlangen nach Schlaf wächst, gemäß täglicher Erfahrung mit der Wachzeit. Nach einer aktuellen Hypothese entspricht dem Ermüden ein Anwachsen der synaptischen Kopplungen im Kortex während des Wachseins. Im Schlaf werden diese Kopplungen auf den Ausgangspunkt zurückgesetzt. In dieser Arbeit wird ein minimales Modell für das Anwachsen der synaptischen Kopplungen während des Wachseins eingeführt und die Gleichung für die mittlere kopplungsstärke analytisch aus den Netzwerkgleichungen abgeleitet.

Die eingeführten Modelle erlauben Simulationen des thalamokortischen Systems in großem Maßstab, die möglicherweise zu in vivo überprüfaren Vorhersagen führen.

# 1 Introduction

## 1.1 Motivation

In the past decades, physicists have successfully applied mathematical and computational methods from physics in other fields, as biology, economics or social sciences. These systems have a common feature: They are far away from the extreme scales that are mostly the subject of physical research. In between these extremes scales at the border between order and disorder and on human length and time scales another exciting frontier of physical research has developed, which is called complex adaptive systems (CAS)(Schuster, 2001). All these systems have the following basic common structure: They consist of many elements which interact in a nonlinear fashion among themselves and their environment. Accordingly they can be described within the framework of nonlinear dynamics or statistical mechanics. As it is the dynamical behavior generated by the nonlinear interactions between the single elements which is of importance, a common theoretical way to describe CAS is to use coarse-grained descriptions of the elements and then study the dynamics of simple models of interacting elements. The most prominent and at the same time least understood example for a CAS is the central nervous system (Schuster, 2001). Major progress has been made in the study of fundamental neural processes over the last ten years. However, the thorough analysis of brain functions continues to be a challenge which, due to the complexity of the dynamic processes involved, is considered even more difficult than the study of structural and functional relations of the human genome.

### 1.1.1 Sleep

One of the great mysteries of modern neuroscience is sleep. Although humans spend nearly one-third of their lives asleep, only little is known about the mechanisms making us fall asleep or the function of sleep. Fortunately, over the past few years scientists have made great advances in understanding some of the brain circuitry that controls wake-sleep states. Sleep disorders are among the most common health problems, in the USA 70 million people are affected by it mostly undiagnosed and untreated. These disorders are one of the least recognized sources of disease, disability, and even death. The costs in the USA are estimated to be in the range of \$100 billion annually in lost productivity, medical bills, and industrial accidents (The National Commission on sleep disorders Research, USA, 1992). Sleep consists of several different stages, the choreography of a night's sleep involves the interplay of these stages, a process that depends upon a complex switching mechanism. The sleep stages are accompanied by daily rhythms in bodily hormones, body temperature, and

other functions (Pinel, 2007; Birbaumer and Schmidt, 1996). Although sleep appears to be a passive and restful time, it actually involves a highly active and well-defined interplay of brain circuits to produce its various stages.

The stages of sleep were discovered in the 1950s in experiments using electroencephalography (EEG) that examined human brain waves during sleep. Researchers also measured movements of the eyes and the limbs during sleep. It was found that during the first hour of sleep each night, the brain waves progressively slow down. This period of slow-wave sleep is accompanied by relaxation of muscles and the eyes. Heart rate, blood pressure and body temperature all fall. These stages of sleep are called NREM sleep. During the next half hour, brain activity changes drastically from the deep slow-wave sleep to neocortical EEG activities that are indistinguishable from those observed during waking. The fast waking-like EEG activity is accompanied by rapid eye movements (REM) what gives this sleep stage its name REM sleep. During REM sleep there is active dreaming. The first REM stage usually lasts 10 to 15 minutes. The above given characterization follows the common practice of referring to sleep characterized by rapid eye movements and waking like EEG activity as REM sleep and the stages characterized by slower EEG activity as NREM or slow-wave sleep (Pinel, 2007). However following Rechtschaffen and Kales (1977) NREM sleep is divided into four stages. These stages can be characterized as follows (see

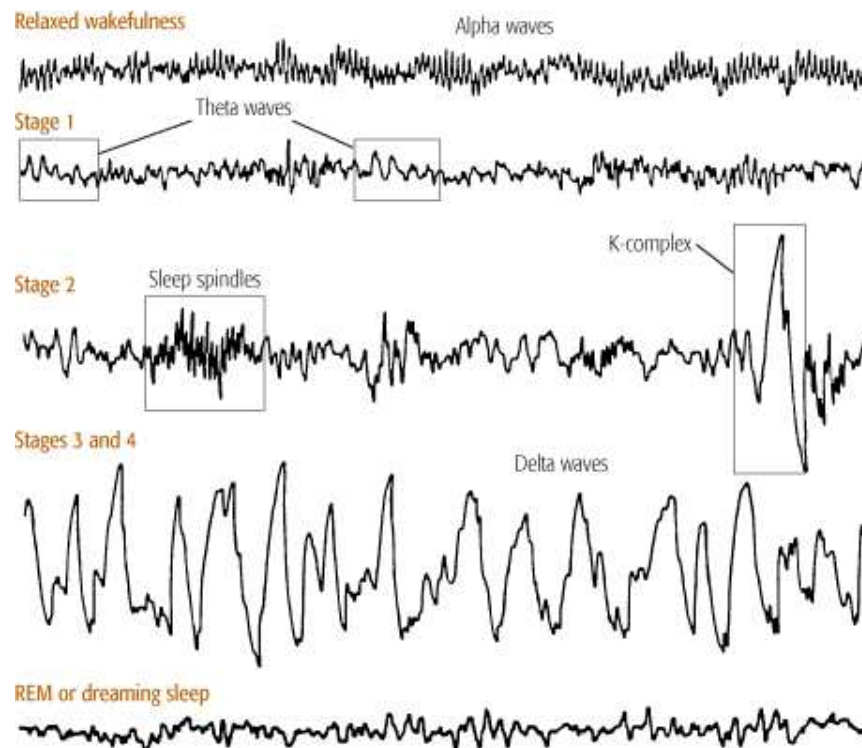


Figure 1.1: Sleep stages and the associated brain wave activity observed by EEG measurements. Picture taken from (HMS, 2008).

also Fig. 1.1):



- NREM 1: Brain waves become smaller, slower, and somewhat irregular characterized by a low-voltage fast EEG in the frequency range of 4-8Hz and an amplitude of 50-100  $\mu V$  (theta waves).
- NREM 2: Larger brain waves and occasional quick bursts of activity which are called sleep spindles in the EEG. The Frequency range is within 4-15Hz and typical amplitudes of 50-150  $\mu V$ .
- NREM 3: Is the beginning of deep sleep. Brain waves are slow (at the rate of 0.5 to 4 per second) and quite large (five times the size of waves in Stage 2).
- NREM 4: The deepest sleep occurs in Stage 4. The brain waves (called delta brain waves) are quite large, making a slow, jagged pattern on the EEG.

During the night, these cycles of slow-wave and REM sleep alternate, the slow-wave sleep becomes less deep and the REM stages become longer until waking occurs (see Fig. 1.2). These patterns of sleep cycles change during lifetime. Babies sleep up to eighteen hours a day, and they spend a lot of time in deep slow-wave sleep. As children grow up, they spend less time asleep and less time in deep slow-wave sleep. Older adults sleep only six to seven hours a day and spend very little time in slow-wave sleep (Ohayon *et al.*, 2004). (For a detailed review, see Steriade (2003)).

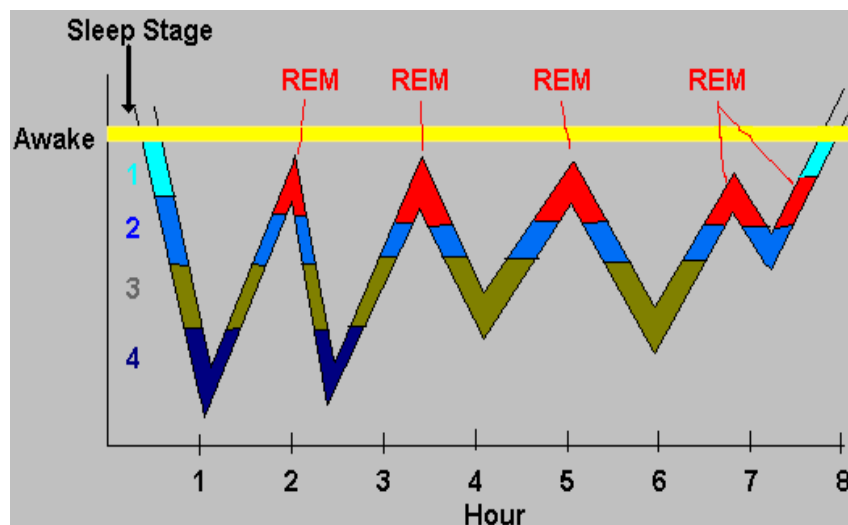


Figure 1.2: Cycles of NREM and REM sleep during sleep, the slow-wave sleep becomes less deep and the REM stages become longer until waking occurs. Picture taken from (Chudler, 2008).

So far an electrophysiological description of sleep and its stages is given, but why do we sleep? This is a question scientists try to answer since centuries and the answer is, the functions of sleep are not entirely known. Some believe that sleep gives the body a chance to recuperate from the day's activities but in reality, the amount of energy saved

by sleeping for even eight hours is minimal – about 50 kCal, the same amount of energy as in a piece of toast. It is a daily live experience that humans have to sleep because it is essential to maintain normal levels of cognitive skills such as speech, memory, innovative and flexible thinking. Further the need for sleep increases with the time awake. Experimental evidence indicates that sleep inspires insight and potentiates memories (Stickgold *et al.*, 2001; Wagner *et al.*, 2004). In other words, sleep plays a significant role in brain development.

### 1.1.2 Sleep and the thalamocortical system

The most prominent feature of sleep is probably the loss of consciousness, which is accompanied by a strong decrease in the perception of sensory information. In this instance, one of the most important functional unit is the thalamus, as it is the major gateway for sensory information. However the thalamus is far from being a passive filter: merely it relays the incoming information depending on the state of arousal. The process of information processing is influenced by further inputs from the brain stem and from the cortex. During NREM sleep the latter play an important role for synchronization of thalamic rhythms. Basically the neurons in the thalamocortical system can be classified in four groups: In thalamocortical relay cells (TC-cells), thalamic reticular neurons (RE-cells), cortical pyramidal neurons and cortical interneurons.

#### Thalamic spindle oscillations

Probably the most studied signal form of the thalamus are spindle oscillations, which are often called spike bursts. Spindle oscillations are waxing and waning waves that originate in the thalamus during NREM sleep or under deep anesthesia in mammals (Marshall *et al.*, 2003), accordingly they can easily be provoked by anesthetics like barbiturates or ketamine. The thalamic source of spindle oscillations was studied by Steriade *et al.* (Steriade, 2001b) *in vitro* and *in vivo*. Sleep spindles are characterized by a large degree of synchrony in the thalamus. The experiments of Steriade (Steriade, 2001a) clearly showed that spindle oscillations are the result of interactions between thalamus and cortex. Spindel oscillations are waxing and waning oscillations of 7-14 Hz, interrupted by silent periods of about 4 seconds, generated by the thalamocortical system (Steriade *et al.*, 1993a). Of particular interest are the dynamical mechanisms underlying the phenomenon of spindle oscillations and its relationship to the decrease of information transmission in the thalamocortical system. This could help to gain more insight into the mechanisms, which deprive the sensory information from the consciousness while mammals are sleeping. As the theoretical understanding of the mechanism remains incomplete, in (Mayer *et al.*, 2006) a computational model for a recent experiment by Le Masson *et al.* (Le Masson *et al.*, 2002) on the thalamocortical loop is analyzed. For this purpose the dynamical behavior of conductance based neuron models, which describe biophysical details with high accuracy, is investigated and reduced models of this behavior are derived. The simplified models derived allow an explanation of how sensory percipience is strongly decreased during sleep within the framework of non-

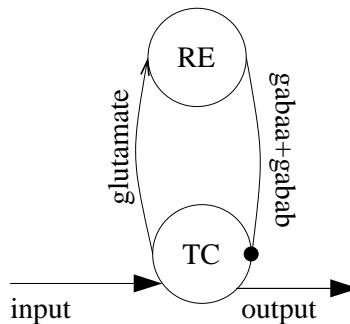


Figure 1.3: Structure of synaptic connections in a pair of reciprocally coupled RE-TC cells.

linear dynamics. It is found that the decrease in spike transfer occurs due to a change between a monostable and a bistable state with increasing inhibitory feedback. A further important condition to efficiently block information transfer through the thalamus is the synchronization of the single thalamic circuits. Up to now only little is known of how synchronous spindle oscillations in the thalamus are organized in the intact brain. Experimental findings suggest, that the simultaneous occurrence of spindle oscillations over widespread territories of the thalamus is due to the corticothalamic projections, as the synchrony is lost in the decorticated thalamus (Steriade *et al.*, 1991). In (Mayer *et al.*, 2007) the influence of cortical slow-wave EEG-data on the synchrony in a computational thalamic network is studied, and the underlying control mechanism uncovered, leading to a control method which might be applicable for several types of oscillations in the central nervous system.

### The sleep slow-wave

During much of sleep, virtually all cortical neurons undergo a slow oscillation ( $<1$  Hz) in membrane potential, cycling from a hyperpolarized state of silence to a depolarized state of intense firing. This slow oscillation is the fundamental cellular phenomenon that organizes other sleep rhythms such as spindles and slow-waves (Massimini *et al.*, 2004a). Experimental results indicate that slow-wave sleep is incorporated in memory consolidation (Gais and Born, 2004). Recently the question, how to influence and control the brain with external stimuli became focus of several studies (Holler *et al.*, 2006; Marshall *et al.*, 2006). As a well-known example, it has been shown that external signals enhance slow-wave activity during NREM sleep and therefore increase memory consolidation (Marshall *et al.*, 2006). However a theoretical study how to influence slow-waves is still missing. The sleep slow-wave is believed to be a travelling wave, originating in the anterior cortex and travelling to the posterior cortex. Some basic questions can be treated by studying travelling waves in a network of simple excitable cortical oscillators. In (Köhler *et al.*, 2008) the well known and experimentally verified Pinto-Ermentrout model (Pinto and Ermentrout, 2001) for cortical activity is simplified and extended by a noisy threshold. It is found that noise allows to tune the dynamical behavior of the computational model for

the cortex in a wide range. These results show that noise has a constructive role for the formation of traveling waves and coherent oscillations in coupled excitable media. While stimulation by either periodic or constant electric or magnetic fields is widely known and applied (Holler *et al.*, 2006; Marshall *et al.*, 2006), the results in (Köhler *et al.*, 2008) on the noise level dependence of travelling waves implicate that brain stimulation by noise might lead to constructive effects, like an enhancement of sleep slow-waves.

### **Plasticity and sleep**

A general hypothesis is that sleep promotes adaptive plastic processes, i.e. processes of memory formation that enable a longer-term stable regulation within different functional systems. As a matter of principle, the sleep-dependent formation of memories represents an active process. Sleep provides optimal conditions for this process since, as introduced above, during this phase interference from environmental stimuli and a potential disruption of underlying plastic processes is minimized. In a hypothesis by Tononi and Cirelli (2003) learning is brought into relation with a mechanism that possibly makes us falling asleep. The determination of the relevant mechanism is still subject of research. It is a daily live experience that the need for sleep increases with the time being awake. The above mentioned hypothesis posts that sleep emerges due to an increase of the average synaptic strength in the cortical network during waking, whilst during sleep the total synaptic strength is reduced back to its base line. During that downscaling weak synaptic couplings are downselected while strong couplings survive what results in consolidation. In (Mayer and Schuster, 2008) a minimal model for cortical synaptic growth is suggested and the equation of motion for the total synaptic strength is derived analytically. Previous models in this direction have mainly been treated by numerical simulations. We show that this mechanism can end up in a stable state of the network, which is robust against external disturbances. Further the mechanism is able to detect correlations, a basic feature of synaptic learning. The simplified models introduced in this thesis allow large scale simulations of the thalamocortical system. An assembly of the model for thalamic activity, cortical activity and spike-timing dependent plasticity, might allow simulations of the thalamocortical system, which lead to in vivo verifiable forecasts. In the conclusions we discuss further important questions that were motivated by this thesis.

## 1.2 Thalamic oscillations and spike transfer

### 1.2.1 Experimental motivation

The cognition and processing of sensory information takes primarily place in the cerebral cortex (Birbaumer and Schmidt, 1996; Pinel, 2007). Before the sensory information reaches the cortex, it has to pass the thalamus, which differentially relays it depending on the state of arousal (Coenen and Vendrik, 1972; Livingstone *et al.*, 2003; Sherman and Guillery, 1996). This active relaying is controlled by inhibition of the thalamic relay neurons by the nucleus reticularis of the thalamus (Yingling and Skinner, 1977; Ahlsén *et al.*, 1985; Steriade *et al.*, 1993a). The thalamus is the first instance where in-coming sensory information can be gated during selective attention (Montero, 1999), anesthesia (Destexhe, 2000), or the transition from general arousal to sleep (Steriade *et al.*, 1993a). However although much is known about the anatomy and the synaptic and cellular properties of the thalamic networks, the underlying mechanisms of the information transmission throughout selective arousal and anesthesia or sleep is not yet well understood (Le Masson *et al.*, 2002). An important step for a deeper understanding of how sensory information is differentially relayed in the thalamus was an experiment by Le Masson *et al.* (2002), where a thalamic circuit was reconstructed as an hybrid and biological network in vitro. The hybrid thalamic circuit consists of a biological thalamocortical relay (TC) and an artificial reticular (RE) thalamic cell as in Fig. 1.4 modeled by a single compartment Hodgkin-Huxley-like model. An artificial cell was necessary to manipulate selectively the synaptic connection of the inhibitory feedback from the RE to the TC cell. The results in (Le Masson *et al.*, 2002) show that the hybrid network resembles the behavior of the network which consists of a biological RE and TC cell. A detailed description of the experiment can be found in (Le Masson *et al.*, 2002). Typically thalamic neurons possess two different firing modes,

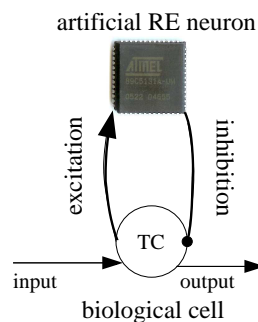


Figure 1.4: Hybrid circuit as used in the Le Masson experiment. The artificial RE cell allows a precise regulation of the inhibition strength from the RE to the TC cell.

depending on their membrane potential. At depolarized potentials, the cells fire in a single spike mode and relay synaptic inputs in a one-to-one manner to the cortex. If the cell gets hyperpolarized, T-type calcium currents generate burst mode firing which

leads to a decrease in spike transfer. In thalamocortical circuits the cell-membrane gets hyperpolarized by recurrent inhibitory feedback loops. In the case of reciprocally coupled excitatory and inhibitory neurons, inhibitory feedback leads to metastable self-sustained oscillations, called spindle oscillations, which mask the incoming input, and thereby reduce the spike transfer significantly (see Fig. 1.5). In contrast for low gain in the feedback inhibition the TC cells relay synaptic inputs in a one-to-one manner to the cortex. By tuning the strength of the inhibitory synapse Le Masson *et al.* showed that inhibitory feedback allows a precise regulation of the spike transfer. Accordingly, inhibitory feedback allows a functional disconnection of the cortex from the sensory input, a typical feature of sleep and anesthesia. The Le Masson experiment suggests that the principle mechanisms of spike transfer in the thalamus can be understood by considering a single thalamic circuit.

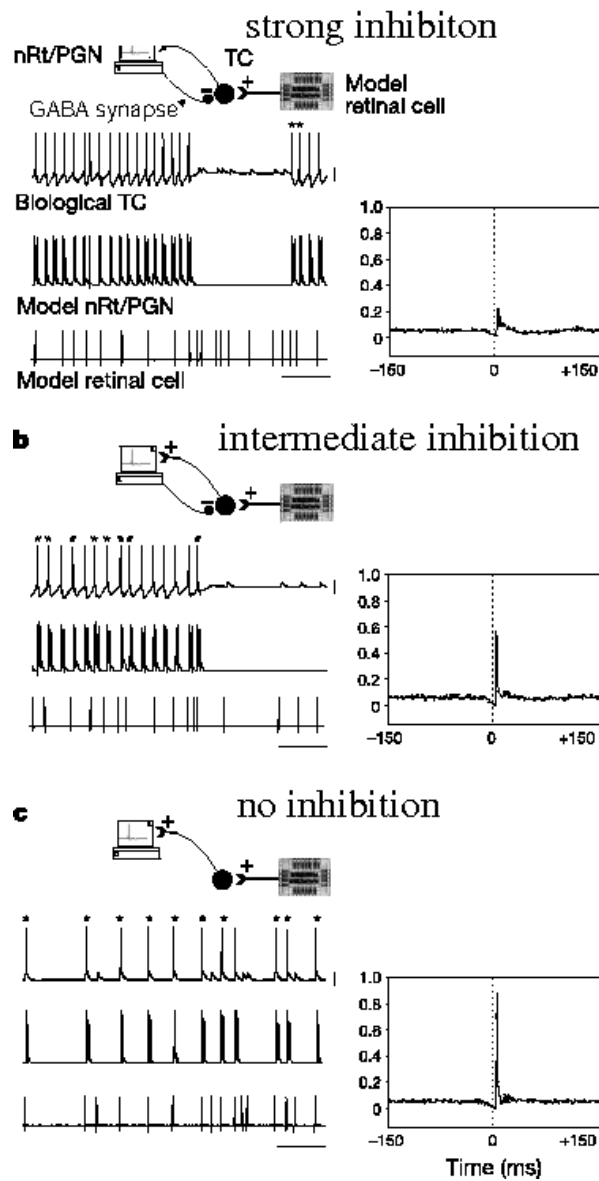


Figure 1.5: Spike transfer in the hybrid thalamic circuit. The TC-cell receives artificial synaptic retinal bombardment modeled by a Poisson-distributed spike train. The number of output spikes in the TC cell triggered by an input spike (marked by dots) diminishes with increase of inhibition, accordingly the correlation between in- and output decreases. **a)** With high gain in the inhibitory feedback, the hybrid thalamic circuit shows spindle oscillations, and little correlation between input and output. **b)** For intermediate levels of inhibition correlation between input and output increases. **c)** Without inhibitory feedback the TC cells relay synaptic inputs in a one-to-one manner resulting in a strong correlation between in and output. Picture modified from (Le Masson *et al.*, 2002).

## 1.2.2 Modeling the thalamic circuit

### Modeling the thalamic circuit using conductance based neuron models

In the early nineties the occurrence of spindle oscillations in interconnected thalamocortical relay cells and thalamic reticular cells was studied intensively by Destexhe, Babloyantz and Sejnowski (Destexhe *et al.*, 1993a; Destexhe and Babloyantz, 1993; Destexhe *et al.*, 1993b). In all that studies Hodgkin-Huxley-like models, with several ion currents were used to study the occurrence of spindle oscillations. The temporal evolution of the membrane potentials is governed by the following cable equations

$$C_m \dot{V}_T = -I_{T_L} - I_T - I_h - I_{T_{Na}} - I_{T_K} - I_{GABA_a} - I_{GABA_b} \quad (1.1)$$

$$C_m \dot{V}_R = -I_{R_L} - I_{T_s} - I_{K[Ca]} - I_{CAN} - I_{R_{Na}} - I_{R_K} - I_{GLU}, \quad (1.2)$$

where  $V_T$  is the membrane potential of the TC cell;  $C_m$  is the capacity of the membrane. According to (Destexhe *et al.*, 1993b), the following ion currents were included: The leakage current  $I_{T_L}$  and  $I_{R_L}$ , the low-threshold  $Ca^{2+}$  currents  $I_T$  and  $I_{T_s}$ , the hyperpolarization activated current  $I_h$ , the  $Ca^{2+}$ -activated currents  $I_{K[Ca]}$  and  $I_{CAN}$ , and, like in the Traub and Miles (Traub and Miles, 1991) model, the fast  $Na^+$  and  $K^+$  currents  $I_{T/R_{Na}}$  and  $I_{T/R_K}$ , which are responsible for the generation of action potentials. The synaptic currents  $I_{GABA_a}$  and  $I_{GABA_b}$  represent the  $GABA_a$  and  $GABA_b$  receptors in the synapses from RE to TC cells, while  $I_{GLU}$  describes the excitatory synapse from the TC to RE cells. All ionic currents are described by the same formalism as described in 2.1.2. A detailed description of each ion current can be found in (Mayer *et al.*, 2006). As this conductance based biophysical motivated models incorporate many features of realistic biological neurons, they allow to identify the key elements which may be responsible for sleep spindle oscillations. The change between active and silent states occurs due to the quite different timescales of the ion currents. According to (Destexhe and Babloyantz, 1993) the  $I_h$  current which works on a very slow time scale is responsible for the slow repetition rate of spindling (0.3–0.1 Hz) and such plays the key role for the long silent phases. The oscillatory period starts in the TC cell due to the current  $I_T$ , which leads to so called post-inhibitory rebound bursts. Post-inhibitory rebound means that a hyperpolarizing current, which is suddenly switched off, results in an overshoot of the membrane potential or even in the triggering of one or more action potentials. Through this mechanism action potentials can be triggered by inhibitory input. These action potentials, however, occur with a certain delay after the arrival of the inhibitory input, i.e. after the end of the inhibitory synaptic current (Gerstner and Kistler, 2002a). In reciprocally coupled RE and TC cells this leads to self-sustained oscillations if the strength of the inhibitory current is strong enough. The spindling terminates due to the activation of the  $Ca^{2+}$  activated current  $I_h$  (see Fig. 1.6). The frequency of the spindling is determined by intrinsic properties of the RE cell, as shown by Destexhe in (Destexhe *et al.*, 1993b), but also the intrinsic properties of the inhibitory synapses play a role. To provide an overview, Fig. 1.6 shows a schematic diagram of the mechanisms leading to spindle oscillations in reciprocally coupled TC and RE cells. Although these models describe experimental observations with high accuracy in



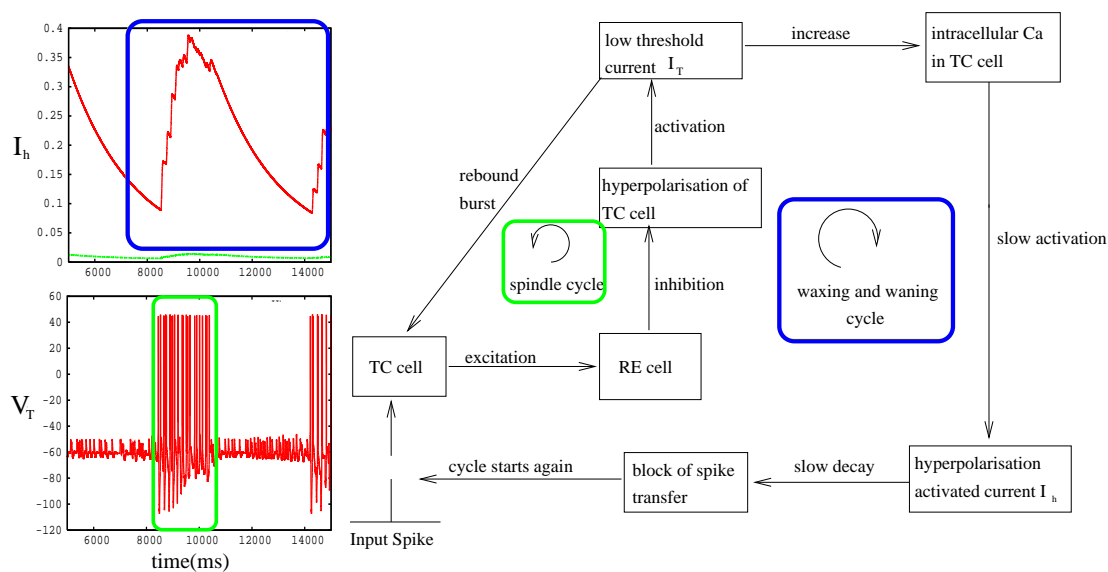


Figure 1.6: Schematic diagram illustrating the generation mechanism of spindle oscillations. Left: Temporal evolution of  $V_t(t)$  and  $I_h$ . We distinguish two cycles: First, the spindle cycle is responsible for the spiking (green); the system runs several time through it before the waxing and waning cycle (blue) is activated leading to bursts of oscillations. The slowly decaying current  $I_h$  leads to the long silent epochs during which spike transfer is blocked. Altogether, the interplay of the currents  $I_T$  and  $I_h$  plays an important role for the genesis of spindle oscillations.

detail, unfortunately, due to the complexity of the high-dimensional biophysical system (all together 38 differential equations for the two connected neurons), the connection between biophysics and dynamics is hard to unravel. Further, the computational effort is very high, making studies of networks on desktop machines almost impossible.

### Simplification of the thalamic circuit

Biological neurons exhibit extremely complex and rich behavior, in order to make neural networks analytically and computationally tractable neuronal dynamics have to be considerably simplified. As mentioned in 1.1 mostly the extremes are considered: On the one hand the relative complex Hodgkin-Huxley (Hodgkin and Huxley, 1952) type models including several ion currents and on the other hand simple binary on/off models like the McCulloch Pitts neuron (McCulloch and Pitts, 1943). Due to the simplicity of binary neurons, extremely detailed studies of the network behavior are possible but out leaves much of biological complexity behind it. Fortunately, models falling between the Hodgkin Huxley model and binary models exist. Most prominent are the integrate and fire models (for a review see Tuckwell (1988); Izhikevich (2003)), the FitzHugh-Nagumo model (FitzHugh, 1961; Nagumo *et al.*, 1962) and the Hindmarsh-Rose model (Hindmarsh and Rose, 1984). The FitzHugh-Nagumo model was constructed to match the basic behavior of the Hodgkin-Huxley model on a phenomenological level, a logical derivation can be found in (Abbott and Kepler, 1990).

$$\begin{aligned}\dot{v}(t) &= v(\alpha - v)(v - 1) - w + I = f(v) - w + I \\ \dot{w}(t) &= \mu(v - \gamma w)\end{aligned}\tag{1.3}$$

An often used set of parameters are  $a = 0.14$ ,  $\mu = 0.01$ ,  $\gamma = 2.54$ . If  $I$  is increased the system undergoes a Hopf bifurcation (see 2.2.2). The Hindmarsh-Rose model (1.4-1.6) is a simplified version of a Hodgkin-Huxley type model which includes an additional ion current, leading to experimentally observed phenomena like spike frequency adaptation (Xia *et al.*, 1997) or post-inhibitory rebound bursts (Beurrier *et al.*, 1999).

$$\dot{v} = w - v^3 + 3v^2 - z + I(t)\tag{1.4}$$

$$\dot{w} = 1.8 - 5v^2 - w\tag{1.5}$$

$$\dot{z} = \epsilon(3.3(v + 1.56) - z),\tag{1.6}$$

Besides the additional slow variable  $z$  (1.6) the main difference to the FitzHugh-Nagumo model is the quadratic equation for  $w$  (1.5), what results in different bifurcation behavior: In the  $(v, w)$  subsystem (1.4,1.5) the stability of the fixed point is lost by a saddle-node bifurcation on an invariant cycle (see 2.2.2). The Hindmarsh-Rose equations show a large variety of dynamical behavior, for a detailed review see (Wang, 1993). However to describe the waxing and waning cycle in Fig. 1.6 the Hindmarsh-Rose equations have to be extended by an additional slow degree of freedom to describe the behavior of the TC

neuron. Accordingly the thalamic circuit is modelled by

$$\begin{aligned}
\dot{v}_{TC/RE} &= w_{TC/RE} - v_{TC/RE}^3 + 3v_{TC/RE}^2 - z_{TC/RE} \\
&\quad - 0.4h_{TC} + I_{TC}(t) + C(v_{RE/TC}) \\
\dot{w}_{TC/RE} &= 1.8 - 5v_{TC/RE}^2 - w_{TC/RE} \\
\dot{z}_{TC/RE} &= 0.006(4(v_{TC/RE} + 1.56) - v_{TC/RE}) \\
\dot{h}_{TC} &= -0.0004(h_{TC} + 1.7(0.85 - z_{TC})),
\end{aligned} \tag{1.7}$$

where  $C(v_{RE/TC})$  is the synaptic coupling function. In (Mayer *et al.*, 2006) the extension of the Hindmarsh-Rose model by the slow variable  $h_{TC}$  is directly motivated from the kinetics of the  $I_h$  current described in (Destexhe and Babloyantz, 1993). The extended Hindmarsh-Rose model allows a description of thalamic circuits on a phenomenological level, coarse graining out details but preserving biological complexity. Overall, the dynamical behavior survives simplifications as long as the basic bifurcations and different time scales of the original system are preserved.

### 1.2.3 Dynamical behavior of thalamic circuits

Spindle oscillations or bursts are often explained by bistability between a fixed point and a limit cycle (Steriade *et al.*, 1991; Fuentealba *et al.*, 2005). In (Mayer *et al.*, 2006) it was shown that the occurrence of spindle oscillations in interconnected RE and TC neurons (Destexhe *et al.*, 1993b) and the accompanied decrease in spike transfer (Le Masson *et al.*, 2002) can be explained by a subsequent shifting between a monostable state, consisting of a fixed point, and a bistable state consisting of a stable fixed point and a stable limit cycle. This shifting is mediated by a slow variable  $h_{TC}$  mimicking the  $I_h$  current in the conductance based model (For a detailed description see Mayer *et al.* (2006)). The decrease in the spike transfer occurs according to two effects: during the oscillatory phase of the spindle oscillation (2 in Fig. 1.7) the incoming signals are masked, during the silent phase (4 in Fig. 1.7) the transfer is blocked. In (Mayer *et al.*, 2007) in a further step of abstraction, spindle oscillations are described by the overdamped movement in a double well potential.

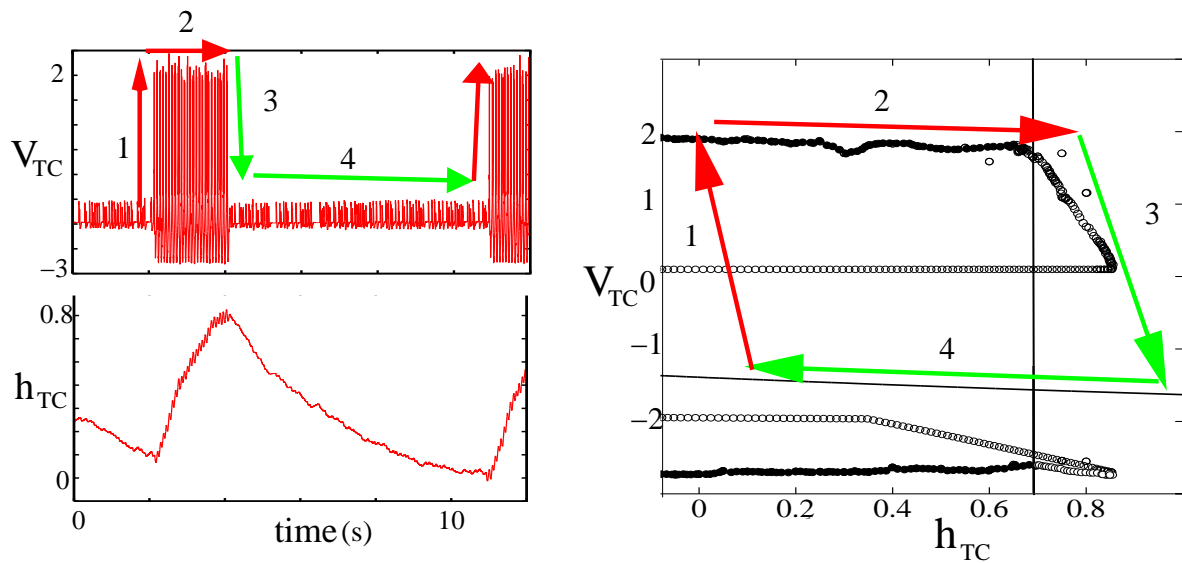


Figure 1.7: Temporal evolution of  $V_{TC}$  and  $h_{TC}$  and max/min bifurcation diagram of the computational model for the thalamic circuit used in (Mayer *et al.*, 2006) with  $h_{TC}$  treated as a slowly varying parameter, solid lines indicate stable fixed points, dashed lines unstable fixed points, filled circles stable limit cycles, open circles unstable limit cycles. For extreme values of  $h_{TC}$  the system is monostable i.e. either a stable fixed point or a stable limit cycle (not shown) exist. In between these areas the system is bistable and can be switched by an input spike from the fixed point to the stable limit cycle (1). During the oscillatory phase  $h_{TC}$  increases (2) accordingly the limit cycle loses stability. Consequently, the system is attracted by the fixed point (3) and rests on it, during the silent state the variable  $h_{TC}$  decays back to its resting value (4). Iteration of this cycle results in spindle oscillations.

## 1.3 Synchronization of thalamic spindles in the thalamocortical system

Synchronization is assumed the oldest scientific studied nonlinear effect, already in 1665, Christiaan Huygens discovered synchronization of the pendulum clocks invented by him. Huygens deduced that the crucial interaction for this effect came from imperceptible movements of the common frame supporting the two clocks (Bennett, 2002). In recent years, synchronization became a focus of nonlinear dynamics research. Synchronization is a widespread phenomenon in populations of periodic, noisy and chaotic oscillators (or maps), studied theoretically (Kuramoto, 1984; Rosenblum *et al.*, 1996) as well as experimentally (Kiss *et al.*, 2002). The synchronizing elements are quite different, ranging from Josephson-Junctions in a high frequency field over swarms of fireflies to neurons of the central nervous system, to mention just a few. A proposition for synchronization is that the observed elements are nonlinear and non-conservative (Pikovsky *et al.*, 2001). Synchronization in nonlinear systems is not restricted to a few particular systems, rather it seems to be a universal concept in nonlinear sciences (Pikovsky *et al.*, 2001).

### 1.3.1 Experimental motivation

#### Synchronization of thalamic spindles

In neural systems, synchronization is a widespread phenomenon (Diesmann *et al.*, 1999). In particular synchronization of cortical activity is putatively connected to information processing and learning (Singer, 1993). In this thesis synchronization of thalamic activity during NREM sleep is of particular interest. Thalamic cells are known to exhibit spike burst activity during periods of drowsiness, inattentiveness and NREM sleep (Destexhe *et al.*, 1993b; Contreras *et al.*, 1996). Thalamic spindle oscillations, a hallmark of early sleep stages, observed in the EEG recordings of sleeping humans and animals as oscillations in a 12-15 Hz frequency range, are considered to be the result of synchronized spike burst activity of millions of thalamic neurons (Steriade, 2001a; Mölle *et al.*, 2002). Despite experimental findings in thalamic slices, where the spindle oscillations propagate like a traveling wave through the network (Kim *et al.*, 1995), in the intact brain, spindle oscillations occur almost synchronously over widespread territories of the thalamus (Contreras *et al.*, 1996; Steriade, 2001a) (see Fig. 1.8). These contrasting results between in vitro and in vivo experiments occur due to the absence of corticothalamic projections (synaptic connections from the cortex to the thalamus) in a thalamic slice, as after ablation of the cortex, synchrony is lost in the thalamus (Contreras *et al.*, 1996; Steriade, 2001a; Destexhe, 2000). In (Möller *et al.*, 2002) it was examined whether in the human EEG, cortical slow-wave oscillations are linked to the occurrence of spindle oscillations. The results clearly show that also in the human sleep the spindles become temporarily grouped by cortical slow-wave oscillations. As the EEG measures an average value of large neuron populations, macroscopic oscillations are only observed if these oscillations are to a high degree synchronous (Rosenblum and Pikovsky, 2004). Therefore, an interpretation of the temporal grouping

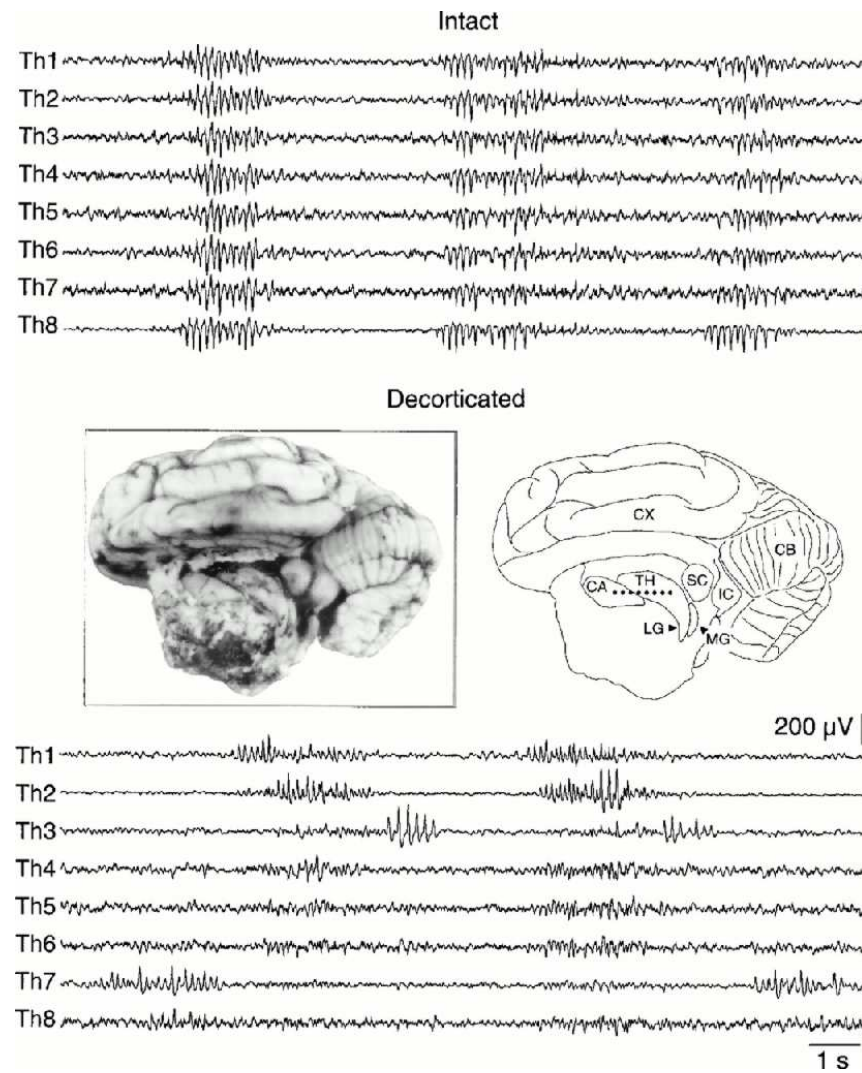


Figure 1.8: Synchronization of thalamic spindles by cortical feedback in the cat. Eight electrodes were placed at different sites in the thalamus of an anesthetized cat. In the intact brain, the spindle oscillations occur synchronous at all eight electrodes. If the cat gets decorticated, synchrony of thalamic spindles is lost. Picture taken from (Contreras *et al.*, 1996).

is that thalamic spindles are synchronized by the cortical slow-waves. This phenomenon was part of several numerical and experimental investigations (Contreras *et al.*, 1996; Bal *et al.*, 2000) however, the dynamical mechanisms how cortical slow-waves lead to coherent spindles in the thalamus are still unknown.

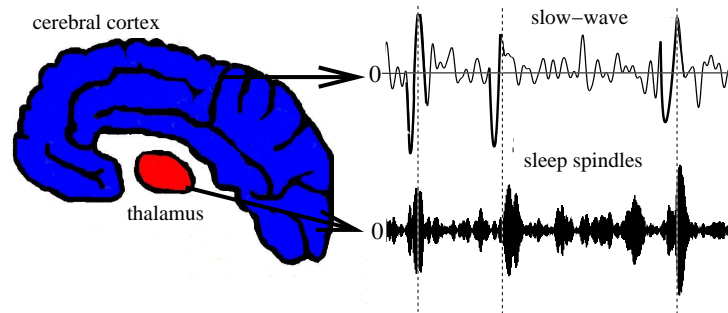


Figure 1.9: Grouping of thalamic spindles by cortical slow-waves in the human EEG. The physical reason for that grouping is that thalamic spindles are synchronized by cortical slow-waves.

### Cortical slow-waves

Low frequency ( $<1$  Hz) oscillations in intracellular recordings from cortical neurons were first reported in the anesthetized cat and then during natural sleep. The slow sequences of hyperpolarization and depolarization were reflected by slow oscillations in the electroencephalogram (Achermann and Borbély, 1997). In human EEG measures, slow-wave sleep manifests as large amplitude ( $75 \mu V$ ) oscillations in a frequency range of about 0.5-3 Hz. During waking thalamic signals form the most important sensory input to the cerebral cortex. However, the cortical slow oscillation seems to be generated, maintained and terminated by the cortex alone (Tononi *et al.*, 2006). Steriade studied the dependence of the slow cortical oscillation upon the thalamus by lesions and stimulation (Steriade *et al.*, 1993b). It was found that the slow cortical rhythm survived extensive destructions of thalamic nuclei that were input sources to the recorded cortical neurons. To further prevent the possibility of thalamic neurons, which were input sources to the other brain hemisphere in the genesis of the slow rhythm, the corpus callosum (i.e. the connection between the two brain hemispheres) was interrupted, and still the slow rhythm was recorded in cortical neurons. These experimental results indicate that the thalamus is not essentially implicated in the genesis of the slow rhythm. Bazhenov studied the slow oscillation in isolated cortical slaps (Bazhenov *et al.*, 2002). It was found that the occurrence of the slow oscillations depends on the size of the slap considered and such on the number of cortical neurons involved. These experimental observations were reproduced in a cortical network model based on Hodgkin-Huxley-like neurons (Bazhenov *et al.*, 2002). The hypothesis that the cortical slow oscillation depends rather on intracortical connections than on subcortical inputs was strengthened by experiments (Amzica and Steriade, 1995b,a)

and computer simulations (Compte *et al.*, 2003), where it was found that dissection of intracortical connections disrupt the slow-wave oscillation.

A further important question is, if the slow-wave oscillation is a travelling wave or coherent over large territories of the cortex. At this point, both observations have been made. In (Massimini *et al.*, 2004a) it was shown by high-density EEG recordings in humans, that the slow oscillation is a traveling wave. However in (Volgushev *et al.*, 2006) simultaneous multisite intracellular recordings in cats, showed that the slow oscillation involves all neocortical neurons and that both activity and silence start almost synchronously in cells located up to 12 mm apart. Because of the high amplitude of the slow oscillation in the EEG, it is conjectured that large ensembles of neurons are in the synchronized state. In (Köhler *et al.*, 2008) a simplification of the Pinto-Ermentrout model (Pinto and Ermentrout, 2001) was used to study the influence of noise on the spreading of cortical oscillations. It was found that via the noise level or via the threshold height, the model can be tuned from the silent, over the traveling wave, to the coherent state. The computational observations suggest that even in the traveling wave state many neurons form a wave front within neurons oscillate coherent.

### 1.3.2 Modeling cortical control of synchrony in the thalamus

The synchronization of thalamic spindles was modeled by Steriade's group based on conductance based neuron models (Destexhe *et al.*, 1998). In this detailed biophysical neuron models the dead time or refractory period between two spindle oscillations is caused by the slow refractory current  $I_h$  (Destexhe *et al.*, 1993a). Coherence of thalamic spindles is established by a reset of the slow refractory variable. In (Mayer *et al.*, 2007) the complex dynamics described in Fig. 1.7 is simplified to the overdamped movement in a double well potential.

$$\begin{aligned}
 U(r, \alpha, \varphi) &= \frac{1}{2}r^2 - \alpha(t)\frac{1}{4}r^4 + \frac{1}{6}r^6, \quad \varphi(t) = \omega t \\
 \frac{dr}{dt} &= -\frac{\partial U(r, \alpha)}{\partial r} + I_{ext} + F(t) \\
 \frac{du}{dt} &= 0.01(r(1-u) - 0.14u), \quad \text{where } \alpha(t) = 2.6(1-u)
 \end{aligned} \tag{1.8}$$

Where  $u$  is a slowly varying process, which switches the system between a monostable and bistable state, it corresponds to  $h$  in Fig. 1.7 (for further details see 2.2.3). Based on the experiments introduced in 1.3.1, in (Mayer *et al.*, 2007) it is conjectured that cortical slow-waves control synchrony of thalamic spindles by open loop control. It was found that the transition from traveling waves to coherent oscillations can be achieved by a low amplitude control signal. To be able compare the results with experimental observations human slow-wave EEG recordings were used as a control signal. The grouping of thalamic spindles in the computational model was quite similar to the grouping observed in the human EEG. The coherence of thalamic oscillations is established by a repetitive reset of the slow variable, switching the system between the oscillatory and the silent state. Here a



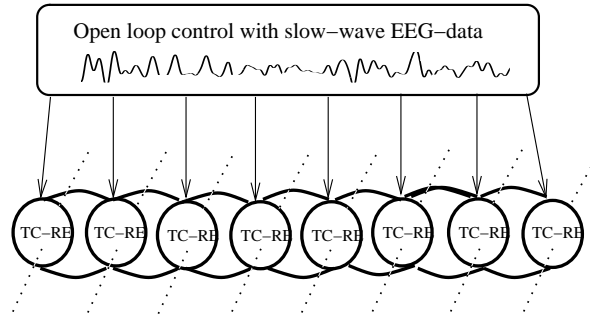


Figure 1.10: Open loop control of a 2-D network of thalamic oscillators described by Equ. (1.8) by slow-wave EEG-data. Here only one row of the network is shown.

qualitative understanding of this control mechanism is given. We assume the slow process  $u$  to be a relaxation oscillator with relaxation time  $\tau$ , this relaxation process is activated during the oscillatory phase of the spindle, in turn the slow process inhibits excitation of the neurons for time  $\tau$ . So the slow process  $u$  can be interpreted as a refractory process which leads to a dead time, in which the single oscillator is not excitable. So the maximum phase difference between any arbitrary chosen oscillators is at most of the magnitude of  $\tau$ . Another way to inhibit the oscillations is a common, sufficiently strong hyperpolarization of all oscillators, i.e.  $F(t)$  in (1.8) is negative. If the duration of this hyperpolarization exceeds  $\tau$ , all neurons will be back in their excitable ground state. That means they all have the same phase. If this phase resetting is done repetitively, the variance of the phases of the single thalamic neurons can be confined. From both, the experimental results (Steriade *et al.*, 1993b; Bazhenov *et al.*, 2002; Compte *et al.*, 2003) and the computational results (Destexhe *et al.*, 1993a; Mayer *et al.*, 2007) one of the main hypothesis in this thesis is that synchronization in the thalamus is mainly controlled through open loop repetitive phase resetting by the cortex. In (Mayer *et al.*, 2007) it was shown that the effects shown in Fig. 1.11 strongly depend on the coupling in the network, and are not just entrainment of a common signal. Thus without internal coupling no synchronization would occur.

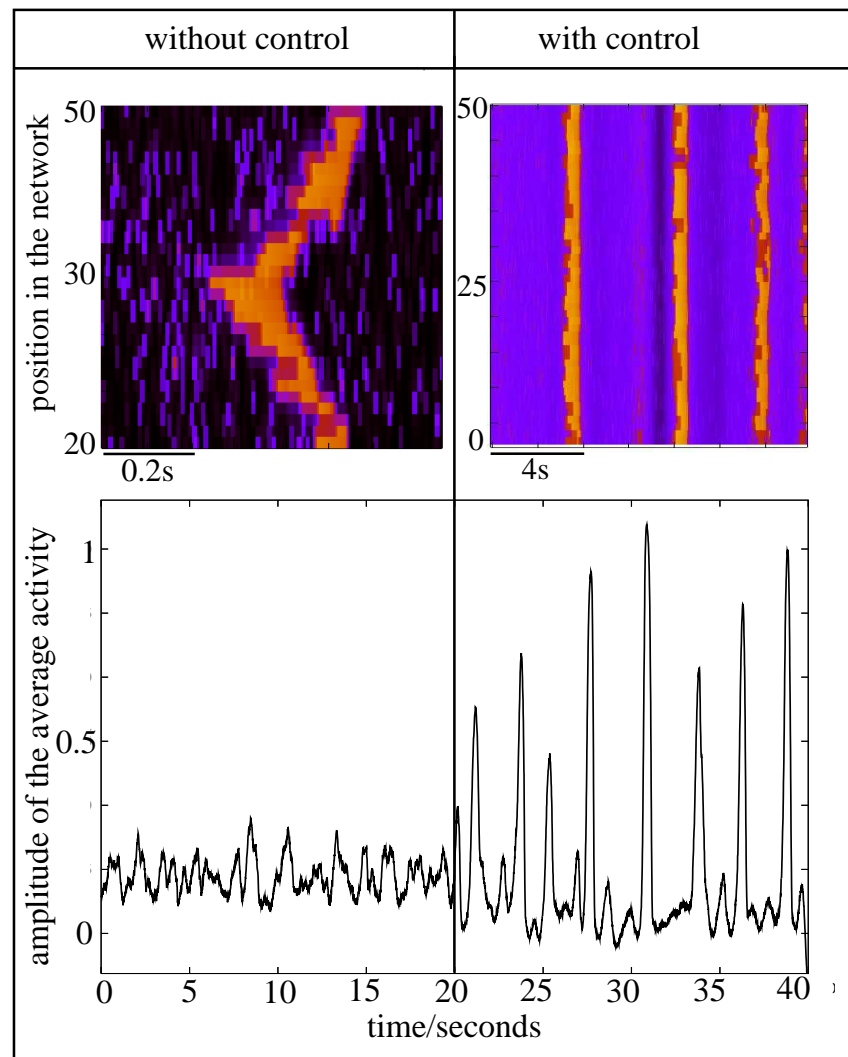


Figure 1.11: Top: Without an external control signal the travelling waves occur in the computational model for thalamic activity used in (Mayer *et al.*, 2007). If cortical slow wave EEG data are used as a control signal, the travelling waves disappear and synchronous oscillations occur. Bottom: The average activity shows only little fluctuations in the travelling wave state, in the synchronous state large fluctuations occur.

## 1.4 Emergence of slow-wave sleep and spike-timing dependent plasticity

While the genesis and the function of spindle oscillations in the thalamus is quite well understood (Destexhe *et al.*, 1993b; Sherman and Guillery, 2001, 2006), only little is known about the emergence of cortical slow-wave oscillations and its function. Several experiments (Wagner *et al.*, 2004; Walker and Stickgold, 2004; Marshall *et al.*, 2006) indicate that slow-wave sleep potentiates memory. However, only little is known about the underlying mechanisms.

### 1.4.1 The hypothesis of synaptic homeostasis

The most promising hypothesis how slow-wave sleep emerges and its functions was proposed by Giulio Tononi (Tononi and Cirelli, 2003, 2006). According to this hypothesis, plastic processes (i.e. changes in the synaptic weight) during wakefulness result in a total synaptic increase of synaptic weights in the cortical network. Following the hypothesis, plastic changes in the form of synaptic potentiation (i.e. an increase of synaptic weight) occur through much of waking life, whenever we are alert and make behavioral choices, whether or not we are specifically engaged in experimental learning paradigms. Because average synaptic strength at the end of the waking period is high, cortical neurons are highly synchronized at the onset of slow-wave sleep. As a result, the EEG of early sleep shows slow-waves of high amplitude. According to Tononi (Tononi and Cirelli, 2003, 2006) the slow-waves are not an epiphenomenon of increased synaptic strength, but have to play a role: The role of sleep is to downscale synaptic strength to a baseline level, which is energetically sustainable and is beneficial for learning and memory (see Fig. 1.12). During the downscaling which decreases all synaptic strengths by a certain factor, some synapses are downscaled under a minimum strength and are downselected. In a network, this leads to consolidation of the important (i.e. strong) connections. In this thesis the synaptic potentiation during waking, which according to the hypothesis induces slow-wave sleep, is of particular interest.

#### Evidences for synaptic potentiation

The synaptic homeostasis hypothesis states that the amplitude of the slow-waves in the EEG is directly coupled to the amount of synaptic potentiation during waking, as it increases the synchrony among cortical neurons. An intriguing prediction of the hypothesis is that synaptic potentiation in certain cortical areas should lead to an increase of slow-wave activity in these areas. In an experiment by Huber *et al.* (2004) high-density EEG measures were used to investigate sleep after learning a visuomotor task, what should lead to synaptic potentiation in the associated cortical area. As predicted by the hypothesis the slow-wave activity, measured by the electrodes in the according cortical area, was increased by about 20% compared to the other electrodes (see Fig. 1.13) (Huber *et al.*, 2004).

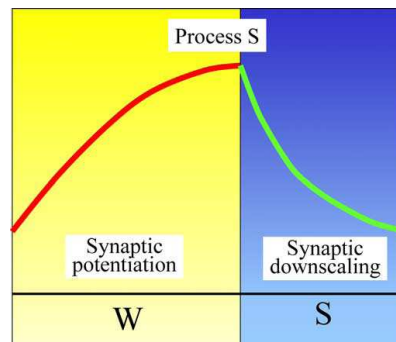


Figure 1.12: The 2 process schema: during waking synaptic potentiation takes place (left), during sleep the synapses are downscaled (right). Picture taken from (Tononi and Cirelli, 2006)

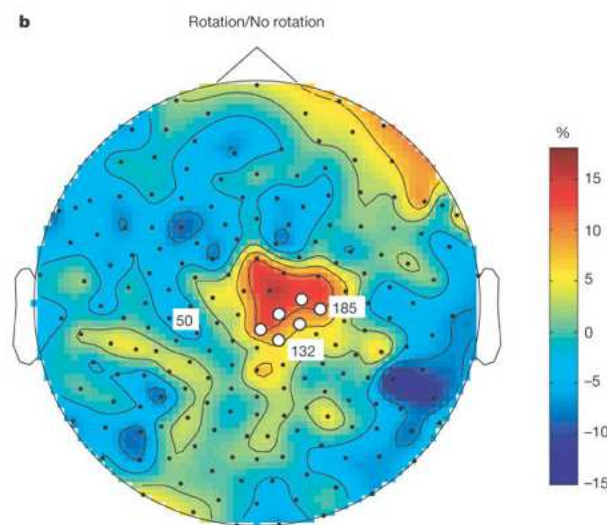


Figure 1.13: Topographic distribution of the percentage change in SWA during NREM sleep between learning the visuomotor task and no learning. White dots indicate the cluster of six electrodes showing increased SWA after learning. In the cortical area involved into learning slow wave activity is increased by about 20%. Picture taken from (Huber *et al.*, 2004).

Another experimental evidence supporting the hypothesis is that the slow-wave activity and the time spend in slow-wave sleep during a night increases with the time awake before falling asleep, what was shown by gentle sleep deprivation in rats (Borbely *et al.*, 1984) and in humans (Achermann *et al.*, 1993). An increase of the slow activity in the EEG is a direct hint towards an increase of synchrony among cortical neurons, as the EEG measures an average value over many neurons (Rosenblum *et al.*, 1996; Mayer *et al.*, 2007). In (Hill and Tononi, 2005) it was shown in computo that an increase of cortico-cortical connections leads to an increase in the degree of synchrony among cortical neurons.

### 1.4.2 Synaptic potentiation by spike-timing dependent plasticity

Synaptic potentiation in local connections between neurons takes place according to certain rules. Probably the most prominent update rule was proposed half a century ago by Donald Hebb (Hebb, 1949). Hebb postulated the change of synaptic weights depends on the correlation of pre and postsynaptic cell activity: Those that fire together wire together. In this thesis a special form of correlation based learning is considered. Experimental evidence indicates that synaptic changes in cortical neurons depend on the precise temporal order between presynaptic and postsynaptic firing (Markram *et al.*, 1997; Bi and Poo, 1998; Wittenberg and Wang, 2006). Spike timing dependent plasticity (STDP) means that synaptic potentiation follows causality, i.e. presynaptic spikes preceding postsynaptic spikes lead to synaptic potentiation whereas reverse time ordering leads to depression (see Fig. 1.14). Recently synaptic changes have been investigated for oscillator networks

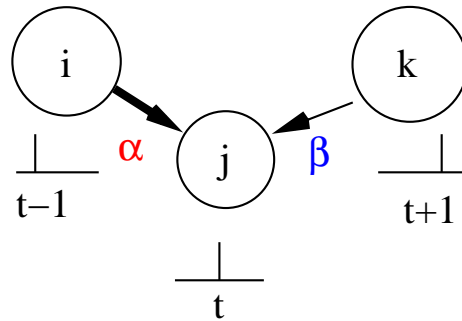


Figure 1.14: Schematic diagram for spike-timing dependent plasticity. If the presynaptic neuron  $i$  fires before neuron  $j$  the strength of the synapse from the  $i$ -th to the  $j$ -th neuron is increased. If neuron  $j$  causes neuron  $k$  to fire the synaptic strength from the  $k$ -th neuron to the  $j$ -th neuron is decreased. Therefore modification of synaptic strengths follows causality

numerically (Tass and Majtanik, 2006; Maistrenko *et al.*, 2007; Rubin *et al.*, 2001). In (Mayer and Schuster, 2008) the spike-timing dependent plasticity rule was reduced to its bare bones by modeling the synaptic change via a time discrete, temporal asymmetric update rule (2.58).

$$J_{ij}^{t+1} = \lambda J_{ij}^t + (\alpha x_i^{t+1} x_j^t - \beta x_i^t x_j^{t+1}), \quad (1.9)$$

For causal firing  $J_{ij}^t$  increases by  $\alpha$  whereas it decreases by  $\beta$  if neuron  $i$  fires before neuron  $j$ . Experimental results suggest that  $\alpha$  is larger than  $\beta$  (Zhang *et al.*, 1998). It is observed that an all to all coupled network of binary neurons connected via Equ. (1.9) shows a transition to the coherent state if driven by uncorrelated white noise. Experiments showed that correlations in neural spike-trains increase during a learning task (Bair *et al.*, 2001). In the model proposed in (Mayer and Schuster, 2008) correlated noise clearly outperforms uncorrelated noise in synaptic potentiation, what is conform to the observation that cortical areas being involved into learning new tasks show a stronger slow-wave activity than others (Huber *et al.*, 2004). The results of this work suggest that spike-timing dependent plasticity might be the mechanism leading to synaptic potentiation during wakefulness.

## 1.5 Survey of the publications

### 1.5.1 Role of inhibitory feedback for information processing in thalamocortical circuits

One way to gain insight into the mechanisms depriving us from sensory information during sleep, is to study the spike transfer of elementary thalamic circuits. Destexhe studied spindle oscillations computationally in interconnected conductance based neuron models for the TC and the RE cell (Destexhe and Babloyantz, 1993; Destexhe *et al.*, 1993b,a) however only the case of constant current injection is studied. In (Mayer *et al.*, 2006) two modeling approaches for the experiment by Le Masson *et al.* (Le Masson *et al.*, 2002) on the thalamocortical loop are considered. In a first step, the transfer of a poisson distributed input spikes is studied in dependence of the inhibitory coupling from the RE to the TC cell, by using conductance based neuron models as used in (Destexhe *et al.*, 1993b). By considering the single ion channels, the key mechanisms for the generation of spindle oscillations are extracted. It is found that spindle oscillations occur due to a multi time scale effect, which seeds in the different time scales of the gating of ion channels in the cell membrane. The insights won by considering the biophysical motivated conductance based neuron model, are used to motivate an extension of the widely used Hindmarsh-Rose model (Hindmarsh and Rose, 1984) by an additional slow degree of freedom, which allows to model the occurrence of spindle oscillations and the spike transfer in the thalamic circuit on an intermediate level of description. The derived model of the thalamic circuit is used to analyze the dynamical mechanisms leading to spindle oscillations and to clarify the relationship between the occurrence of spindle oscillations and the decrease in information transmission. Two measures are used to characterize the information transmission. First, the signal-to-noise ratio (SN) examines the amplitude of the TC-cell signals and quantifies the percentage  $N_{tr}$  of output spikes  $N_{out}$  which are exactly triggered by an input spike. Second, the transfer efficiency (TE) measures the global efficiency in the input-output spike transfer, and indicates the ratio of input spikes being actually transmitted as output spikes. The decrease in the spike transfer with increasing inhibitory feedback occurs according to two effects:

- the oscillatory phase of the spindle oscillation is a very robust self-oscillation of the circuit, during that phase the system is stable against external disturbance, i.e. the incoming signals are masked, which leads to decrease of SN.
- during the silent phase of the spindle, the threshold of the system is strongly increased, so incoming spikes only lead to subthreshold oscillation, what results in a block of the transfer and such a decrease of TE.

The two effects described above are typical for hysteresis between a limit cycle and a fixed point. The additional slow degree of freedom switches the system between these two existing dynamical states, namely a fixed point and a bistable state where limit cycle and

a fixed point coexist. Without this further current, two reciprocal coupled Hindmarsh-Rose neurons exhibit so called hard self-excitation (Haken, 1983) as response to an input spike, resulting in stable self-sustained oscillations. The additional slow current makes this oscillatory state metastable, resulting in waxing and waning oscillations. An increase of the inhibitory coupling changes the responsibility of the system: Without, or with only little inhibition, the system responds to an input pulse with an output spike, so that spikes are transmitted in a one to one manner. With high gain in inhibitory feedback, the system responds to an input spike by an output burst. The transmission behavior depends critically on the rate of rise and fall of the slow current.

### 1.5.2 Corticothalamic projections control synchrony in locally coupled bistable elements

In (Mayer *et al.*, 2006) spindle oscillations were studied in an elementary thalamic circuit. Sleep spindles can also be seen outside the brain during NREM sleep by EEG measurement, resembling a mean-field observation of neural electric activity (Steriade *et al.*, 1993a; Mölle *et al.*, 2002; Mayer *et al.*, 2007). Spindle oscillations are generated in the thalamocortical system (Hill and Tononi, 2005; Steriade *et al.*, 1993a). Physiological cortex and thalamus form a closed feedback loop (Sherman and Guillery, 2006). However, several experimental evidences indicate that during NREM sleep the cortical action does not essentially depend on thalamic inputs (Steriade *et al.*, 1993b; Tononi *et al.*, 2006). Large-scale computational models of the thalamocortical system, based on Hodgkin-Huxley (Hodgkin and Huxley, 1952) type neuron models, have shown that thalamic spindles are synchronized within the thalamocortical network (Destexhe, 2000; Hill and Tononi, 2005). However only little is known about the mechanisms underlying this synchronization. In the human EEG thalamic spindles are grouped by the cortical slow-waves during non REM sleep (Möller *et al.*, 2002). Further it was shown in several experiments of the Steriade group that spindles occur as travelling waves in thalamic slices or if the cortex is removed, whereas in the intact brain they occur synchronously (Contreras *et al.*, 1996; Steriade, 2001a) In (Mayer *et al.*, 2007) the control of thalamic oscillations is studied on an intermediate model level, course-graining out details but preserving essential biophysical elements that distinguish the neurons from simple phase oscillators: stochastically driving, slow-fast dynamics, and bistable switching. As a control signal human slow-wave EEG data are used, the results are directly comparable with the experimental results in (Möller *et al.*, 2002). It is found that cortical slow-waves as a control signal induce the transition from travelling waves to synchronized states in the artificial thalamic network. For this synchronization both the internal coupling within the network and an external control signal is needed. Responsible for this synchronization is, that the external field modulates the threshold. The synchronization in the model thalamus is mainly controlled through open loop repetitive phase resetting of the slow process, leading to the long silent periods between the oscillatory phases. The results obtained by this computational model provide a phenomenological explanation of the experimental results in (Möller *et al.*, 2002). Further the grouping of the



mean-field activity of the computational thalamic network in (Mayer *et al.*, 2007) by the slow-wave signal, reproduces the experimental results in (Möller *et al.*, 2002).

### 1.5.3 Excitation of coherent oscillations in a noisy medium

Although our knowledge of the brain and its functions has increased over the last decades, we still understand very little about the internal mechanisms. The question, how to influence and control the brain with external stimuli became focus of many recent studies (Chen, 1997; Huber *et al.*, 2004; Nitsche *et al.*, 2003; Marshall *et al.*, 2006). As a well-known example, it has been shown that external signals enhance slow-waves during NREM sleep (Marshall *et al.*, 2006). In (Richardson *et al.*, 2005a) computational predictions (Pinto and Ermentrout, 2001) that modulation of the neuronal threshold with electrical fields can speed up, slow down, and even block traveling waves, were experimentally confirmed in neocortical slices. A biological example for the occurrence of traveling waves is the deep sleep of mammals (Massimini *et al.*, 2004b). During most of NREM sleep, almost all cortical neurons undergo a slow oscillation in the membrane potential, switching between a silent hyperpolarized state, and an active depolarized state of high frequency firing (Massimini *et al.*, 2004b; Marshall *et al.*, 2006). In (Köhler *et al.*, 2008) noise induced transitions of threshold elements with self-inhibition to synchronous oscillations are studied. Experimentally acquired EEG-data of slow-wave oscillations resemble only the average activity of populations of neurons and give no information about biophysical details. Following Freeman (Freeman, New York 1975) and Wilson and Cowan (Wilson and Cowan, 1973) in (Köhler *et al.*, 2008) it is assumed that the functional units of the single brain regions consist of populations of neurons and not of single neurons. Accordingly, the dynamical behavior of neural networks can be studied by coupled elements in which the variables describe whole neuron populations. Probably the best-known model following this approach is the Wilson Cowan model for cortical activity (Wilson and Cowan, 1973). Pinto and Ermentrout (Pinto and Ermentrout, 2001) modified this model to represent traveling pulse propagation in the disinhibited neocortex. However the Pinto-Ermentrout traveling wave model assumes a continuous medium, as all real neural networks consist of single elements, i.e. the neurons, a continuum model is only valid for very large neural populations. In (Köhler *et al.*, 2008) it is shown that the Pinto-Ermentrout traveling wave model can be simplified to a spatial discrete network with nearest neighbor coupling, without losing the main feature – the dependence of the spreading velocity of the traveling wave on the threshold. By introducing threshold noise, it is found that the network shows pronounced coherence resonance. In a 2-dimensional network, it is shown that the transition from the silent, to the self-induced traveling wave, to the coherent oscillation network state can be achieved by either tuning the threshold or the noise intensity. Furthermore, the influence of a threshold modulation by external signals, i.e. electric fields, is studied for different amplitudes of the noise. For small noise intensities, a threshold modulation with a periodic signal has nearly the same effect as threshold modulation with a constant signal. For larger noise intensities, however a constant threshold modulation has no effect, while symmetric, positive and negative modulation increase the oscillation of the network.

### 1.5.4 Dynamical mean-field equations for synaptic plasticity

How do we acquire new knowledge and skills through instruction or experience? This is one of the most fascinating questions in understanding the function of our brain. In order to learn or memorize a fact or skill, there must be persistent functional changes in the brain that represent the new knowledge. Synaptic plasticity is thought to be the neuronal correlate of learning. Moreover, modification of synapses contributes to the activity-dependent homeostatic maintenance of neurons and neural networks (Abbott and Gerstner, 2004). This change obeys certain rules. Recent experiments indicate that synaptic changes in cortical neurons depend on the precise temporal order between presynaptic and postsynaptic firing (Markram *et al.*, 1997; Bi and Poo, 1998; Wittenberg and Wang, 2006). This effect is called spike-timing dependent plasticity. Several computational models for this kind of synaptic change have been proposed and studied numerically (Song *et al.*, 2000; Rubin *et al.*, 2001; Tass and Majtanik, 2006; Maistrenko *et al.*, 2007). In (Mayer and Schuster, 2008), the discrete dynamics of a fully connected network of threshold elements interacting via dynamically evolving synapses displaying spike-timing dependent plasticity is studied. The update rule for spike-timing dependent plasticity is reduced to its bare bones. By using dynamical functionals a dynamical mean-field theory for uncorrelated and correlated input noise is derived analytically from the network equations. It is shown that noise with an appropriate amplitude plays a beneficial role for the evolution of the couplings in the network. An important question is whether results depend on the color of the noise, as the spectral properties of human EEG measurements change during different states of consciousness (Shen *et al.*, 2003). The results in (Mayer and Schuster, 2008) show that colored noise outperforms white noise in enhancement of synaptic couplings. This is a realistic result, as measurements show that cortical areas involved into a learning task resolve stronger correlations than cortical areas not involved into learning (Singer and Gray, 1995). Furthermore it was shown that cortical areas involved into learning during day show stronger low wave activity as others, indicating more synaptic potentiation during day (Huber *et al.*, 2004). Although spike-timing dependent plasticity is described on a phenomenological level the main feature—the detection of spatiotemporal correlations—is preserved. As in many physical systems (solid state physics, neuro-physics, socio-econophysics, statistical physics in general) dynamical evolving couplings occur, the methods presented in (Mayer and Schuster, 2008) can widely be applied. Further the model suggested in (Mayer and Schuster, 2008) allows a computational efficient treatment of further important questions like for example the evolution of initially imprinted activity-patterns or synchronization of threshold elements with a dead time, coupled via synapses showing STDP.

## 2 Methods

### 2.1 Modeling the electrophysiology of the neuron

Electrophysiology is the study of the electrical properties of biological cells and tissues. It ranges from measurements of voltage change or electrical current flow of single ion channels to EEG measurements in clinical applications. A prominent example of electrophysiology are measurements of the electrical activity of neurons, and particularly the action potential activity (often called spike or spiking), which led to the work of Hodgkin and Huxley (Hodgkin and Huxley, 1952) in elucidating the mechanisms of action potentials in the squid giant axon - one of the major breakthroughs in dynamical modeling in physiology. The theoretical framework of nonlinear dynamics can be used to understand and explain neurophysiologic observations on different levels. Biophysical approved and well understood is the ionic basis of neural excitability. The dynamical generation of action potentials at the single neuron level is fundamental in computational neuroscience. The membrane of a neuron acts as a barrier separating the intracellular fluid from the extracellular fluid. It is permeable for water but not for large molecules. Ions like  $Na^+$ ,  $K^+$ , and  $Cl^-$  can pass through so-called ion channels, driven by electrical forces and diffusion. This movement of electric charge underlies the generation of electrophysiologic signals in the nervous system. Differences in the intra/extracellular ionic concentrations create a potential difference across the membrane. Roughly, the electric behavior can be described as follows (Wilson, 1999):

- In the absence of a signal there is a resting potential of  $\simeq -65\text{mV}$
- During an action potential (i.e. if the neuron fires a spike), the membrane potential increase rapidly to  $\simeq 20\text{mV}$ , returns slowly to  $\simeq -75\text{mV}$  and then slowly relaxes to the resting potential
- The fast membrane depolarization corresponds to an influx of  $Na^+$  across the membrane. The return to  $-75\text{mV}$  corresponds to an efflux of  $K^+$  of the cell. The final recovery back to the resting potential is associated with the passage of  $Cl^-$  out of the cell.

#### 2.1.1 Conductance based neuron models

The dynamical mechanisms of neural excitability are shared by broad classes of neural models. These features manifest in models of a single cell by threshold behavior, beating

and bursting behavior, bistability and hysteresis. The conceptual idea behind conductance based electrophysiological models is that cell membranes behave like electrical circuits. The equivalent elements of this electric circuit can be categorized as follows:

- the phospholipid bilayer, is the analogous to a capacitor: It accumulates electric charge as the electrical potential across the membrane changes
- the ionic permeabilities of the membrane, are the analogous to resistors
- the electrochemical driving forces, are the analogous to batteries driving the ionic currents

These ionic currents are arranged in a parallel circuit. Accordingly the electrical behavior of a cell is determined by the transfer and storage of ions such as  $K^+$  and  $Na^+$ . Ion channels create voltage differences, which are described by the Nernst potential (Nernst, 1889; Nernst and Riesenfeld, 1902):

$$\Delta V \sim \log \frac{[\text{ion}]_{\text{out}}}{[\text{ion}]_{\text{in}}}, \quad (2.1)$$

where  $[\text{ion}]_{\text{out}}$  denotes the concentration of the ions outside the cell and  $[\text{ion}]_{\text{in}}$  inside the cell.

### 2.1.2 The Hodgkin-Huxley model for action potentials

Perhaps the best-known intrinsic electrical property of neurons is the action potential. The action potential is an all-or-none dynamic electrical event that is caused by voltage dependent ion channels. Real neurons possess several different ion channels working on quite different time scales. However, the underlying biophysical mechanisms are the same for almost all ion currents in biophysical neurons. As conductance based neuron models form the basis of the simplifications introduced in this thesis the Hodgkin-Huxley formalism will be described in detail here. Still today most computational models of neurons are widely influenced by Hodgkin and Huxley's approach to membrane biophysics. Hodgkin and Huxley (1952) showed that action potentials occur due to the voltage dependent gating of  $Na^+$  and  $K^+$  ionic currents. The electrical properties of the membrane are treated as idealized resistive and capacitive elements. This approach leads to the following electrical circuit model for the membrane:

$$C_m \dot{V} = -g_l(V_T - E_l) - I_{Na} - I_K \quad (2.2)$$

The circuit in Fig. 2.1 obeys the equation

$$C_m \frac{dV}{dt} = -g_l(V - E_l) - g_{Na}(V)(V - E_{Na}) - g_K(V)(V - E_K), \quad (2.3)$$

where

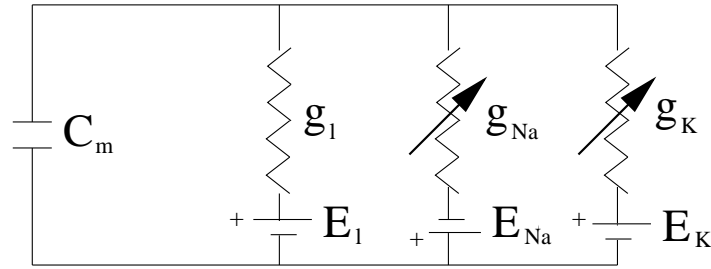


Figure 2.1: Equivalent electrical circuit for an active membrane. While  $g_l$  is a constant  $g_{Na}$  and  $g_K$  are functions of the membrane potential  $V$ .

- $V$  is the membrane potential,
- $C_m$  is the capacity of the membrane,
- $g_l$  is the leakage conductance,
- $E_l$  is the leakage reversal potential,
- $g_i(V)$  are the ionic conductances,
- and  $E_i$  are the reversal potentials,

The conductances  $g_{Na}(V)$  and  $g_K(V)$  depend explicitly on the membrane potential and implicitly on time. Essential for generating an action potential is the activation dynamics of the active currents  $I_{Na}$  and  $I_K$ . Consider the simplest case, a channel that can have two configurations, a closed and an open state, and transitions that obey

$$C \rightleftharpoons O, \quad (2.4)$$

where  $C$  and  $O$  represent the closed and the open state of the channel, with  $\alpha(V)$  as the forward transition rate and  $\beta(V)$  as the backward transition rate. Both  $\alpha(V)$  and  $\beta(V)$  depend on the membrane potential. According to Hodgkin and Huxley (Hodgkin and Huxley, 1952)  $m$  is defined as the fraction of channels in the open state

$$m = \frac{[O]}{[O] + [C]}, \quad (2.5)$$

with Equ. (2.4) one obtains

$$\frac{dm}{dt} = \alpha_m(V)(1 - m) - \beta_m(V)m, \quad (2.6)$$

The ionic current is then

$$I_{ion} = \bar{g}_{ion}m(V)(V - E_{ion}). \quad (2.7)$$

Where  $\bar{g}_{ion}$  is the maximal conductance in the case that every channel is in the open state that means  $m = 1$  and  $E_{ion}$  is the reversal potential, in reality it has to be calculated after the Nernstian relation (2.1) but for simplicity it is assumed to be constant.

With

$$\tau_m(V) = \frac{1}{\alpha_m(V) + \beta_m(V)}, \text{ and } m_\infty(V) = \alpha_m(V)\tau_m(V), \quad (2.8)$$

Equ. (2.6) can be written as

$$\dot{m} = -\frac{1}{\tau_m(V)}(m - m_\infty(V)), \quad (2.9)$$

where  $m_\infty$  is called steady state activation and  $\tau_m$  is the *activation time constant* of the current.

If  $\frac{dV_c}{dt} = 0$  equation 8 reduces to a first order equation with constant coefficients  $\alpha$  and  $\beta$ , with the solution

$$m(t) = m_\infty(V_c) [1 - \exp[-t/\tau_m(V_c)]] \quad (2.10)$$

However, in most cases  $\alpha$  and  $\beta$  cannot be considered as constant coefficients.

### The Hodgkin-Huxley formalism

Hodgkin and Huxley (Hodgkin and Huxley, 1952) described the  $Na^+$  and  $K^+$  currents by assuming that each current was controlled by several independent gates in the single ion channel. The sodium channel possesses three activation gates ( $m$ ) that open with depolarization, and one inactivation gate ( $h$ ) that closes with depolarization. The potassium current needs four activation gates to open.

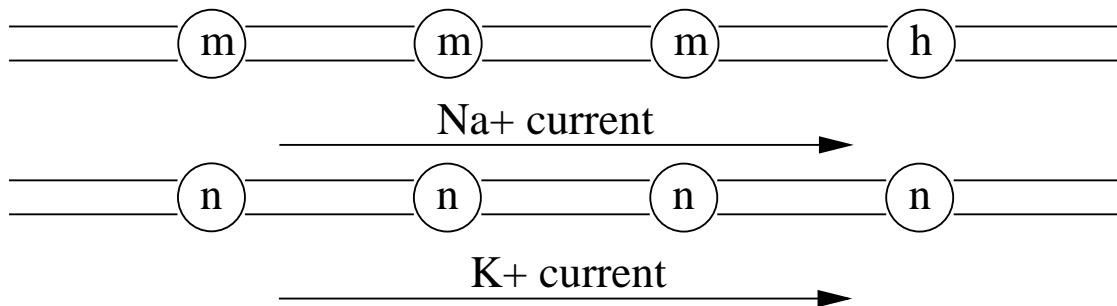


Figure 2.2: Top: The  $Na^+$ -channel with three activating gates  $m$  and one deactivating gate  $h$  in series. Bottom: The  $K^+$ -channel with four serial activating gates  $n$ .

As every single gate follows an independent simple first order open-close dynamic like in

Equ. (2.8) we obtain:

$$\dot{m} = -\frac{1}{\tau_m(V)}(m - m_\infty(V)) \quad (2.11)$$

$$\dot{h} = -\frac{1}{\tau_h(V)}(h - h_\infty(V)) \quad (2.12)$$

$$\dot{n} = -\frac{1}{\tau_n(V)}(n - n_\infty(V)) \quad (2.13)$$

where

$$\tau_x(V) = \frac{1}{\alpha_x(V) + \beta_x(V)} \quad x_\infty(V) = \alpha_x(V)\tau_x(V) \quad (2.14)$$

with  $x \in m, h, n$ . As a reflection of the independence of the single gates Eqs. (2.11-2.13) are not directly coupled but only over  $V$ . The currents are given by:

$$I_{Na} = g_{Na}(t)(V(t) - E_{Na}), \quad (2.15)$$

$$I_K = g_K(t)(V(t) - E_K) \quad (2.16)$$

where  $g_{Na}(t) = \bar{g}_{Na}m(t)^3h(t)$  and  $g_K(t) = \bar{g}_Kn(t)^4$ . The behavior of the cell depends strongly on the rate constants  $\alpha_x(V)$  and  $\beta_x(V)$ . As an example, the rate constants of Hodgkin and Huxley and the constants of Traub and Miles (Traub and Miles, 1991) are given. Although they look quite similar the Hodgkin-Huxley constants lead to a qualitative different behavior than those of Traub and Miles (see 2.2.2).

Table 2.1: With gating variables as used by Hodgkin and Huxley (1952) the resting potential loses its stability by a subcritical Hopf bifurcation (see 2.2.2 )

m	$\alpha_m(V) = -0.1 \frac{(V+40)}{1 - \exp(-\frac{V+40}{4})}$	$\beta_m(V) = 4 \cdot \exp(\frac{V+65}{18})$
h	$\alpha_h(V) = 0.07 \exp(-\frac{V+65}{20})$	$\beta_h(V) = \frac{1}{\exp(-\frac{V+35}{10})+1}$
n	$\alpha_n(V) = 0.01 \frac{(V+55)}{1 - \exp(-\frac{V+55}{10})}$	$\beta_n(V) = 0.125 \exp(-\frac{V+65}{40})$

Table 2.2: With gating variables of Traub and Miles (1991) the resting potential loses its stability by a saddle-node bifurcation (see 2.2.2)

m	$\alpha_m(V) = 0.32 \frac{(V+37)}{1 - \exp(-\frac{V+37}{5})}$	$\beta_m(V) = 0.28 \frac{(V+10)}{\exp(\frac{V+10}{5})-1}$
h	$\alpha_h(V) = 0.128 \exp(-\frac{V+33}{5})$	$\beta_h(V) = \frac{4}{\exp(-\frac{V+10}{5})+1}$
n	$\alpha_n(V) = 0.032 \frac{(V+35)}{1 - \exp(-\frac{V+35}{5})}$	$\beta_n(V) = 0.5 \exp(-\frac{V+40}{5})$

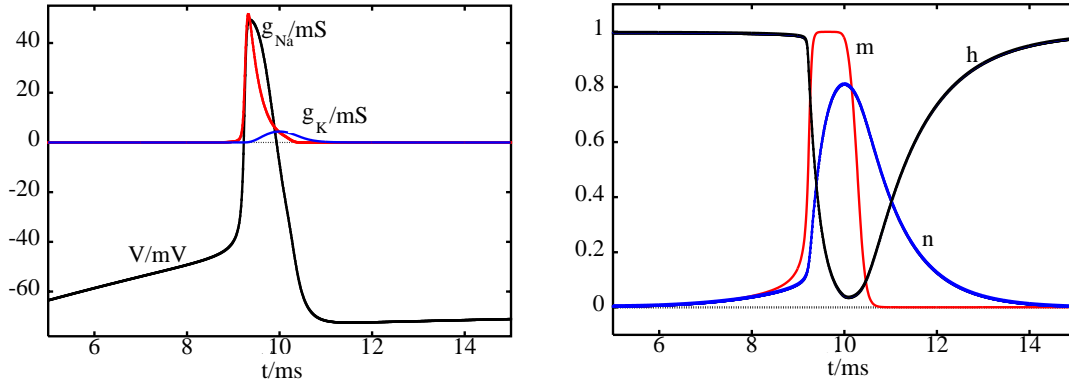


Figure 2.3: **right:**  $V(t)$ ,  $g_{Na}$  and  $g_K$  as functions of  $t$  after a stimulation with a pulse of 5mV amplitude and 5ms duration **left:** The corresponding gating variables  $m$ ,  $h$  and  $n$  as functions of  $t$ .

### Generation of an action potential

To understand the biophysics of action potential generation it is necessary to discuss the Eqs. (2.11-2.13, 2.15,2.16) which display the kinetics of activation and inactivation of the ionic currents.

The steady state activation of the  $Na^+$  current ( $m_\infty$ ) forms a sigmoid shaped curve that increases with voltage, in contrast the steady-state value of the inactivation variable  $h$  decreases with voltage. The action potential occurs due to a multi time scale effect: The kinetics of activation is much faster than that of inactivation ( $\tau_m \ll \tau_h$ ). The reaction of the  $Na^+$  current to an external pulse can be derived from the kinetics of the gating variables: A sufficient strong external pulse leads to an increase of the membrane voltage  $V$ . Initially  $V \approx -65mV$  is at its steady state that means  $m = m_\infty(-65) \approx 0$  and  $h = h_\infty(-65) \approx 1$ . When the voltage increases to  $\approx 0mV$  because of an external stimulus,  $m$  moves to  $m_\infty$  of about one (activation) and simultaneously  $h$  moves to  $h_\infty$  of about zero (inactivation). As  $\tau_m \ll \tau_h$ ,  $m$  quickly reaches  $m_\infty \approx 1$  while  $h$  has not yet decreased to zero (see Fig. 2.3 left). This leads to a sudden increase of the inward Na-conductance ( $\sim m^3h$ ) (Fig. 2.3 right). After a few milliseconds,  $h$  reaches zero and the current decays back to zero. At the same time the outward  $k^+$  current activates and repolarizes the cell (see Fig. 2.3 right) (Matthews, 2001, 2003). As it does not stop abrupt when the steady state voltage is reached, it even hyperpolarizes the cell. This after hyperpolarization is also observed in experiments (Hodgkin and Huxley, 1952; Sah and McLachlan, 1992).



## 2.2 Mathematical tools

As mentioned in 1.1 the nervous system is inherently both highly complex and highly nonlinear. Despite the enormous complexity of the brain, a major goal in neuroscience (and science in general) is to understand the mechanisms underlying the experimental observations. The most powerful analytical tool for understanding and predicting the behavior of complex systems is nonlinear dynamics. In particular, the local bifurcation theory allows to understand the basic dynamics by using canonical models, what is a big help when a rather complex system should be analyzed.

### 2.2.1 Linear stability analysis

Mathematically neuronal systems are described by nonlinear dynamic systems, which can be written as a set of ordinary differential equations

$$\dot{x} = F(x) \quad (2.17)$$

where  $F$  is a nonlinear function of the vector  $x$ . Although it is in general not possible to give a closed solution of the system (2.17), within the framework of nonlinear dynamics the general properties can be discussed. Particularly if  $F(x_0) = 0$   $x_0$  is a fixed point and the system will stay on  $x_0$  forever. However if the system gets disturbed the dynamical evolution depends on the stability of the fixed point. If the fixed point is stable the system is robust against small or even large perturbations, if the fixed point is unstable it will move away from the fixed point. To determine the stability of the fixed point a multivariate Taylor expansion of the right hand side of Equ. (2.17) is made:

$$\begin{aligned} \dot{x} &= F(x_0) + \left. \frac{\partial F}{\partial x} \right|_{x_0} + \dots \\ &= \left. \frac{\partial F}{\partial x} \right|_{x_0} + \dots \end{aligned} \quad (2.18)$$

The partial derivative in Equ. (2.18) is the Jacobian Matrix. By considering small perturbations  $\delta x = x - x_0$  only the first term of the Taylor expansion (2.17) is significant. Therefore, for the temporal evolution of small disturbances of the fixed point, it is sufficient to consider

$$\dot{\delta x} = J_0 \delta x \quad (2.19)$$

where  $J_0$  is the Jacobian evaluated at the fixed point. As the matrix  $J_0$  is just a constant, Equ. (2.19) is a linear differential equation. According to the theory of linear differential equations the solution can be written as a superposition of terms of the form  $e^{\lambda_j t}$  where  $\lambda_j$  is the set of eigenvalues of the Jacobian. In general the eigenvalues of the Jacobian are complex numbers, if  $\mu_j$  and  $\nu_j$  are, respectively the real and imaginary part of the eigenvalue, each exponential term can therefore be written as

$$e^{\lambda_j t} = e^{\mu_j t} e^{\nu_j t} \quad (2.20)$$

Accordingly, the complex part of the eigenvalue only contributes an oscillatory part to the solution. For the stability, the real part matters: If one of  $\mu_j > 0$  even small disturbances will tend to move away from the equilibrium point. A fixed point  $x_0$  is only stable if all real eigenvalues of the Jacobian  $\mu_j$  are negative. It is unstable if at least one  $\mu_j$  is larger than zero. The case that several  $\mu_j$  are zero while the others are negative cannot be treated within linear stability analysis. As the oscillatory subsystems of the simplified models for neural activity used in this thesis are two-dimensional, a short overview of the dynamics in planar systems will be given here

### Linear planar systems

Any two dimensional autonomous linear system can be written in the form

$$\begin{aligned} \dot{x}_1 &= ax_1 + bx_2 \\ \dot{x}_2 &= cx_1 + dx_2 \end{aligned} \tag{2.21}$$

introducing the vector  $x = (x_1, x_2)^T$ , leads to

$$\dot{x} = Ax, \quad A = \begin{bmatrix} a & b \\ c & d \end{bmatrix} \tag{2.22}$$

The ansatz  $x = e^{\lambda t}x_0$  leads to the linear homogeneous equation

$$(A - \lambda I_2)x_0 = 0, \tag{2.23}$$

where  $I_2$  is the  $2 \times 2$  the identity matrix. The system above has only non trivial systems if

$$\det(A - \lambda I_2) = 0, \tag{2.24}$$

what is called characteristic equation. Substituting the components of  $A$  in (2.24) yields

$$\lambda^2 - (a + d)\lambda + (ad - bc) = 0, \tag{2.25}$$

and accordingly

$$\lambda_{\pm} = \frac{1}{2}\{TrA \pm \sqrt{(TrA)^2 - 4detA}\} \tag{2.26}$$

So the behavior of (2.21) can be classified in dependence of  $TrA$  and  $detA$ .

- $\lambda_{\pm}$  are real if  $(TrA)^2 > 4detA$ .
- Real Eigenvalues have the same sign if  $detA > 0$  and are positive if  $TrA > 0$  (negative if  $TrA < 0$ )  $\implies$  stable (unstable) node
- Real Eigenvalues have opposite sign if  $TrA < 0 \implies$  saddle-node
- The Eigenvalues are complex if  $(TrA)^2 < 4detA \implies$  focus

## 2.2.2 Bifurcations of equilibrium points

Neuronal models show a large variety in their dynamical behavior, including resting on equilibrium points, periodic spiking, bursting and chaotic behavior. Neurons change their qualitative behavior in dependence of an applied external current  $I$ , if this current is below a threshold the neuron rests on an equilibrium point, this state is called excitable, if  $I$  exceeds the threshold they fire a periodic spike train. In simplified models, this important feature is modeled by a 2-dimensional system. These two types of dynamics correspond to a stable equilibrium and a limit cycle attractor respectively. The transition between these two qualitative different types of dynamics is called bifurcation. As this transition can be observed by varying only one parameter, i.e.  $I$ , they are called codimension 1 bifurcations. For every local bifurcation a normal form can be defined, that describes the simplest possible system showing such a bifurcation. Here definitions and examples of the codimension 1 bifurcations from an equilibrium point on a limit cycle, which occur in this thesis, are provided. A classification of the equilibrium points being possible in a two Dimensional system was done in 2.2.1.

### The saddle-node bifurcation

A saddle-node bifurcation is a collision and disappearance of two equilibria in a dynamical system. The saddle-node bifurcation can easily be understood by considering the one-dimensional case

$$\dot{x} = f(x, \lambda) \quad (2.27)$$

A one-dimensional dynamic system  $\dot{x} = f(x, \lambda)$  undergoes a saddle-node bifurcation in  $(\bar{x}, \bar{\lambda})$ , if:

- $a(0) = f_{xx}(0, 0) \neq 0$
- $f_{\lambda} \neq 0$

where  $f_{ij\dots}$  is an abbreviation for  $\partial_i \partial_j \dots f$ . In this case, the system is locally topological equivalent to the origin of

$$\dot{y} = \beta + \sigma y^2 \quad (2.28)$$

where  $\sigma = \text{sgn}(a(0))$ . Equ. (2.28) is the normal form of a saddle-node bifurcation. If  $f_{\beta} f_{xx} < 0$ , a pair of a stable and an unstable fixed point exists, for  $\beta > 0$ . For  $f_{\beta} f_{xx} > 0$  the pair exists for  $\beta < 0$ . For  $\beta = 0$  the fixed points coalesce, what is called saddle-node. In higher dimensional systems, things get more complicated. Consider a dynamical system of the form

$$\dot{x} = f(x, \lambda), \quad x \in \mathbb{R}^m, \quad \lambda \in \mathbb{R}^l \quad (2.29)$$

which has an equilibrium point in  $(\bar{x}, \bar{\lambda})$

$$f(\bar{x}, \bar{\lambda}) = 0$$

Equ. (2.29) undergoes a saddle-node bifurcation if it is reducible to the above mentioned normal form (2.28) in a local surrounding of the equilibrium point  $(\bar{x}, \bar{\lambda})$ . This is the case if the Jacobian matrix  $A$  at the saddle-node bifurcation has

- a simple zero eigenvalue  $\mu_1 = 0$ ,
- $n_s$  eigenvalues with  $\text{Re } \mu_j < 0$ , and
- $n_u$  eigenvalues with  $\text{Re } \mu_j > 0$

with  $n_s + n_u + 1 = n$ . According to the center manifold theorem, there is a family of smooth one-dimensional invariant manifolds  $W_\alpha^c$  near the origin. The  $n$ -dimensional system restricted on  $W_\alpha^c$  is one-dimensional. Moreover, the following conditions have to be fulfilled

- The function  $f(x, \bar{\lambda})$  has non vanishing quadratic terms along the eigenvector  $v_1, w_1$  corresponding to  $\mu_1$ , that means

$$w_1(D_x^2 f(\bar{x}, \bar{\lambda}))(v_1, v_1) \neq 0$$

where  $D_x^2 f(\bar{x}, \bar{\lambda})(\cdot, \cdot) : \mathbb{C}^m \times \mathbb{C}^m \rightarrow \mathbb{C}^m$  is a bilinear vector form.

- The  $n$ -dimensional vector

$$w_1 D_\lambda f(\bar{x}, \bar{\lambda}) \neq 0$$

what is called transversality condition.

Under these conditions, the  $n$ -dimensional system is locally topologically equivalent near the origin to the suspension of the normal form by the standard saddle-node bifurcation (2.28), i.e. the  $n$ -dimensional system decouples to

$$\begin{aligned} \dot{y} &= \beta + \sigma y^2, \\ \dot{y}^s &= -y^s, \\ \dot{y}^u &= +y^u, \end{aligned} \tag{2.30}$$

where  $y \in \mathbb{R}$ ,  $y^s \in \mathbb{R}^{n_s}$ ,  $y^u \in \mathbb{R}^{n_u}$ . An example of this formalism applied to a 2d system can be found in (Mayer, 2004).

### Saddle-node on invariant circle bifurcation

As its name indicates the saddle-node on invariant circle bifurcation (often called snic-bifurcation) is a standard saddle-node bifurcation which takes place on an invariant circle. The invariant circle consists of two heteroclinic trajectories connecting the node and the saddle. It is called invariant because any solution starting on the circle stays on the circle. As the saddle and the node coalesce, the short heteroclinic trajectory vanishes and the other one becomes a homoclinic invariant circle. In this case a ,larger' invariant set, a periodic orbit, collides with equilibria. This causes changes in the topology of the trajectories in the

phase space, which cannot be confined to a small neighborhood, as it is the case for local bifurcations. Accordingly, there is no locally topologically equivalent system as for the standard saddle-node bifurcation. The saddle-node on invariant circle is a relative simple example of a global bifurcation. As an example the  $(v, w)$  subsystem of the extended

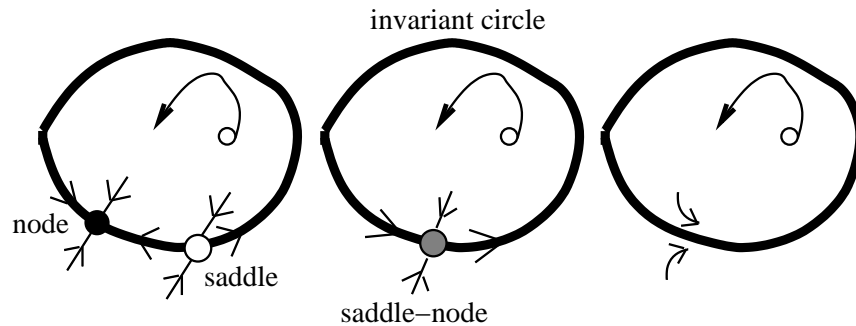


Figure 2.4: Schematic diagram of saddle-node on invariant circle bifurcation.

Hindmarsh-Rose model used in (Mayer *et al.*, 2006) is considered. The conductance based neuron models used in (Mayer *et al.*, 2006) undergo a snic bifurcation too.

$$\begin{aligned}\dot{v}(t) &= w - v^3 + 3v^2 + I \\ \dot{w}(t) &= 1 - 5v^2 - w\end{aligned}\tag{2.31}$$

$$\tag{2.32}$$

The saddle-node bifurcation which results in a stable limit cycle is here shown in a bifurcation diagram, obtained numerical with xpp (Ermentrout, 1999). The inlay in Fig. 2.5 shows the frequency of the oscillation on the limit cycle as a function of the bifurcation parameter  $I$ . For small distances from the critical point, the system fires with arbitrary low frequency. This can be understood by considering the picture in the middle of Fig. 2.4. A homoclinic trajectory originates from the saddle-node and leaves its small neighborhood to wander around the orbit and then reenters the neighborhood and terminates in the saddle-node. This homoclinic orbit is a limit cycle with zero frequency. A mathematical treatment of the frequency dependence near the critical point can be found in (Izhikevich, 2000, 2007) and for time discrete models in (Mayer, 2004).

### The Hopf bifurcation

The other important scenario for a transition from a resting state to an oscillatory state is the Hopf bifurcation. Contrary to the saddle-node bifurcation the resting state does not disappear, rather it loses its stability. The loss of stability of the equilibrium point is accompanied either by the appearance of a stable limit cycle (supercritical Hopf bifurcation) or by the disappearance of an unstable limit cycle (subcritical Hopf bifurcation). The Hopf bifurcation involves a nonhyperbolic fixed point with linearized eigenvalues  $\pm i\omega$  and a two-dimensional center manifold. As done in (Schuster and Just, 2006; Argyris *et al.*, 1994)

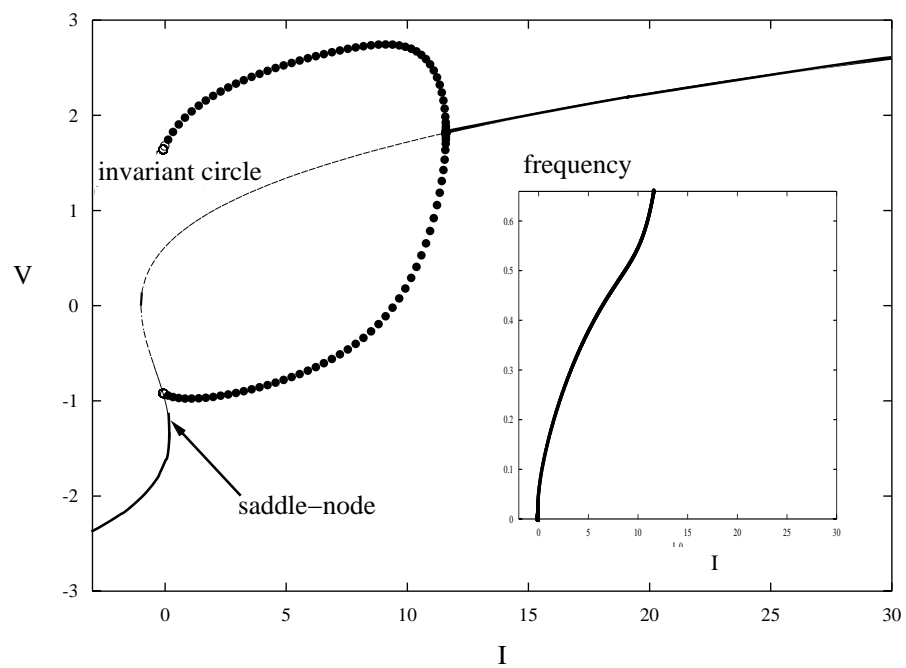


Figure 2.5: Maximum/Minimum bifurcation diagram of  $v$  in system (2.31) as a function of  $I$ . Heavy lines indicate stable fixed points (limit cycles) and thin lines indicate unstable fixed points (limit cycles). The inlay shows the frequency of the oscillation on the limit cycle as a function of the bifurcation parameter  $I$ .

the following normal form is considered.

$$\begin{aligned}\dot{x} &= \mu x - \omega y - (x^2 + y^2)x \\ \dot{y} &= \omega x - \mu y - (x^2 + y^2)y\end{aligned}\tag{2.33}$$

Linearizing around the origin shows that the origin is a stable focus if  $\mu < 0$  and an instable focus if  $\mu > 0$  (since the eigenvalues of the linearized flow are  $\mu \pm i\omega$ ). Hence the origin is non-hyperbolic if  $\mu = 0$  and a bifurcation should occur if  $\mu$  passes the zero. This is easily analyzed in polar coordinates

$$\dot{r} = \mu r - r^3, \quad \dot{\theta} = \omega\tag{2.34}$$

Here the case of a 2-dimensional system is considered

$$\dot{x} = f(x, y, \mu), \quad \dot{y} = g(x, y, \mu)\tag{2.35}$$

where  $f(0, 0, \mu) = g(0, 0, \mu) = 0$ , what can always be reached by a simple coordinate transformation. The following conditions have to be fulfilled:

- The Jacobi Matrix

$$J = \begin{bmatrix} \partial_x f & \partial_y f \\ \partial_x g & \partial_y g \end{bmatrix}$$

has a pair of pure imaginary eigenvalues  $\pm i\omega$  in the origin for  $\mu = 0$ :

$$J = \begin{bmatrix} 0 & -\omega \\ \omega & 0 \end{bmatrix}$$

This is equivalent to

$$\text{Tr}L = \partial_x f + \partial_x g = 0, \quad \det L = \partial_x f \partial_y g - \partial_y f \partial_x g > 0\tag{2.36}$$

- If  $\alpha(\mu) \pm i\omega(\mu)$  are the eigenvalues of  $J(\mu)$  at the fixed point, then

$$\frac{d\alpha(\mu)}{d\mu} \neq 0 \quad (\text{transversality condition})\tag{2.37}$$

or equivalent

$$f_{\mu x} + g_{\mu y} \neq 0 \text{ in } (x, y, \mu) = (0, 0, 0)\tag{2.38}$$

Then a limit cycle bifurcates from the origin, with an amplitude that grows like  $|\mu|^{1/2}$  whereas its period tends to  $2\pi/\omega$ , if  $|\mu| \rightarrow 0$ . the bifurcation is supercritical for  $\sigma < 0$  and subcritical for  $\sigma > 0$  where

$$\begin{aligned}\sigma &= \frac{1}{16}[f_{xxx} + g_{xxy} + f_{xxy} + g_{yyy}] \\ &+ \frac{1}{16\omega}\{f_{xy}(f_{xx} + f_{yy}) - g_{xy}(g_{xx} + g_{yy}) - f_{xx}g_{xx} + f_{yy}g_{yy}\}\end{aligned}\tag{2.39}$$

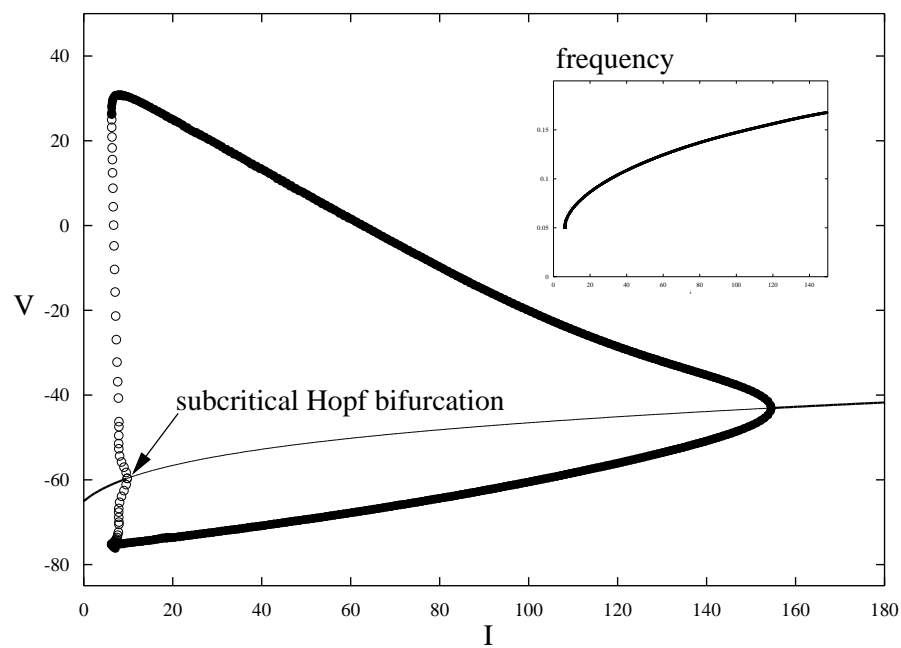


Figure 2.6: Maximum/Minimum bifurcation diagram of  $V$  for the Hodgkin-Huxley model described in 2.1.2 as a function of  $I$ . Heavy lines indicate stable fixed points (limit cycles) and thin lines indicate unstable fixed points (limit cycles). The inlay shows the frequency of the oscillation on the limit cycle as a function of the bifurcation parameter  $I$ .



If the dimension of the system is larger than 2 in the critical point (i.e. when the fixed point loses stability) the Jacobi matrix has exactly one pair of pure imaginary eigenvalues  $\pm i\omega$  while all other eigenvalues have negative real parts. As an example for a subcritical Hopf bifurcation, we consider the Hodgkin-Huxley system in 2.1.2. The inlay in Fig. 2.6 shows that the oscillation starts with non zero frequency, as discussed above. In (Mayer *et al.*, 2006) it is shown that a slowly periodic driving of a subcritical Hopf bifurcation leads to bursting oscillations. Other widely occurring local codimension 1 bifurcations are the

- Transcritical bifurcation
- Pitchfork bifurcation
- Period-doubling (flip) bifurcation

as they do not occur in the systems discussed in this thesis, they are not treated here. For a review, see (Schuster and Just, 2006).

### 2.2.3 Bifurcations of limit cycles

Spindle oscillations and bursts are of particular interest in this thesis. As mentioned before they consist of a subsequent series of alternating oscillatory and silent phases. While in section 2.2.2 scenarios for the emergence of limit cycles have been discussed, scenarios which describe the disappearance of limit cycles have not been discussed yet. In the case that only a fixed point and a limit cycle without hysteresis occur, the bifurcations mentioned above also explain the disappearance of limit cycles.

#### Saddle-node bifurcation of limit cycles

In a saddle-node bifurcation of limit cycles a pair of limit cycles, one stable, the other unstable are involved. This situation occurs in subcritical Hopf bifurcations. Another example are neural systems where a slow variable alternates a fast subsystem between a monostable state where only a fixed point exists and a bistable state where a stable fixed point and a stable limit cycle exist. The two attractive areas are divided by a repulsive area, a separatrix, which consists of an unstable limit cycle. At the transition point from the bistable to the monostable state the unstable limit cycle coalesces with the stable limit cycle and both disappear. This behavior is qualitative equivalent to the saddle-node bifurcation. In several computational models for bursting oscillations the above described scenario takes place (Destexhe and Babloyantz, 1993; Destexhe *et al.*, 1993b; Mayer *et al.*, 2006, 2007). In (Mayer *et al.*, 2007) the dynamics of a thalamic circuit is reduced to the overdamped movement of a particle in a time dependent rotation symmetric double well potential:

$$U(r, t, \varphi) = \frac{1}{2}r^2 - \frac{1}{4}\alpha(t)r^4 + \frac{1}{6}r^6 \quad (2.40)$$

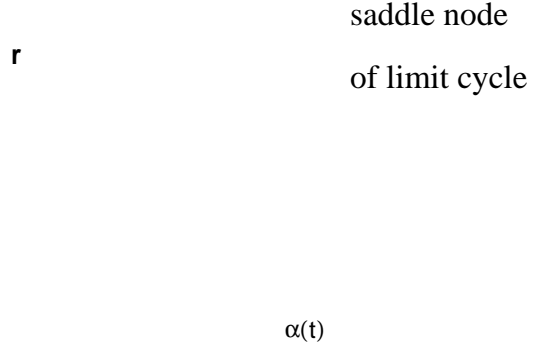


Figure 2.7: Depending on  $\alpha$ , the system (2.41) possesses either one stable fixed point or it shows bistability with a stable fixed point and a stable limit cycle. Left:  $U(r, t)$  for different values of  $\alpha$ . Right: Bifurcation diagram of (2.41) with  $\alpha(t)$  considered as a bifurcation parameter. Solid lines indicate a stable fixed point, open circles an unstable limit cycle and filled circles a stable limit cycle. The limit cycle disappears by a saddle-node of limit cycle bifurcation.

$$\begin{aligned} \frac{dr}{dt} &= -\frac{\partial U(r, \alpha)}{\partial r} \\ \frac{du}{dt} &= 0.01 * (r * (1 - u) - 0.14 * u) \end{aligned} \quad (2.41)$$

where  $\alpha(t)$  is given by  $a(1 - u)$ . (see Fig. 2.7),  $r = \sqrt{x^2 + y^2}$  and  $\varphi(t) = \omega t$  captures the oscillation in phase (mod  $2\pi$ ). A similar model was also used in (Aoyagi, 1995) to model neural oscillators. Several other scenarios can occur and destroy a limit cycle, mostly these scenarios are global bifurcations

- Heteroclinic bifurcation in which a limit cycle collides with two or more saddle-nodes.
- Infinite-period bifurcation in which a stable node and saddle-node simultaneously occur on a limit cycle.
- Blue-sky catastrophe in which a limit cycle collides with a nonhyperbolic cycle.
- Bogdanov-Takens bifurcation, in which a saddle-node bifurcation, a Hopf bifurcation and a homoclinic bifurcation occur nearby. It is a codimension 2 bifurcation.

as they do not appear in the systems considered in this thesis no details will be described here, for details see (Schuster and Just, 2006; Izhikevich, 2007).

### 2.2.4 Singular approximation

Singular approximation is used in nonlinear dynamics to separate fast and slow subsystems (Pontryagin, 1957; Zeeman, 1972). Slow variables can be treated as slowly varying parameters and the rest of the system can be studied as function of these new parameters. This approximation has been successfully applied to uncover the underlying dynamics of several bursting systems (Rinzel, 1987; Destexhe *et al.*, 1993b; Mayer *et al.*, 2006). In neural systems ionic currents work on well-separated timescales, which makes them suitable for singular approximation in a natural way. Singular approximation is often called quasi-adiabatic approximation, as the underlying physical mechanism is the same (Haken, 1983). Another name often used is slaving principle, resembling the fact that the fast subsystem is slaved by the slow parameters. However, in chaotic systems this is not always the case.

### 2.2.5 Noisy dynamical systems

In (Mayer *et al.*, 2006, 2007; Köhler *et al.*, 2008; Mayer and Schuster, 2008) the behavior of dynamical systems driven by stochastic input is discussed. Neural systems are always noisy due to several sources of noise. Each neuron is under the influence of multiple sources of noise e.g. synaptic noise, channel noise and Johnson noise (Gerstner and Kistler, 2002b). Mostly neuronal activity is described by stochastic differential equations with an additive noise in the form of a fluctuating input current.

#### Stochastic differential equations and path integrals

A stochastic differential equation (SDE) is a differential equation in which one or more of the terms are a stochastic process, thus resulting in a solution, which is itself a stochastic process. Typically, SDEs incorporate white noise, which can be thought of as the derivative of Brownian motion (or the Wiener Process); however, it should be mentioned that other types of random fluctuations are possible, such as jump processes e.g. Poisson distributed spike trains. In physics, SDEs are typically written in the Langevin form. In one dimension such a SDE is given by

$$\dot{x} = F(x) + g(x)\xi(t), \quad (2.42)$$

If  $g$  is a constant, the system is said to be subject to additive noise, otherwise it is said to be subject to multiplicative noise. The correct solution can often be found using ordinary calculus. In particular, the ordinary chain rule of calculus can be used. However, in the case of multiplicative noise, the Langevin equation is not a well-defined entity on its own, and it must be specified whether the Langevin equation should be interpreted as an Ito SDE or a Stratonovich SDE. In this thesis, only the case of additive noise is considered. The main method of solution is to find the probability distribution function as a function of time using the equivalent Fokker-Planck equation (FPE). The Fokker-Planck equation is a deterministic partial differential equation. Other techniques include the path integration that draws on the analogy between statistical physics and quantum mechanics or by writing down ordinary differential equations for the statistical moments of

the probability distribution function (Schuster, 2001; Gardiner, 1985). Following (Schuster, 2001) discretization in time is used to consider equations of type (2.42) with  $g(x) = 1$ , i.e. the time derivative is replaced by

$$\dot{x} \rightarrow \frac{x^{t+\tau} - x^t}{\tau} \quad (2.43)$$

and obtain

$$x^{t+\tau} = x^t + \tau [F(x^t) + \xi(t)] \quad (2.44)$$

measuring time in units of  $\tau$  yields the stochastic map

$$x^{t+1} = f(x^t) + \xi(t), \quad (2.45)$$

where  $f(x^t) = x^t + F(x^t)$ . The probability  $P^t(x)$  to find the particle at time  $t$  at site  $x$  is given by the Frobenius Perron equation

$$P^{t+1}(x) = \int dy K(x|y) P^t(y) \quad (2.46)$$

where  $K(x|y)$  is the kernel function, it is given by

$$K(x|y) = \int d\xi \delta[x - f(y) - \xi] p(\xi) = p[x - f(y)] \quad (2.47)$$

for Gaussian noise  $p(\xi) = (2\pi\sigma^2)^{-1/2} e^{-\frac{\xi^2}{2\sigma^2}}$  the kernel  $K(x|y)$  becomes

$$K(x|y) = (2\pi\sigma^2)^{-1/2} \exp\left[-\frac{[x - f(y)]^2}{2\sigma^2}\right] \quad (2.48)$$

$$= \frac{1}{2\pi} \int d\hat{y} \exp\left[-\frac{\sigma^2}{2} \hat{y}^2 + i\hat{y}[x - f(y)]\right] \quad (2.49)$$

iterating (2.50) yields

$$P^{t+1}(y^{t+1}) = \int dy^t K(y^{t+1}|y^t) P^t(y^t) \quad (2.50)$$

$$= \int dy^t \dots \int dy^0 K(y^{t+1}|y^t) \dots K(y^1|y^0) P^0(y^0) \quad (2.51)$$

$$= \int dy^0 K^t(y^{t+1}|y^0) P^0(y^0) \quad (2.52)$$

with (2.51) the kernel  $K^t(y^{t+1}|y^0)$  can be written as a path integral

$$\begin{aligned} K^t(y^{t+1}|y^0) &= \int dy^t \dots \int dy^1 K(y^{t+1}|y^t) \dots K(y^1|y^0) \\ &= \int Dy Dx \exp\left[\sum_{\tau=1}^t \left[-\frac{\sigma^2}{2} \hat{y}^{2\tau} + i\hat{y}^\tau [y^{\tau+1} - f(y^\tau)]\right]\right] \end{aligned} \quad (2.53)$$

where

$$\int Dy Dx \dots = \frac{1}{2\pi} \prod_{\tau=1}^t \int dy^t d\hat{y}^t \dots \quad (2.54)$$

## 2.2.6 Dynamic mean-field equations for spike-timing dependent plasticity

Neural systems, or complex systems in general, can often be described by many interacting units, which individually have the same structure, but obtain stochastic independent input. If these networks are fully connected, their behavior can often be described by dynamic mean-field theories. Path integrals provide a useful tool to study such systems (Sompolinsky, 1981; Sompolinsky and Zippelius, 1981; Molgedey *et al.*, 1992; Schuster, 2001). In (Mayer and Schuster, 2008) a dynamical mean-field equation for a fully connected network of neurons coupled via spike-timing dependent plasticity, is derived. As only the results are presented in (Mayer and Schuster, 2008), the most important steps in the derivation of the dynamical mean-field equation are presented here. The model consists of  $i = 1 \dots N$  neurons whose time dependent activities  $x_i^t$  are updated in parallel according to

$$x_i^t = g(h_i^t) \quad (2.55)$$

$$h_i^{t+1} = \frac{1}{N} \sum_j J_{ij}^t g(h_j^t) + \xi_i^t \quad (2.56)$$

Where  $g = \theta(h_i^t - \vartheta)$  is the Heaviside function and  $\vartheta$  the threshold. The variable  $\xi_i^t$  describes stationary uncorrelated or correlated external Gaussian noise

$$\langle \xi_i^t \xi_j^{t'} \rangle = \sigma^2 A(t, t') \delta_{ij} \quad (2.57)$$

where  $A(t, t') = \exp(-|t - t'|/\tau)$ ,  $\sigma^2$  is the noise intensity,  $\tau$  is the correlation time and the angular brackets denote the average over the noise.  $A(t, t') = \sigma^2 \delta_{tt'} \delta_{ij}$  describes uncorrelated Gaussian noise. Whereas  $\tau > 0$  describes correlated noise.  $J_{ij}^t$  obeys

$$J_{ij}^{t+1} = \lambda J_{ij}^t + (\alpha x_i^{t+1} x_j^t - \beta x_i^t x_j^{t+1}), \quad (2.58)$$

with the decay time

$$\tau_d = 1/|\ln \lambda|. \quad (2.59)$$

$J_{ij}^t$  measures the strength of a synapse that leads from neuron  $j$  to neuron  $i$ . For  $J_{ij}^0 = 0$  we obtain from (2.58)

$$J_{ij}^t = \sum_{\tau=0}^{t-1} \lambda^{t-1-\tau} (\alpha x_i^{\tau+1} x_j^\tau - \beta x_i^\tau x_j^{\tau+1}) \quad (2.60)$$

and from (2.55) and (2.56)

$$h_i^{t+1} = \sum_{\tau=0}^{t-1} \frac{\lambda^{t-1-\tau}}{N} \left( \alpha x_i^{\tau+1} \sum_j x_j^\tau x_j^t - \beta x_i^\tau \sum_j x_j^{\tau+1} x_j^t \right) + \xi_i^t \quad (2.61)$$

Following 2.2.5, from (2.61) the following path integral (2.62) is obtained

$$Z = \int_{-\infty}^{+\infty} \prod_{i,t} \frac{dh_i^t d\hat{h}_i^t}{2\pi} \exp \left\{ - \sum_{i,t,t'} \frac{\sigma^2}{2} \hat{h}_i^t R(t,t') \hat{h}_i^{t'} - \sum_{i,t} i\hat{h}_i^t \right. \\ \left. \times \left[ h_i^{t+1} - \sum_{\tau=0}^{t-1} \frac{\lambda^{t-1-\tau}}{N} \left( \alpha x_i^{\tau+1} \sum_j x_j^\tau x_j^t - \beta x_i^\tau \sum_j x_j^{\tau+1} x_j^t \right) \right] \right\}, \quad (2.62)$$

where  $R(t,t')$  is the inverse of the correlation function (Wio *et al.*, 1989; Colet *et al.*, 1989). In this path integral terms of the form

$$\exp \left( ih_i^t \sum_{\tau=0}^{t-1} \frac{\lambda^{t-1-\tau}}{N} \alpha x_i^{\tau+1} \sum_j x_j^\tau x_j^t \right), \exp \left( ih_i^t \sum_{\tau=0}^{t-1} \frac{\lambda^{t-1-\tau}}{N} \beta x_i^\tau \sum_j x_j^{\tau+1} x_j^t \right) \quad (2.63)$$

occur. These occurring products can be decoupled via two Hubbard-Stratonovich transformations (Stratonovich, 1957; Hubbard, 1959).

$$e^{\frac{ab}{2N}} = \int dQ \int dQ^* \exp \left[ -\frac{N}{2} QQ^* + \frac{1}{2} [Qa + Q^*b] \right] \quad (2.64)$$

The path integral can now be rewritten as

$$Z = \int_{-\infty}^{+\infty} \prod_{i,t,\tau < t} N^2 \frac{dh_i^t d\hat{h}_i^t dQ_1^{t,\tau} dQ_1^{*t,\tau} dQ_2^{t,\tau} dQ_2^{*t,\tau}}{2\pi (2\pi)^2} \exp [-NF(Q_1^{t,\tau}, Q_1^{*t,\tau}, Q_2^{t,\tau}, Q_2^{*t,\tau})] \quad (2.65)$$

where  $F$  is given by

$$F = \sum_{t,\tau < t} (Q_1^{t,\tau} Q_1^{*t,\tau} + Q_2^{t,\tau} Q_2^{*t,\tau}) + \\ \frac{1}{N} \sum_i \ln \int_{-\infty}^{+\infty} \prod_t \frac{dh_i^t d\hat{h}_i^t}{2\pi} \exp \left[ -f_i(Q_1^{t,\tau}, Q_1^{*t,\tau}, Q_2^{t,\tau}, Q_2^{*t,\tau}, h_i^t, \hat{h}_i^t) \right] \quad (2.66)$$

and

$$f_i(Q_1^{t,\tau}, Q_1^{*t,\tau}, Q_2^{t,\tau}, Q_2^{*t,\tau}, h_i^t, \hat{h}_i^t) = \\ \sum_t \left\{ \sum_{t'} -\frac{\sigma^2}{2} (\hat{h}_i^t R(t,t') \hat{h}_i^{t'}) - i\hat{h}_i^t \right. \\ \left. \times \left[ h_i^{t+1} - \sum_{\tau=1}^{t-1} \frac{\lambda^{t-\tau-1}}{N} \left( \alpha Q_1^{*t,\tau} \sum_j x_j^\tau x_j^t + Q_1^{t,\tau} x_i^{\tau+1} - \beta x_i^\tau Q_2^{*t,\tau} \sum_j x_j^{\tau+1} x_j^t - Q_2^{t,\tau} x_i^\tau \right) \right] \right\} \quad (2.67)$$

the integration over  $Q_1^{t,\tau}, Q_1^{*t,\tau}, Q_2^{t,\tau}, Q_2^{*t,\tau}$  can be performed for  $N \gg 1$  by the saddle-point approximation (Schuster, 2001) which leads to

$$Q_1^{t,\tau} = \frac{\alpha}{N} \sum_j \langle x_j^\tau x_j^t \rangle = \alpha C^{t,\tau} \quad (2.68)$$

$$Q_2^{t,\tau} = \frac{\beta}{N} \sum_j \langle x_j^{\tau+1} x_j^t \rangle = \beta C^{t,\tau+1} \quad (2.69)$$

$$Q_1^{*t,\tau} = \frac{1}{N} i \sum_j \langle \hat{h}_i^t x_i^{\tau+1} \rangle = G^{t,\tau+1} \quad (2.70)$$

$$Q_2^{*t,\tau} = \frac{1}{N} i \sum_j \langle \hat{h}_i^t x_i^\tau \rangle = G^{t,\tau} \quad (2.71)$$

here  $\langle \dots \rangle$  denotes the average over the noise,  $C^{t,\tau}$  is the correlation function and  $G^{t,\tau}$  is the responsefunction which describes the reaction of the system at time  $t$  to an external field at time  $\tau$ . Causality requires  $G^{t,\tau} = 0$  for  $\tau \leq t$ , because this is just the condition in the sums over  $\tau$  we can drop the terms  $Q_1^{*t,\tau} = 0$ ,  $Q_2^{*t,\tau} = 0$ . Thus  $Z = \prod_i Z_i^{eff}$ , after dropping  $i$  follows

$$Z^{eff} = \int_{-\infty}^{+\infty} \prod_t \frac{dh^t d\hat{h}^t}{2\pi} \exp[-f\{C^{t,\tau}, h^t, \hat{h}^t\}] \quad (2.72)$$

and  $f$  is the site independent functional

$$f = \sum_t \left\{ \sum_{t'} \frac{\sigma^2}{2} \hat{h}^t R(t, t') \hat{h}^{t'} - i \hat{h}^t \left[ h^{t+1} - \sum_{\tau=1}^{t-1} \lambda^{t-1-\tau} \left( \alpha C^{t,\tau} x^{\tau+1} - \beta C^{t,\tau+1} x^\tau \right) \right] \right\} \quad (2.73)$$

We can translate (2.73) back to an effective single neuron equation for the mean-field which depends only on time

$$h^{t+1} = \sum_{\tau=1}^{t-1} \lambda^{t-1-\tau} \left( \alpha C^{t,\tau} x^{\tau+1} - \beta C^{t,\tau+1} x^\tau \right) + \xi^t \quad (2.74)$$

Equ. (2.74) is a selfconsistence equation for the dynamical evolution of the mean-field.





## 3 Publications

This chapter contains the following Publications

- Jörg Mayer, Heinz Georg Schuster and Jens Christian Claussen, The role of inhibitory feedback for information processing in thalamocortical circuits, *Physical Review E* 73, 031908 (2006).
- Jörg Mayer, Heinz Georg Schuster, Jens Christian Claussen and Matthias Mölle, Corticothalamic projections control synchronization in locally coupled bistable thalamic oscillators *Physical Review Letters* 99, 068102 (2007)
- Jan Köhler, Jörg Mayer, and Heinz Georg Schuster, Excitation of coherent oscillations in a noisy medium, *Physical Review E* 77, 021916 (2008)

and the following submitted manuscript

- Jörg Mayer and Heinz Georg Schuster, Dynamical mean-field equations for a neural network with spike-timing dependent plasticity, submitted to *Physical Review Letters* (2008)

### **3.1 Role of inhibitory feedback for information processing in thalamocortical circuits**

PHYSICAL REVIEW E 73, 031908 (2006)

**Role of inhibitory feedback for information processing in thalamocortical circuits**

Jörg Mayer, Heinz Georg Schuster, and Jens Christian Claussen

*Institut für Theoretische Physik und Astrophysik, Christian-Albrechts Universität, Olshausenstraße 40, 24098 Kiel, Germany*

(Received 19 October 2005; revised manuscript received 21 December 2005; published 13 March 2006)

The information transfer in the thalamus is blocked dynamically during sleep, in conjunction with the occurrence of spindle waves. In order to describe the dynamic mechanisms which control the sensory transfer of information, it is necessary to have a qualitative model for the response properties of thalamic neurons. As the theoretical understanding of the mechanism remains incomplete, we analyze two modeling approaches for a recent experiment by Le Masson *et al.* [Nature (London) **417**, 854 (2002)] on the thalamocortical loop. We use a conductance based model in order to motivate an extension of the Hindmarsh-Rose model, which mimics experimental observations of Le Masson *et al.* Typically, thalamic neurons possess two different firing modes, depending on their membrane potential. At depolarized potentials, the cells fire in a single spike mode and relay synaptic inputs in a one-to-one manner to the cortex. If the cell gets hyperpolarized, *T*-type calcium currents generate burst-mode firing which leads to a decrease in the spike transfer. In thalamocortical circuits, the cell membrane gets hyperpolarized by recurrent inhibitory feedback loops. In the case of reciprocally coupled excitatory and inhibitory neurons, inhibitory feedback leads to metastable self-sustained oscillations, which mask the incoming input, and thereby reduce the information transfer significantly.

DOI: [10.1103/PhysRevE.73.031908](https://doi.org/10.1103/PhysRevE.73.031908)

PACS number(s): 87.19.La, 05.45.-a, 87.19.Nn, 84.35.+i

**I. INTRODUCTION**

Spindle oscillations are waxing and waning waves that originate in the thalamus at the transition to slow wave sleep in mammals [1]. In a pioneering experiment [2], spindle oscillations have been investigated in a hybrid thalamic circuit consisting of a biological thalamocortical (TC) and an artificial reticular (RE) thalamic cell [2]. An artificial cell was necessary to manipulate selectively the synaptic connection of the inhibitory feedback from the RE to the TC cell (Fig. 1). Spindle oscillations depended critically on the presence of the synaptic connections between TC and RE cells [3,4]. Further, the occurrence of spindle oscillations comes along with a significant decorrelation between input and the output of the TC cells. Clarification of the relationship between the occurrence of spindle oscillations and the decrease in information transmission could help to gain more insight into the mechanisms which deprive the sensory information from the consciousness while mammals are sleeping.

Spindle, or bursting, oscillations in excitable media are widespread observed in a variety of physical [5], chemical [6], and biological [7] oscillators. Typically, the potential of a bursting neural cell undergoes subsequent shifting between active and silent phases. In the active phase, the membrane potential oscillates quickly, and in the silent phase, it evolves slowly without or only with subthreshold oscillations [8]. In this work, we focus on bursting or spindle oscillations in neural systems, and investigate their role for information transfer through the thalamus. The thalamus, our major gateway for all sensory information, relays the incoming information depending on the state of arousal [9,10]. To process and relay information [11] is a generally important, but not equally well understood, feature of neural systems; here we contribute to the understanding of the underlying dynamics of a key mechanism in the thalamocortical loop.

The paper is organized as follows. In Sec. II, we use biophysical models of TC and RE neurons interconnected with

realistic model synapses as introduced in [3] and also used in the hybrid network investigated by Le Masson in [2]. In Sec. III, we establish an extension of the Hindmarsh-Rose model [12]. For this purpose, we use dynamically coupled Hindmarsh-Rose neurons to reproduce the experimental results of [2]. We show that the Hindmarsh-Rose system has to be extended by a fourth variable working on a very slow time scale, in order to describe the experimental results.

For both models, we investigate the influence of the inhibitory synaptic connection on the information transfer of the TC cell and compare the results with the experiment of Le Masson *et al.* [2]. An additional goal is to answer the question whether the complicated biophysical conductance-based model can be replaced by the much simpler Hindmarsh-Rose model without loss of the most important dynamical features. We show how to achieve this by introducing an extended Hindmarsh-Rose model with an additional degree of freedom. Some important features are better reproduced by the extended Hindmarsh-Rose neuron than by the biophysical model. Our model is by far less computationally costly, yet simple enough to understand dynamical mechanisms.

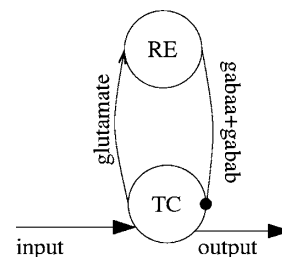


FIG. 1. Structure of synaptic connections in a pair of reciprocally coupled RE-TC cells.

MAYER, SCHUSTER, AND CLAUSSEN

PHYSICAL REVIEW E 73, 031908 (2006)

## II. INFORMATION TRANSFER IN A BIOPHYSICAL MODEL OF A THALAMOCORTICAL OSCILLATOR

A common approach to model the thalamocortical system are conductance-based models [13–16]. Descriptions of the properties of single neural cells can be found for example in [3,4]. The case of two interconnected cells without external forcing has been investigated in [4]. To our knowledge the case of two interconnected cells as shown in Fig. 1 which get excited by an unregularly distributed realistic synaptic bombardment as used in the experiment of Le Masson *et al.* [2] has not been studied in detail upto now. In this section we will investigate the influence of the inhibitory synaptic connection on the information transfer of the TC cell for this case. Destexhe *et al.* [4] model the TC cell and the RE thalamic cell by using a conductance-based single compartment model. The time evolution of the membrane potentials is governed by the following cable equations:

$$C_m \dot{V}_T = -I_{T_L} - I_T - I_h - I_{T_{Na}} - I_{T_K} - I_{GABA_a} - I_{GABA_b}, \quad (1)$$

$$C_m \dot{V}_R = -I_{R_L} - I_{T_s} - I_{K[Ca]} - I_{CAN} - I_{R_{Na}} - I_{R_K} - I_{GLU}, \quad (2)$$

where  $V_T$  is the membrane potential of the TC cell;  $C_m$  is the capacity of the membrane. According to [4], we included the following ion currents: The leakage current  $I_{T_L}$  and  $I_{R_L}$ , the low-threshold  $Ca^{2+}$  currents  $I_T$  and  $I_{T_s}$ , the hyperpolarization activated current  $I_h$ , the  $Ca^{2+}$ -activated currents  $I_{K[Ca]}$  and  $I_{CAN}$ , and, like in the Traub and Miles [17] model, the fast  $Na^+$  and  $K^+$  currents  $I_{T/R_{Na}}$  and  $I_{T/R_K}$ , which are responsible for the generation of action potentials. The synaptic currents  $I_{GABA_a}$  and  $I_{GABA_b}$  represent the  $GABA_a$  and  $GABA_b$  receptors in the synapses from RE to TC cells, while  $I_{GLU}$  describes the excitatory synapse from the TC to RE cells.

Destexhe *et al.* [4] refer to several sources for the description of the ion currents. The kinetic equations of the TC cell have been described in detail in [15]. The  $I_T$  kinetics was taken from Wang *et al.* [18].  $I_h$  was described by the model of Destexhe *et al.* [15], which incorporates a regulation by intracellular calcium. For the RE cell  $I_{T_s}$  was taken from Huguenard and Prince [19]. The kinetics of the  $Ca^{2+}$ -dependent currents  $I_{K[Ca]}$  and  $I_{CAN}$  are adjusted to the clamp data of RE neurons [20]. For both cells,  $I_{Na}$  and  $I_K$  were taken from [17]. The calcium dynamics in both cells are described by a simple model which was introduced in [15]. All details are described in Appendix A.

In biology, the typical input signal for the TC cells is a spike train with unregularly distributed interspike intervals, which can be modeled by a Poisson process with a refractory period. For example, the retinal cells fire such unregularly distributed spikes in darkness or under constant illumination. The refractory period is necessary because every biological cell needs some time  $\tau_r$  to recover after it has fired a spike, so the cell cannot fire spikes with arbitrary low interspike intervals (ISIs). In our model, the ISI are distributed according to the following distribution:

$$\tilde{f}(\tau) = \begin{cases} 0 & \text{for } \tau < \tau_r \\ \bar{r} e^{\bar{r}\tau_r} e^{-\bar{r}\tau} & \text{for } \tau \geq \tau_r, \end{cases} \quad (3)$$

where  $e^{\bar{r}\tau_r}$  is a scaling factor,  $\bar{r}=1/100$  and  $\tau_r=30$  ms here. If we stimulate our model by such a modified Poisson process, we have a computational model for the experiment of Le Masson *et al.* [2], which allows us to compare our computational model with the experiment.

### A. Simulation results of the biophysical model: Spindle oscillations, waxing and waning, and influence on information transfer

With the TC and RE cells interconnected, the computational thalamic circuit receiving this realistic synaptic bombardment [2] showed waxing and waning oscillations. These spindle sequences consisted of bursts of 8–10 Hz oscillations lasting a few seconds, and were separated by silent phases of around 8–10 s. The periodical occurrence of this oscillations is very similar to biological spindle waves which occur in sleep-related states. As in the experiment, each spindling state is terminated by an after-depolarization of the membrane potential. The reason for this effect is the hyperpolarization activated current  $I_h$  (see Appendix A); when this after-depolarization adds to the synaptic bombardment, it forms a depolarization which deactivates the low threshold  $Ca^{2+}$  current  $I_T$  and subsequently blocks the input signal transfer.

### B. Measuring the information transfer

During the spindling state, the firing pattern of the TC cells (excitor), which is very different from the input [see Figs. 2(a) and 2(b)], shows that obviously the information transfer of the input is low. Le Masson *et al.* [2] answer the question whether this low transfer is still reliable, by calculating two different indices. First, the contribution index ( $T_{CI}$ ) examines the TC cell discharge and quantifies the percentage of output spikes  $N_{out}$  which are precisely correlated with retinal input spikes. It estimates the reliability with which a TC spike can be considered as being triggered by an input spike rather than being spontaneous. It is computed as the peak of the cross correlation, normalized by the number of output spikes. Second, the correlation index ( $T_{CC}$ ) measures the global efficiency of the input-output spike transfer and indicates the ratio of input spikes being actually transmitted as output spikes in the TC neuron. It is computed as the peak of the cross correlation between retinal and TC neuron spikes, normalized by the number of retinal cell spikes. To be able to compare our numerical results with the experimental results of Le Masson *et al.* [2] quantitatively, we will use exactly these measures here.

To be able to compare the numerical results obtained from the biophysical model with the simplified model introduced in this paper, we will define two new measures for the information transfer which are equivalent to the measures used by Le Masson *et al.* in [2], but do not depend on the detailed form of the signals. First, the signal-to-noise ratio ( $T_{SN}$ ) examines the amplitude of the TC-cell signals and quantifies

ROLE OF INHIBITORY FEEDBACK FOR INFORMATION

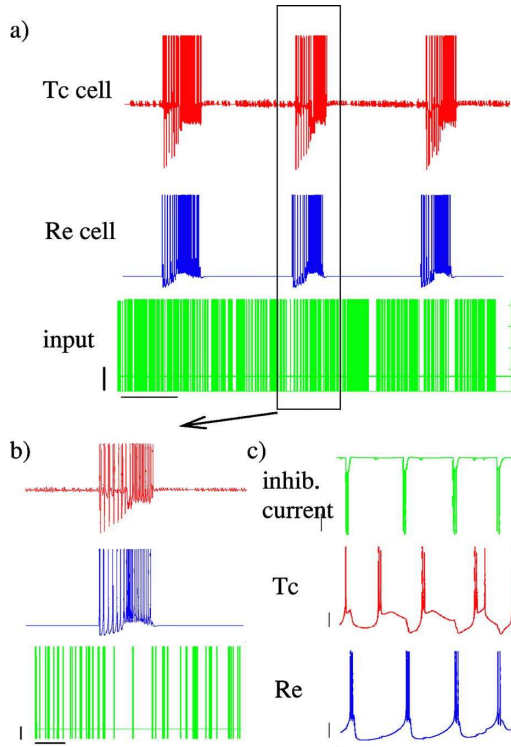


FIG. 2. (Color online) (a) Spontaneous spindle activity in the computational thalamic circuit. The TC cell receives artificial synaptic retinal bombardment, modeled by a Poisson-distributed spike train. The RE-TC oscillator shows spindle activity. (b) Detail of (a). (c) Total synaptic current injected into the biological TC cell and simultaneous voltage of the TC and RE cell. Bottom: The hyperpolarization of the TC cell activates the  $I_T$  current, what initiates a post-inhibitory rebound burst (see also Fig. 5). Calibration bars: 10 s, 20 mV (a); 1 s, 20 mV (b); 10 ms, 6 nA, 20 mV, 1 nA (c).

the percentage  $N_{tr}$  of output spikes  $N_{out}$  which are exactly triggered by an input spike; such it is a measure equivalent to the  $T_{CI}$  used. An output spike is considered to be triggered by an input spike if it occurs within a delay of  $<50$  ms after an input spike. As the  $T_{CC}$ , it is a measure for the reliability with which an output spike can be considered as being triggered by an input spike rather than being due to the intrinsic dynamic of the circuit

$$T_{SN} = \frac{N_{tr}}{N_{out}}. \quad (4)$$

Second, the transfer efficiency  $T_{TE}$  measures the global efficiency in the input-output spike transfer, and indicates the ratio of input spikes being actually transmitted as output spikes, obviously it is equivalent to the measure  $T_{CC}$ . It is computed by the number of triggered spikes  $N_{tr}$  divided by the total number of input spikes

$$T_{TE} = \frac{N_{tr}}{N_{in}}. \quad (5)$$

PHYSICAL REVIEW E 73, 031908 (2006)

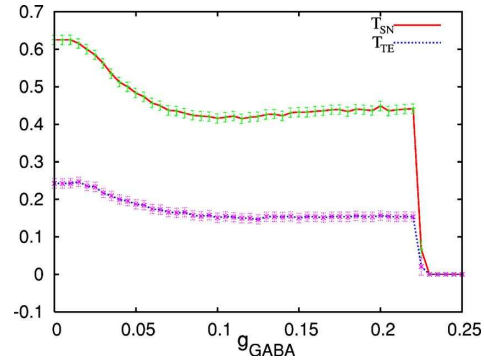


FIG. 3. (Color online) Percentage of output spikes triggered by an input spike ( $T_{SN}$ ) (solid) and transfer efficiency  $T_{TE}$  (dashed) for different values of the inhibitory feedback. Both indices show no significant change when the inhibitory feedback is varied within the stability borders.

The difference between the measures ( $T_{SN}$ ) and ( $T_{CI}$ ) is that our measure checks if an output spike occurs within a certain delay after an input spike, while the contribution index counts the spikes at a fixed time delay defined by the maximum of the cross correlation. The  $T_{CC}$  and  $T_{TE}$  differ in the same way as mentioned above, further  $T_{TE}$  only takes values between zero and one. As our measures only count the spikes, and such treat spikes like binary events, they can be used for any spiking system and allow a comparison of the transmission properties of different models. The disadvantage is that they do not shed light on the amplified details of a signal system such as  $T_{CI}$  and  $T_{CC}$  do.

These two measures, the transfer efficiency and the transfer reliability, are necessary to characterize the information transfer appropriately. The usage of two different transfer measures allows us to answer the question whether the transfer gets blocked or if incoming signals get masked by autonomous oscillations of the system. The results are given in Fig. 3.

In the presence of strong inhibitory feedback ( $g_{GABA_a} = 0.1$  mS and  $g_{GABA_b} = 0.01$  mS) the ( $T_{CI}$ ) and ( $T_{SN}$ ) were low ( $\approx 0.4$ ), indicating that less than half of the output spikes were triggered by an input spike; thus the thalamus is not transferring spikes in a one-to-one manner. To answer the question whether the degree of inhibition produced by the RE neurons could directly control the precision of spike transfer, we varied the strength of inhibition. Our simulations show that the influence of the inhibitory feedback is by far not so strong as in the experiment [2]. In our computational model, the  $T_{SN}$  varied only between  $\approx 0.6$  and  $\approx 0.4$ . In agreement with the experimental data [2], the global efficiency of spike transfer  $T_{TE}$  was not significantly different in the absence or presence of inhibitory feedback.

### C. Discussion of the biophysical model

Altogether, our simulation cannot reproduce the transmission behavior of the thalamic circuit observed [2] experimentally. When we compare the numerical achieved values for

MAYER, SCHUSTER, AND CLAUSSEN

PHYSICAL REVIEW E 73, 031908 (2006)

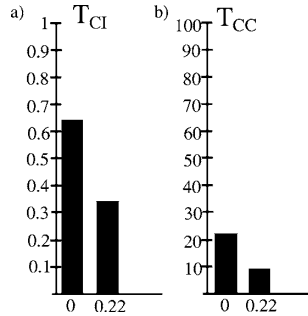


FIG. 4. Averaged contribution ( $T_{CI}$ ) (a) and correlation ( $T_{CC}$ ) (b) indices versus synaptic strength.

the  $T_{CI}$  and  $T_{CC}$  (Fig. 4) quantitatively with the values from the experiment, we find that the effect of input-output spike decorrelation is present, but lacks some features. First, even without or very low inhibitory feedback, the  $T_{CC}$  is not more than  $\approx 25$ ; in the experiment the  $T_{CC}$  varied in a range from about 85–45 (see Fig. 3(e) in [2]). For a biological system this would mean that the animal would always be drowsy. Second, the system does not allow precise up and down regulation of the signal reliability in a wide range, the  $T_{CI}$  only varies in range from around 0.7–0.35, that is about a factor 2, while in the experiment the  $T_{CI}$  varies from about 0.8–0.2 (see Fig. 3(d) in [2]) which corresponds to a factor 4. Further, spindle oscillations occurred even with very little or no inhibitory feedback, which is also in contrast to the experimental results.

At this point it appears questionable whether the detailed biophysical model described above—with its high dimensionality and parameter space quite too detailed to gain systematic understanding—provides the appropriate level of description to analyze coupled systems, e.g., of the thalamocortical loop investigated here. We will however use

the biophysical model to establish our simplified model. As the biophysical model incorporates many features of realistic biological neurons, it allows us to identify the key elements which may be responsible for sleep spindle oscillations. The slow repetition rate of spindling (0.3–0.1 Hz) is due to intrinsic mechanisms of the TC cell. The slow variables  $F_2$  and  $S_2$  (Fig. 11) of the  $I_h$  current (see Sec. III D and Appendix A) play the key role for these long silent phases. The spindling starts in the TC cell due to the hyperpolarization low threshold  $Ca^{2+}$  current  $I_T$  [see Figs. 2(c) and 5]. The spindling terminates due to the activation of the  $Ca^{2+}$  activated current  $I_H$  (see Fig. 5). The frequency of the spindling is determined by intrinsic properties of the RE cell, as shown by Destexhe in [4], but also the intrinsic properties of the inhibitory synapses play a role. To provide an overview, Fig. 5 shows a schematic diagram of the mechanisms leading to spindle oscillations.

Unfortunately, due to the complexity of the high-dimensional biophysical system, the connection between biophysics and dynamics is hard to unravel. Further, the computational effort is very high, making studies of networks almost impossible. To solve these problems, we propose a reduced model to reproduce the experimental data of Le Masson *et al.* by using the simpler Hindmarsh-Rose [12] type neurons, and modify them in a way that the features described above are reproduced.

### III. THE REDUCED SYSTEM: AN EXTENDED HINDMARSH-ROSE MODEL

#### A. The Hindmarsh-Rose model

The Hindmarsh-Rose equations are a simple polynomial model of bursting in thalamic cells, which reproduce several features, like for example rebound bursts, of more complicated biophysical models [3,21,22]. The original Hindmarsh-Rose equations are given by

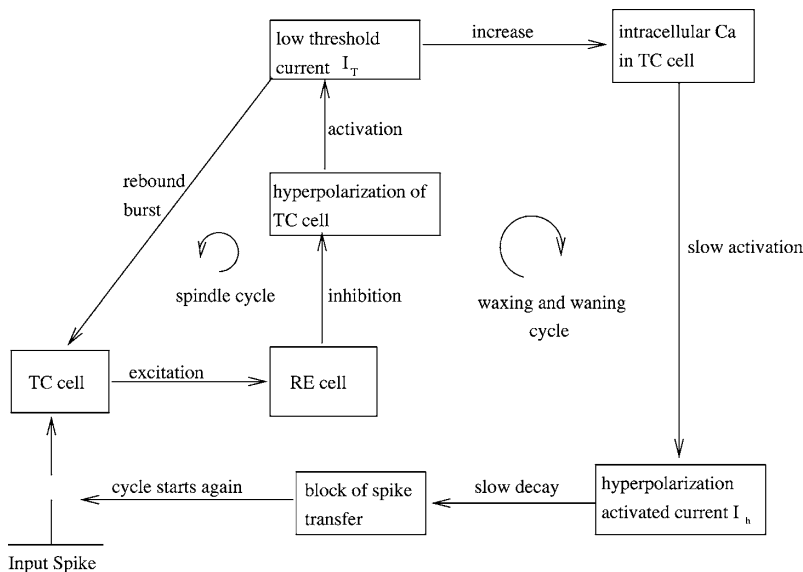


FIG. 5. Schematic diagram illustrating the generation mechanism of spindle oscillations. We distinguish two cycles: First, the spindle cycle is responsible for the spiking; the system runs several time through it before the waxing and waning cycle is activated, leading to bursts of oscillations. The slowly decaying current  $I_h$  leads to the long silent epochs during which spike transfer is blocked. Altogether, the interplay of the currents  $I_T$  and  $I_h$  plays an important role for the genesis of spindle oscillations. (See also Figs. 2 and 3.)

ROLE OF INHIBITORY FEEDBACK FOR INFORMATION

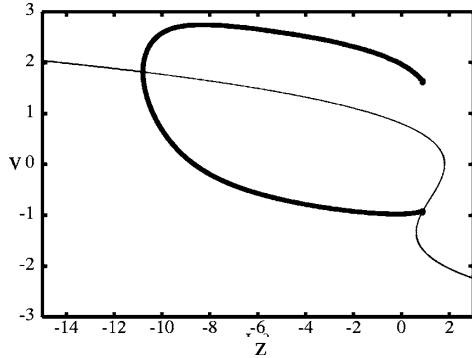


FIG. 6. Maximum and or minimum bifurcation diagram of  $v$  in the fast subsystem (4) as a function of  $z$ . Heavy lines indicate stable fixed points (limit cycles) and thin lines indicate unstable fixed points (limit cycles). (See Appendix B 3.)

$$\dot{v} = w - v^3 + 3v^2 - z + I(t), \quad (6)$$

$$\dot{w} = 1.8 - 5v^2 - w, \quad (7)$$

$$\dot{z} = \epsilon[3.3(v + 1.56) - z], \quad (8)$$

where  $v$  is the voltage,  $w$  is a recovery variable,  $I(t)$  is an external forcing, and  $z$  is a slow variable. In order to understand the behavior of Eqs. (6)–(8), we first consider the limit  $\epsilon \rightarrow 0$ , so  $z(t) = z$ , which results in a planar reaction-diffusion system. This fast subsystem is responsible for the spiking dynamics of the Hindmarsh-Rose system. The dynamics of this subsystem is also crucial for  $\epsilon \neq 0$ . This procedure is called singular approximation, or slaving principle, and is widely used to separate fast and slow subsystems [23–25]. Slow variables (here  $z$ ) can be treated as slowly varying parameters and the rest of the system can be studied as a function of these new parameters. We apply this method to the Hindmarsh-Rose model.

To understand the influence of the variable  $z$  on the  $(v, w)$  subsystem, Eqs. (6) and (7) with  $I(t) = 0$  are transformed to a Lienard system [7,26], yielding (Appendix B 2)

$$0 = \ddot{v} + f(v)\dot{v} + g(v), \quad (9)$$

where  $g(v) = v^3 + 2v^2 - 1$  can be considered as the gradient of a potential  $\Phi(v, z)$ , and  $f(v) = 1 - 6v + 3v^2$  as a damping term. The roots of  $g(v, z)$  give the fixed points of the equation. Depending on the parameter  $z$ , there exist either one or three real roots.

The bifurcation diagram of Eqs. (6) and (7) as a function of  $z$  is shown in Fig. 6 (the bifurcation diagram was computed with the auto interface [27] of xpp [28]). If we start with  $z = 2$  from the fixed point ( $v = -2.05, w = -19.67$ ) of the fast subsystem and go to the left in the bifurcation diagram, the stable fixed point loses its stability by a saddle node bifurcation at  $z \approx 0.6148$ . For values of  $z$  between  $[0.6148, 0.8891]$ , a stable limit cycle and a stable fixed point coexist. At  $z = -10.4$ , the upper branch of the steady state

PHYSICAL REVIEW E 73, 031908 (2006)

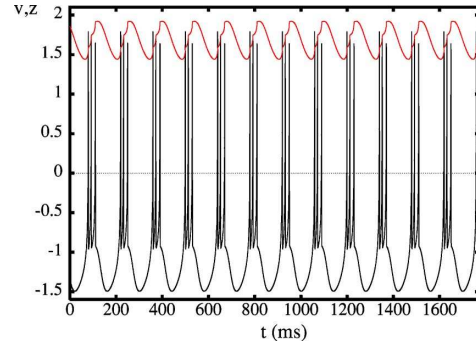


FIG. 7. (Color online)  $v(t)$  (black) and  $z(t)$  (red, upper curve) with  $I = 1.0$ . When  $z(t)$  is periodic,  $v(t)$  oscillates with the same period; thus the slow variable  $z(t)$  slaves  $v(t)$ .

loses stability by a Hopf bifurcation (for further details see [7,29]). Here we will only focus on values of  $z$  between  $[-5, +5]$ .

### B. Periodic forcing of the Hindmarsh-Rose neuron

Another important case is that of  $z$  being a periodic function  $p(t)$ ; this is the case for certain values of a constant external forcing  $I$  [29], or when the neuron is coupled to another periodic spiking or bursting neuron. So in a next step we consider the fast  $(v, w)$  subsystem with periodic forcing

$$\dot{v}(t) = w - v^3 + 3v^2 + p(t),$$

$$\dot{w}(t) = 1.8 - 5v^2 - w, \quad (10)$$

or, in Lienard form

$$p(t) = \ddot{v} + f(v)\dot{v} + g(v), \quad (11)$$

where  $f$  and  $g$  are defined as above. According to [30], theorem 4.3.1 and 4.3.3, Eq. (11) has a nonconstant periodic solution with the same period as the forcing term  $p(t)$  if several conditions (i–vi) (given in Appendix B 4) are fulfilled. Hence, we make the following proposition: When  $p(t)$  is a  $T$ -periodic function, then (11) has a periodic solution with the same period  $T$ . The detailed proof is in Appendix B 4.

For illustration, we show the behavior of the Hindmarsh-Rose Eqs. (6)–(8) excited with a constant forcing  $I(t) = I_0$  (see Fig. 7), thus again  $z(t)$  is a periodic function. This is an example for a typical intrinsic burster, where the slow variable slaves the fast subsystem [27]. The theorem presented above proves that the fast  $(v, w)$  subsystem of the Hindmarsh-Rose model shows mode locking when it is driven by a periodic forcing, no matter what frequency or amplitude this forcing has.

If we assume  $\epsilon$  to be small ( $\approx 0.006$  as used by [31]),  $z$  can be treated like a slowly varying parameter in the  $(v, w)$  system (10). To understand the influence of  $v$  on Eq. (8), we write it in the form of a relaxation process

MAYER, SCHUSTER, AND CLAUSSEN

PHYSICAL REVIEW E 73, 031908 (2006)

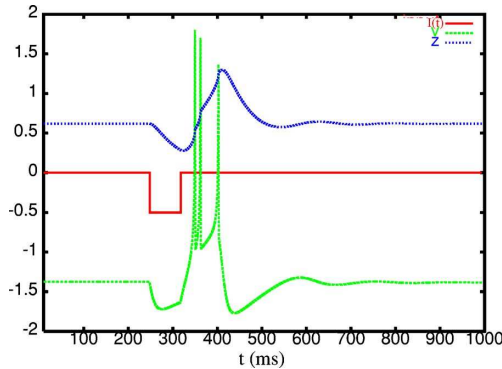


FIG. 8. (Color online)  $v(t)$ ,  $z(t)$ , and  $I(t)$ . The system shows a post-inhibitory rebound burst after a hyperpolarizing step of  $I(t)=-0.5$  and a duration of 70 ms.

$$\dot{z} = -\epsilon[z - z_\infty(v)], \quad (12)$$

where  $z_\infty(v)=3.3(v+1.56)$ . As  $\epsilon$  is very small, the fast dynamics of  $v$  has only little influence on Eq. (12), as its own dynamics is too slow to follow the fast  $z_\infty(v)$ . Because of this,  $z$  will arrive in a steady state if  $v$  is spiking quickly, and then just oscillate with a very little amplitude around it. This effect leads to the so-called spike frequency adaption (for details see [12]), which is also observed in biological neurons [22]. For small enough values of  $I(t)$  this effect can also lead to an effect similar to intrinsic bursting [29].

### C. Post-inhibitory rebound bursts in the Hindmarsh-Rose neuron

Post-inhibitory rebound bursts are a dynamical feature being also present in the biophysical neuron model [3]. As it is crucial for spindle oscillations and for the information transfer, we will describe it in detail here, see also Fig. 8. If the Hindmarsh-Rose model [12] is hyperpolarized for a period similar to the burst duration, the adaption current  $z$  will de-

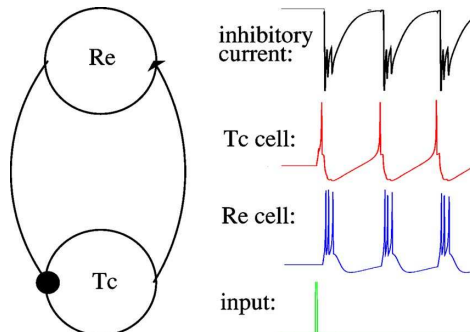


FIG. 9. (Color online) Right: Reciprocally coupled RE and TC cell. Left: If the excitor cell gets activated by an external pulse, it excites the inhibitor cell, which leads to an inhibitory current. This current hyperpolarizes the excitor cell and evokes a rebound burst in it, and the mechanism repeats, which leads to self-sustained oscillations.

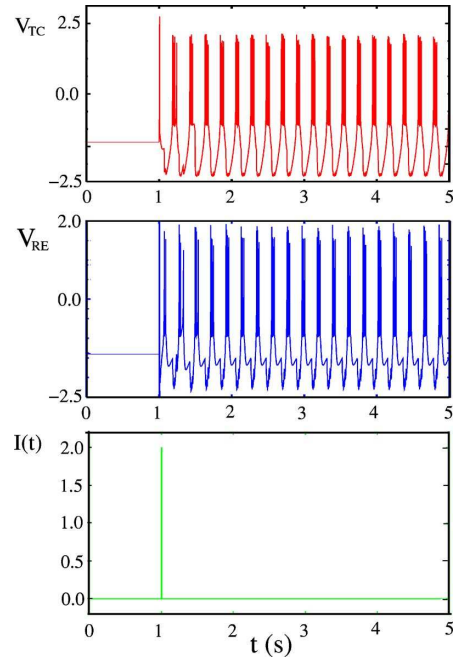


FIG. 10. (Color online) Reciprocally coupled inhibitor and excitor; without the  $h$  current, the oscillation does not terminate.

crease below its steady state. If the hyperpolarizing current is released, the  $z$  current stays below its steady state for some time due to its slow timescale. As a consequence, the model behaves as if some extra current had been applied, so it will cross the saddle node bifurcation in Fig. 6 and stay on the limit cycle. Due to the spikes,  $z$  will increase above its steady state, stopping the burst (see Figs. 8 and 9). Due to the slow time scale, a post-inhibitory rebound burst will only appear if slowly decaying dynamic synapses are used, as otherwise  $z$  will not decrease below its steady state. In the biophysical model, the same effect occurs due to the low threshold calcium current  $I_T$  [see Fig. 2(c)] [3], so the variable  $z$  can be interpreted as a calcium current.

In reciprocally coupled neurons, the effect described above leads to self-sustained oscillations if the excitor gets activated by a single input spike; this effect is an example for so-called hard-excited self-oscillations [25]. During this oscillation, the two neurons exhibit antiphase synchronization. We show this for the case of two Hindmarsh-Rose neurons, which are coupled like in a typical thalamocortical circuit (see Fig. 9).

### D. Motivation of a simplified calcium current: Extending the Hindmarsh-Rose model

The self-sustained oscillations in Fig. 10 are stable and do not terminate; this is contrary to the experimental observations of Le Masson *et al.* [2]. A spindle oscillation or a burst consists of a series of metastable self-oscillations enhanced by rebound bursts which terminate after a few seconds. Above we argued that the slow variable  $z$  can be inter-



ROLE OF INHIBITORY FEEDBACK FOR INFORMATION

preted as a calcium current, and such corresponds to the low threshold calcium current  $I_T$  in the biophysical model. The schematic diagram in Fig. 5 shows that the reason for the termination of the oscillation is a further ion current  $I_h$  [2–4,32]. As the original Hindmarsh-Rose model does not incorporate a variable which corresponds to the  $I_h$  current in the biophysical model, we will extend the Hindmarsh-Rose model by an equation motivated directly by the dynamics of  $I_h$  in the biophysical model. Destexhe *et al.* [4] model  $I_h$  by a double activation kinetic, consisting of slow and fast activation variables, regulated by intracellular  $\text{Ca}^{2+}$

$$S_0 \rightleftharpoons S_1, \quad (13)$$

$$F_0 \rightleftharpoons F_1, \quad (14)$$

were  $S_{0/1}$  and  $F_{0/1}$  represent the closed and open states of the slow and fast activation gates, respectively. The open state gates are assumed to have  $n$  bindings for  $\text{Ca}^{2+}$  which lead to the open bounded gates  $S_2$  and  $F_2$ ,

$$S_1 + n\text{Ca}^{2+} \rightleftharpoons S_2, \quad (15)$$

$$F_1 + n\text{Ca}^{2+} \rightleftharpoons F_2. \quad (16)$$

In this model the activation function of  $I_h$  is shifted during the oscillatory phase by the entry of  $\text{Ca}^{2+}$ , and thus terminates the oscillation. Destexhe *et al.* [4] find that the length of the silent phase and of the oscillatory phase were directly proportional to the time constant of intracellular  $\text{Ca}^{2+}$  binding to  $I_h$  channels,  $k_2^{-1}$ . Further it is assumed that the binding of  $\text{Ca}^{2+}$  is critical for the onset and termination of the oscillatory phase [4]. So the length of the oscillatory phase depends on the rate of rise of the variables  $S_2$  and  $F_2$ , while the length of the silent phase depends on the rate of relaxation of  $S_2$  and  $F_2$  back to their resting values (see Fig. 11 and [4]). According to (A20), both the length of rising and relaxation of  $S_2$  (red) and  $F_2$  are proportional to  $k_2^{-1}$ . As Fig.11 shows,  $F_2$  only displays small variations of amplitude compared to  $S_2$  and therefore plays a less important rule. In our further simplification we will neglect the influence of  $F_2$ . The slow variable  $S_2$  slaves the system and switches between the oscillatory and the resting state leading to waxing and waning oscillations [4]. Our simplified model will be motivated from the kinetic equation of  $S_2$ . As the transition from  $S_0$  to  $S_1$  is much faster than the one from  $S_1$  to  $S_2$ , we will assume it to be instantaneous, what leads to  $S_2 \approx S_0$ , so we get

$$S_0 + n\text{Ca}^{2+} \rightleftharpoons S_2. \quad (17)$$

In Eq. (5) in [4], the number of binding sites  $n$  for  $\text{Ca}^{2+}$  is assumed to be 2, in our model we use  $n=1$  with the backward rate  $k_2=4 \times 10^{-4}$ , the forward rate  $k_1=k_2/(5 \times 10^{-4})$  and  $C=[\text{Ca}_{in}]/(5 \times 10^{-4})$ , where  $[\text{Ca}_{in}]$  is the intracellular calcium concentration, thus altogether we get

$$\dot{S}_2 = -k_2[S_2 - CS_0]. \quad (18)$$

The essential features of Eq. (18) can be summarized as follows:  $S_2$  opens and closes proportional to the same rate constant  $k_2$ ; due to  $C$ , the activation depends critically on the

PHYSICAL REVIEW E 73, 031908 (2006)

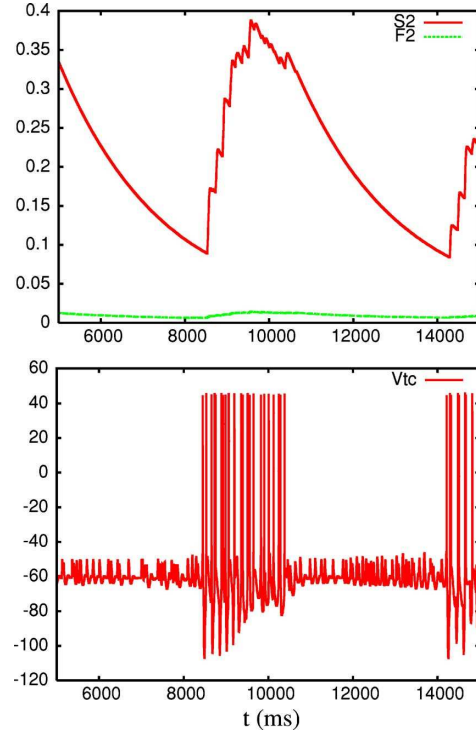


FIG. 11. (Color online) Top: Time course of the gating variables  $S_2$  (red, upper curve) and  $F_2$  (green, lower curve) during a spindle cycle. Bottom: The membrane potential  $V_{TC}$  of the biophysical model.

concentration of intracellular  $\text{Ca}^{2+}$ . This features should also be present in our simplified model. In the Hindmarsh-Rose model the calcium current is mimicked by the variable  $z$  [12], in our model for the  $h$  current will get activated by the variable  $z$ . The rate of activation and deactivation will be equal to the constant used in the biophysical model. For convenience and to be consistent with the notation used in biophysics, we call this current  $h$

$$\dot{h}_{TC} = -k_2[h_{TC} - 0.88(0.9 - z_{TC})]. \quad (19)$$

As  $z$  decreases when the cell gets hyperpolarized, we use the difference between the maximum magnitude of  $z$  and  $z$  itself as an activation term in (19). In order to reproduce the behavior of the biological TC cell, we extend the Hindmarsh-Rose equations as follows:

$$\dot{v}_{TC} = w_{TC} - v_{TC}^3 + 3v_{TC}^2 - z_{TC} - h_{TC}, \quad (20)$$

$$\dot{w}_{TC} = 1.8 - 5v_{TC}^2 - w_{TC}, \quad (21)$$

$$\dot{z}_{TC} = \epsilon[3.3(v_{TC} + 1.56) - z_{TC}], \quad (22)$$

$$\dot{h}_{TC} = -0.0004[h_{TC} + 0.88(0.9 - z)]. \quad (23)$$

MAYER, SCHUSTER, AND CLAUSSEN

PHYSICAL REVIEW E 73, 031908 (2006)

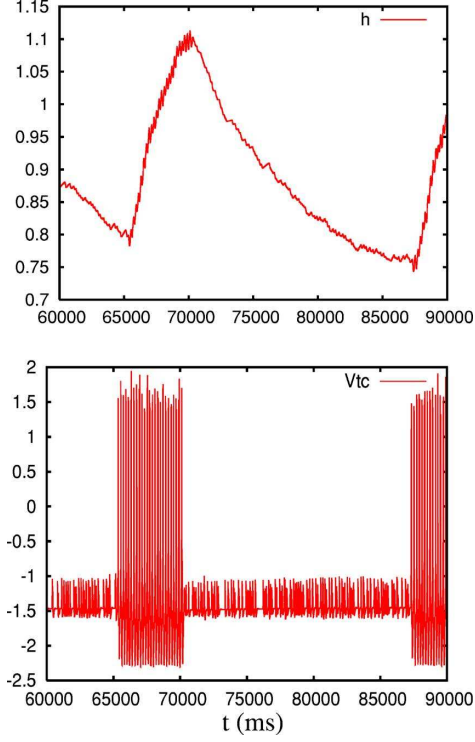


FIG. 12. (Color online) Top: Time course of  $h$  during a spindle cycle. Bottom: The membrane potential  $v_{TC}$  of the extended Hindmarsh-Rose model.

Equations (20)–(23) define our central model, and will be used to model the reciprocally coupled neurons in the remainder. As Fig. 12 shows, the time course of the variable  $h$  is very similar to the time course of  $s_2$  in the biophysical model. To understand the influence of the variable  $h$  we proceed in the same way as before. The time scale of the dynamics of  $h$  is less than a tenth than the time scale of  $z$ . As declared above, the reason for the self-sustained oscillations is the after-hyperpolarization activation by the variable  $z$ . In the presence of  $h$ , the slowly varying parameter in the  $(v, w)$  system is the sum  $[z(t) + h(t)]$ . As  $h(t)$  gets activated by  $z(t)$ , after some rebound bursts the sum  $[z(t) + h(t)]$  is below the threshold of the  $(v, w)$  system, as a consequence, the oscillation terminates. When the excitor cell is inactive, there are no more inhibitory currents, that means that  $t$  is inactive too, so  $h$  decays slowly until it is small enough that the system can get activated again by an input spike.

#### E. Reciprocally coupled TC-RE neurons using the extended Hindmarsh-Rose model

As the  $h$  current is absent in the biological RE neuron, we have to extend the Hindmarsh-Rose system by the  $h$  Eq. (23) for the TC neuron only

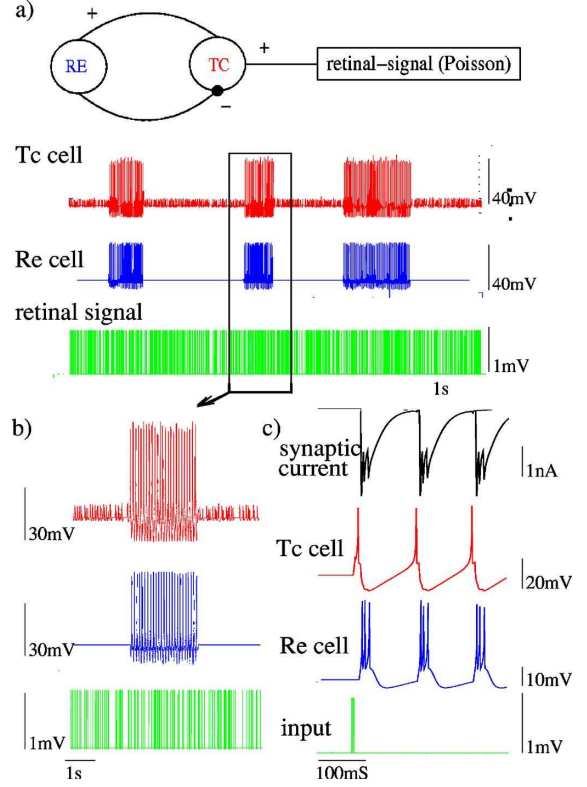


FIG. 13. (Color online) Spontaneous spindle activity in our computational model (the numerical values of the voltages are scaled by a factor of 30 to match with the biophysical values). Similar rescalings have been also necessary in the underlying Hindmarsh-Rose model (see, e.g. [22]). (a) The computational circuit: A TC cell (excitor) modeled by the extended Hindmarsh-Rose model is reciprocally coupled to a model RE cell (inhibitor) represented by the original Hindmarsh-Rose model. The TC cell receives artificial synaptic retinal bombardment modeled by a Poisson distributed spike train. Like in the experiment the system shows spindle activity. (b) Detail of (a). (c) Like in Fig. 8.

$$\dot{v}_{TC} = w_{TC} - v_{TC}^3 + 3v_{TC}^2 - z_{TC} - h_{TC} + I_{GABA} + I(t),$$

$$\dot{w}_{TC} = 1.8 - 5v_{TC}^2 - w_{TC},$$

$$\dot{z}_{TC} = 0.006[4(v_{TC} + 1.56) - z_{TC}],$$

$$\dot{h}_{TC} = -0.0004[h_{TC} + 0.88(0.9 - z)],$$

$$\dot{v}_{RE} = w_{RE} - v_{RE}^3 + 3v_{RE}^2 - z_{RE} + I_{GLU},$$

$$\dot{w}_{RE} = 1.8 - 5v_{RE}^2 - w_{RE},$$

$$\dot{z}_{RE} = 0.006[4(v_{RE} + 1.56) - z_{RE}]. \quad (24)$$

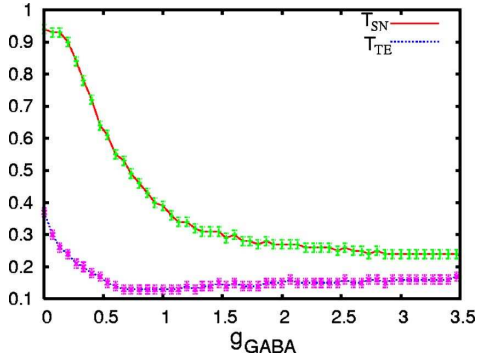


FIG. 14. (Color online) Percentage of output spikes triggered by an input spike. An increase of the strength of the inhibitory coupling  $g_{GABA}$  comes along with a significant decrease in the reliability of the information transfer. As in the experiment of Ref. [2] and in the biophysical model, the transfer efficiency does not vary significantly.

$I_{GABA}$  and  $I_{GLU}$  are governed by Eqs. (B4) and (B5) in Appendix B 1, respectively. The external input was modeled as described above for the biophysical model, with modified parameters adapted to the Hindmarsh-Rose model,  $\bar{r}$  was  $1/100$  and  $\tau_0$  was  $30$  ms. If we stimulate our model by such a modified Poisson process, we have a computational model for the experiment of Le Masson *et al.* [2], which allows us to compare our computational model with the experiment and the biophysical model [3], so that we can validate our extension of the Hindmarsh-Rose model.

A comparison of Fig. 13 and ([2], Fig. 2) shows that our system reproduces the experimental results of Le Masson *et al.* [2] quite well. During the spindling state, the firing pattern of the TC cells (excitor), which is very different from

the input, shows that the information transfer of the input is low. The question whether this low transfer is still reliable is calculated in the same way as for the biophysical system. With a strong inhibitory feedback, the  $T_{SN}$  was low, showing that most of the TC spikes were not triggered by an input spike and thus that the system is not transferring spikes in a one-to-one manner. This result encouraged us to screen the strength of inhibition to test if recurrent feedback inhibition could be a way to control the precision of input-output transfer in a wide range, or if there is just a switching between a relay state and masquerading state. Our numerical investigation leads to the following results. An increase of the inhibitory coupling strength leads to a smooth decrease in  $T_{SN}$  from a maximum value of around 1 to a minimum value of less than 0.3 (Fig. 14). Despite this significant decrease in the reliability of spike transfer, the efficiency of spike transfer  $T_{TE}$  was not significantly diminished by the strength of the inhibitory coupling (Fig. 14). Thus inhibitory feedback has a direct decorrelating effect, which is able to reduce the reliability of the spike transfer.

**F. Dynamical behavior of coupled TC-RE neurons using the extended Hindmarsh-Rose model**

As we argued in Sec. III A for the Hindmarsh-Rose model, Destexhe *et al.* [4] use singular approximation to characterize the spindle oscillations as a transition between a hyperpolarizing stationary phase and an oscillatory phase. Here we will apply this method to our simplified model of a thalamocortical oscillator. In Fig. 13, the  $h$  current evolves according to a much slower time scale as the dynamics of the coupled TC-RE neurons.

We assume  $h$  to be a slow varying parameter in (24) with  $I(t)=0$ , so we consider the limit  $k_2 \rightarrow 0$  in (19). We will consider  $h$  as bifurcation parameter of (24) in an interval be-

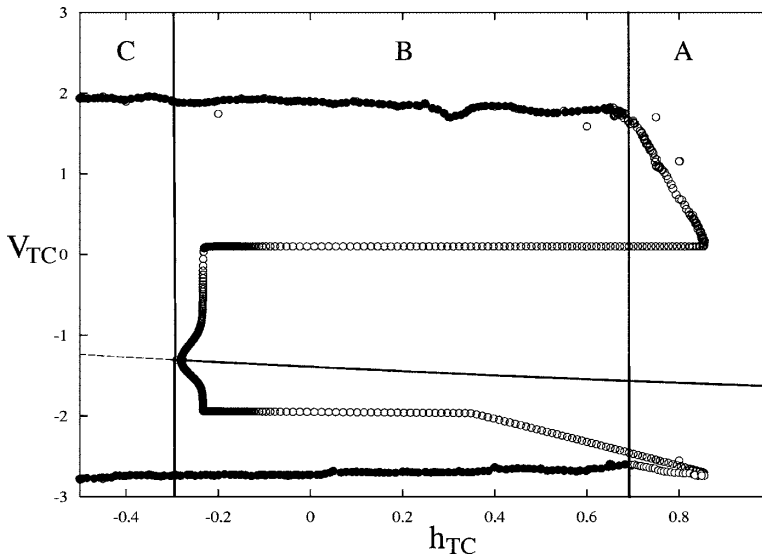


FIG. 15. Bifurcation diagram of (24) with  $h_{TC}$  treated as a slowly varying parameter; solid lines indicate stable fixed points, dashed lines unstable fixed points, filled circles stable limit cycles, open circles unstable limit cycles. For extreme values of  $h$ , the system is monostable, i.e., either a stable fixed point or a stable limit cycle coexist.

MAYER, SCHUSTER, AND CLAUSSEN

PHYSICAL REVIEW E 73, 031908 (2006)

tween  $-1$  and  $1.5$  as a parameter. In this range of  $h$  the dynamical state of the system can be divided in three areas: For high values of  $h$  the system is in a stable resting state, for intermediate values of  $h$  both a stable resting state and a stable oscillatory state exist, separated by an unstable limit cycle. For negative values of  $h$  the stable resting state gets unstable, while the stable oscillatory state persists. The transition between the stable fixed point and the oscillatory state occurs by a subcritical Hopf bifurcation [33]. The existence of a region of parameters where stable solutions overlap is typical for a subcritical Hopf bifurcations; our system shows this typical behavior in a wide range of the bifurcation parameter. In this states the system is bistable, i.e., a stable fixed point and a stable limit-cycle coexist (see Fig. 15). In this area, the state of the system depends on its history: If the initial conditions or the past state of the system lie within the basin of attraction of the limit cycle, the system exhibits stable oscillations; if the starting point lies within the basin of attraction of the fixed point, the system rests on the fixed point. These two attractive areas are separated by an unstable limit cycle. Further, the system can be switched between these two states by an input pulse.

#### G. Discussion of the transfer properties of the extended Hindmarsh-Rose model

The  $h$  current switches the system between two existing dynamical states, namely a fixed point and a bistable state where a limit cycle and a fixed point coexist. Without this further current (i.e.,  $h=0$ ), two reciprocally coupled Hindmarsh-Rose neurons exhibit so-called hard self-excitation [25] as response to an input spike, resulting in stable self-sustained oscillations. The  $h$  current makes this oscillatory state metastable, resulting in waxing and waning oscillations. An increase of the inhibition changes the responsivity of the system: Without, or with only little inhibition, the system responds to an input pulse with an output spike, so that spikes get transmitted in a one-to-one manner. With high gain in inhibitory feedback, the system responds to an input spike by an output burst (range  $B$  in Fig. 15), followed by a silent period where transmission is totally blocked (range  $A$  in Fig. 15). During the burst, the system is in an autonomous self-oscillatory state which masquerades the input, this leads to an increase of the  $T_{SN}$ . As the system is still excitable, but with a different responsivity the  $T_{TE}$  does not change as strong as the  $T_{SN}$ . So the transmission behavior depends critically on the rate of rise and fall of the  $h$  equation. This insight might also help to improve the biophysical model in terms of information transfer.

#### IV. CONCLUSIONS

We have shown that an extended Hindmarsh-Rose model is able to reproduce the behavior of a biological thalamocortical relay neuron in the recent experiment of Le Masson *et al.* To gain more insight into the dynamical mechanisms, a simplification or reduction of the detailed biophysical model, which did not convincingly reproduce the experimentally observed decrease of the signal-to-noise ratio, was necessary.

The widely used Hindmarsh-Rose model however does not show the characteristic waxing and waning oscillations. Further it does not exhibit the quiescence periods necessary for transfer of information. Especially, we have analytically proven that the fast subsystem of the Hindmarsh-Rose model gets slaved by periodic forcing, which can lead to intrinsic bursting if the forcing is slow. To account for the waxing and waning mechanism, we propose an extended Hindmarsh-Rose neuron model for the TC cell, directly motivated from the biophysical model, taking the low threshold calcium current explicitly into account.

In this paper, we have demonstrated that our extended Hindmarsh-Rose model serves as a computational model for the setup in the Le Masson *et al.* experiment, showing that the information transfer can be adjusted within a wide range by the gain of the recurrent feedback inhibition. Our numerical investigations strongly suggest that the low threshold calcium current plays an important role for the information transfer in thalamocortical circuits. From the technical simplicity of our approach and its agreement with the experiment, this approach may give rise to similar models for neural systems where a third time scale is apparent, and a second slow degree of freedom is necessary to describe the dynamics.

#### ACKNOWLEDGMENTS

This research has been supported by the Deutsche Forschungsgemeinschaft (DFG) within SFB 654 "Plasticity and Sleep." The authors thank Jan Born, Lisa Marshall, and Matthias Mölle for intensive and fruitful discussions.

#### APPENDIX A: THALAMOCORTICAL CIRCUIT

The thalamocortical circuit consists of a pair of TC and thalamic RE neurons connected as shown in Fig. 1. For each TC and RE cell several ion currents were included which will be described in detail here. All intrinsic currents are described by the same general equation [16]

$$I_j = \bar{g}_j m^M h^N (V - E_j). \quad (\text{A1})$$

Here the current  $I_j$  is the product of the maximal conductance,  $\bar{g}_j$ , activation  $m$  and inactivation  $h$  variable, and the difference between the membrane potential  $V$  and the Nernst reversal potential  $E_j$ . The powers  $N$  and  $M$  are the respective numbers of ion channels to be open synchronously. The gating of a membrane channel is described by a first order kinetic scheme



where  $O$  and  $C$  stand for the open and the closed state of the gate, with  $\alpha(V)$  and  $\beta(V)$  as the transition rates. According to the Hodgkin-Huxley model [20], the variables  $m$  and  $h$  represent the fraction of independent gates in the open state and are described by simple first order differential equations

ROLE OF INHIBITORY FEEDBACK FOR INFORMATION

$$\dot{m} = -\frac{1}{\tau_m(V)}[m - m_\infty(V)], \quad (\text{A4})$$

$$\dot{h} = -\frac{1}{\tau_h(V)}[h - h_\infty(V)]. \quad (\text{A5})$$

The steady states  $m_\infty(V)$  and  $h_\infty(V)$  and the time constants  $\tau_{m/h}(V)$ , respectively, can be written as functions of the transition rates  $\alpha$  and  $\beta$ , using  $x \in \{m, h\}$ , as

$$\tau_x(V) = \frac{1}{\alpha_x(V) + \beta_x(V)},$$

$$x_\infty(V) = \alpha_x(V)\tau_x(V). \quad (\text{A6})$$

### 1. The TC cell

Here we summarize the results of the previously mentioned investigations of TC cell membrane properties. The membrane potential of the TC neuron is given by

$$C_m \dot{V}_T = -I_{T_L} - I_T - I_h - I_{T_{Na}} - I_{T_K} - I_{GABA_a} - I_{GABA_b}. \quad (\text{A7})$$

The area of a TC cell membrane is about  $2.9 \times 10^{-4} \text{ cm}^2$  which is according to a cell capacity of  $C_m = 0.29 \text{ nF}$ . All constants used in the simulations correspond to a cell of this size.

The leakage current  $I_{T_L}$  is the only passive current, and is governed by the Ohm law

$$I_{T_L} = g_{T_L}(V_T - E_L), \quad (\text{A8})$$

where  $g_{T_L} = 0.05 \text{ mS}$ ,  $E_L = -86 \text{ mV}$ .

All the other currents are active currents, and more complicated, as detailed below.

The sodium current  $I_{Na}$  has the form

$$I_{T_{Na}} = g_{Na}m(t)^3h(t)(V_T - E_{Na}), \quad (\text{A9})$$

with  $g_{T_{Na}} = 30 \text{ mS}$  and  $E_{Na} = 50 \text{ mV}$ . In addition we have for the gating variables  $m(t)$  and  $h(t)$

$$m_\infty(V_T) = \frac{\alpha_m(V_T)}{\alpha_m(V_T) + \beta_m(V_T)},$$

$$h_\infty(V_T) = \frac{\alpha_h(V_T)}{\alpha_h(V_T) + \beta_h(V_T)},$$

$$\tau_m(V_T) = \frac{1}{\alpha_m(V_T) + \beta_m(V_T)},$$

$$\tau_h(V_T) = \frac{1}{\alpha_h(V_T) + \beta_h(V_T)}, \quad (\text{A10})$$

where

$$\alpha_m(V_T) = 0.32 \frac{(V_T + 37)}{1 - \exp\left(-\frac{V_T + 37}{4}\right)},$$

PHYSICAL REVIEW E 73, 031908 (2006)

$$\beta_m(V_T) = 0.28 \frac{(V_T + 10)}{\exp\left(\frac{V_T + 10}{5}\right) - 1},$$

$$\alpha_h(V_T) = 0.128 \exp\left(-\frac{V_T + 33}{5}\right),$$

$$\beta_h(V_T) = \frac{4}{\exp\left(-\frac{V_T + 10}{5}\right) + 1}. \quad (\text{A11})$$

With Eqs. (A4) and (A5) the sodium current is completely described.

The potassium current  $I_K$  has the form

$$I_{T_K} = g_{T_K}m(t)^4(V_T - E_k), \quad (\text{A12})$$

with  $g_{T_K} = 2 \text{ mS}$  and  $E_k = -95 \text{ mV}$ . The gating and transition variables are given by

$$m_\infty(V_T) = \frac{\alpha_m(V_T)}{\alpha_m(V_T) + \beta_m(V_T)},$$

$$\tau_m(V_T) = \frac{1}{\alpha_m(V_T) + \beta_m(V_T)},$$

$$\alpha_m(V_T) = 0.032 \frac{(V_T + 35)}{1 - \exp\left(-\frac{V_T + 35}{5}\right)},$$

$$\beta_m(V_T) = 0.5 \exp\left(-\frac{V_T + 40}{5}\right). \quad (\text{A13})$$

With Eq. (A4) the potassium current is completely described.

The low threshold  $\text{Ca}^{2+}$  current  $I_T$  is taken to be

$$I_T = g_{Ca}m(t)^3h(t)(V - E_T), \quad (\text{A14})$$

where  $g_{Ca} = 1.75 \text{ mS}$  and the reversal potential  $E_T$  depends on the  $\text{Ca}^{2+}$  concentration inside ( $[\text{Ca}]_{in}$ ) and outside ( $[\text{Ca}]_{out}$ ) the cell. It is defined by the Nernst equation

$$E_T = 1000 \frac{RT}{2F} \ln \frac{[\text{Ca}]_{out}}{[\text{Ca}]_{in}}, \quad (\text{A15})$$

where  $R = 8.31441 \text{ J/K mol}$ ,  $T = 309.15 \text{ K}$ ,  $F = 96489 \text{ C/mol}$ , and  $[\text{Ca}]_{out} = 2 \text{ mM}$  is considered to be constant. In the remainder, all concentrations will be denoted by square brackets, following an usual convention (see e.g., [13]).

The calcium dynamics in the cell are described by a simple model which was introduced in [13],

$$\frac{d[\text{Ca}]_{in}}{dt} = -A I_T - K_T [\text{Ca}]_{in} / ([\text{Ca}]_{in} + K_d), \quad (\text{A16})$$

where  $A = 0.179 \text{ m mol/ms } \mu\text{A}$ ,  $K_T = 10^{-4} \text{ m mol/ms}$  and  $K_d = K_T$ .

The gating variables are governed by the following system which was proposed by Wang [18]

MAYER, SCHUSTER, AND CLAUSSEN

PHYSICAL REVIEW E 73, 031908 (2006)

$$\begin{aligned} \dot{m} &= [\tau_m(V_T)]^{-1}[m - m_\infty(V_T)], \\ \dot{h} &= \alpha_1(V_T)[1 - h - d - K(V_T)h], \\ \dot{d} &= \alpha_2(V_T)[K(V_T)(1 - h - d) - d]. \end{aligned} \quad (\text{A17})$$

In addition, for this current the constants are

$$\begin{aligned} m_\infty(V_T) &= \left[ 1 + \exp\left(\frac{V_T + 65}{7.8}\right) \right]^{-1}, \\ \tau_m(V_T) &= 0.15m_\infty(V_T) \left[ 1.7 + \exp\left(-\frac{V_T + 30.8}{13.5}\right) \right], \\ \alpha_1(V_T) &= \exp\left(-\frac{(V_T + 162.3)}{17.8}\right) / 0.26, \\ K(V_T) &= \sqrt{0.25 + \exp\left(\frac{(V_T + 85.5)}{6.3}\right)} - 0.5, \\ \alpha_2(V_T) &= \frac{1}{\tau_2(V_T)[K(V_T) + 1]}, \\ \tau_2(V_T) &= \frac{62.4}{1 + \exp\left(\frac{V_T + 39.4}{30}\right)}. \end{aligned} \quad (\text{A18})$$

The numerical values are fits to experimental data [19].

The hyperpolarization-activated cation current  $I_h$  finally is described by

$$I_h = g_h(S_1 + S_2)(F_1 + F_2)(V_T - E_h), \quad (\text{A19})$$

where  $g_h=0.15$  mS and  $E_h=-43$  mV. The gating variables for this current are governed by

$$\begin{aligned} \dot{S}_1 &= \alpha_s(V_i)S_0 - \beta_s(V_i)S_1 + k_2(S_2 - CS_1), \\ \dot{F}_1 &= \alpha_f(V_i)F_0 - \beta_f(V_i)F_1 + k_2(F_2 - CF_1), \\ \dot{S}_2 &= -k_2(S_2 - CS_1), \\ \dot{F}_2 &= -k_2(F_2 - CF_1), \end{aligned} \quad (\text{A20})$$

where  $C=[\text{Ca}_{im}]/(5 \times 10^{-4})$ ,  $k_2=4 \times 10^{-4}$ , the rate constants  $\alpha_{s/f}(V_i)$  and  $\beta_{s/f}(V_i)$  are related to the activation function  $H_\infty$  and the time constants  $\tau_{s/f}$ 

$$\begin{aligned} \alpha_s(V_i) &= H_\infty/\tau_s, \\ \alpha_f(V_i) &= H_\infty/\tau_f, \\ \beta_s(V_i) &= (1 - H_\infty)/\tau_s, \\ \beta_f(V_i) &= (1 - H_\infty)/\tau_f, \end{aligned} \quad (\text{A21})$$

where

$$\begin{aligned} H_\infty &= \left[ 1 + \exp\left(\frac{V_i + 68.9}{6.5}\right) \right]^{-1}, \\ \tau_s &= \exp[(V_i + 183.6)/15.24], \\ \tau_f &= \exp\left(\frac{V_i + 158.6}{11.2}\right) / \left[ 1 + \exp\left(\frac{V_i + 75}{5.5}\right) \right]. \end{aligned} \quad (\text{A22})$$

This makes the biophysical description of TC cell complete. While it contains a lot of simplifications, for example the single compartment assumption, it reproduces almost all important features of TC cells quite good. We will use this model in our computer experiment to verify theories obtained by using simplified models. For more details see [15].

## 2. The RE cell

The membrane potential of the thalamic RE neuron is governed by the cable equation

$$C_m \dot{V}_R = -I_{R_L} - I_{T_s} - I_{K[Ca]} - I_{CAN} - I_{R_{Na}} - I_{R_K} - I_{GLU}. \quad (\text{A23})$$

For the RE cell the membrane capacity is  $C_m=0.143$  nF, the leakage conductance is  $g_{R_L}=0.05$  mS and the reversal potential of the leakage current is  $E_L=-80$  mV. This model of thalamic RE cell was introduced by Destexhe *et al.* in [34].

The equations for the sodium  $I_{R_{Na}}$  and potassium  $I_{R_K}$  current in the RE cell are the same as for the TC cell, except that the conductance  $g_{Na}=100$  mS is different. The description of the RE cell potassium current is reached by putting  $g_K=10$  mS.

The kinetics of the low threshold  $\text{Ca}^{2+}$  current  $I_{T_s}$  was established as a model for voltage clamp data on rat RE cells using a so-called  $m^2h$  formalism [19]

$$I_{T_s} = g_{T_s}m(t)^2h(t)(V_R - E_{T_s}), \quad (\text{A24})$$

where  $g_{T_s}=1.75$   $\mu\text{S}$  and  $E_{T_s}$  depends on the calcium concentration in the same way as described for the TC cell. The calcium dynamics are described by Eq. (A9), when  $I_T$  is replaced by  $I_{T_s}$ . In addition we have for this current

$$\begin{aligned} m_\infty(V_R) &= \left[ 1 + \exp\left(-\frac{V_R + 52}{7.4}\right) \right]^{-1}, \\ \tau_m(V_R) &= 1 + \frac{1}{3} \left[ \exp\left(\frac{V_R + 27}{10}\right) \right. \\ &\quad \left. + \exp\left(-\frac{V_R + 102}{15}\right) \right]^{-1} h_\infty(V_R), \\ &= \left[ 1 + \exp\left(\frac{V_R + 80}{5}\right) \right]^{-1}, \end{aligned}$$

ROLE OF INHIBITORY FEEDBACK FOR INFORMATION

$$\tau_h(V_R) = \frac{85}{3} + \frac{1}{3} \left[ \exp\left(\frac{V_R + 48}{4}\right) + \exp\left(-\frac{V_R + 407}{50}\right) \right]^{-1}. \quad (\text{A25})$$

The full kinetics of the  $I_T$  current is reached if  $m_\infty$ ,  $\tau_m$ ,  $h_\infty$ , and  $\tau_h$  are inserted in Eqs. (A4) and (A5).

*The calcium dependent currents:* The RE cell possesses further two calcium dependent currents the slow  $K^+$  current  $I_{K[Ca]}$ , and the slow nonspecific cation current  $I_{CAN}$ . According to [15] they are modeled as voltage-independent currents described by Eq. (A1) with  $M=2$  and  $N=0$ . The activation variable  $m$  obeys

$$\dot{m} = \alpha[Ca_i]^2(1 - m) - \beta m, \quad (\text{A26})$$

where  $\alpha$  and  $\beta$  are rate constants and  $[Ca_i]$  is the intracellular calcium concentration. For  $I_{K[Ca]}$   $\alpha=48 \text{ ms}^{-1}$ ,  $mM^{-2}$ , and  $\beta=0.03 \text{ ms}^{-1}$ , for  $I_{CAN}$ ,  $\alpha=20 \text{ ms}^{-1}$ ,  $mM^{-2}$ , and  $\beta=0.002 \text{ ms}^{-1}$ . With this the description of the RE cell is complete.

### 3. Synaptic currents

Kinetic models of synaptic currents have been directly fitted to experimental data [3], based on whole cell recorded synaptic currents obtained in hippocampal neurons [35]. The  $GABA_A$  and  $GLU$  (=glutamate) receptor mediated currents are both represented by a first order kinetic scheme [36]



where the transition between closed ( $C$ ) and open ( $O$ ) states depend on the binding of the transmitter ( $T$ ). The current is given by

$$I_{syn} = g_{syn}[O](t)[V(t) - E_{syn}], \quad (\text{A28})$$

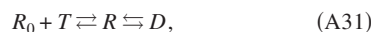
where  $g_{syn}$  is the maximal conductivity and  $E_{syn}$  is the reversal potential. For AMPA receptors  $E_{syn}=0 \text{ mV}$  and for  $GABA_A$  receptors  $E_{syn}=-80 \text{ mV}$ .  $g_{syn}=0.05$  for  $GABA_A$  and  $g_{syn}=0.1$  for glutamate synapses.  $[O](t)$  is the fraction of open channels

$$\frac{d[O](t)}{dt} = \alpha[1 - [O](t)][T](t) - \beta[O](t), \quad (\text{A29})$$

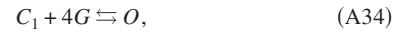
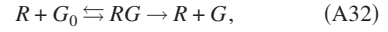
and  $[T](t)$  is the concentration of transmitter released from time  $t$  to time  $t_{max}$

$$[T](t) = A\Theta(t_{max} - t)\Theta(t), \quad (\text{A30})$$

where  $\Theta(x)$  is the Heaviside function. The synaptic parameter values used in the simulation are  $A=0.5$  and  $t_{max}=3 \text{ ms}$  for  $GABA_A$  and  $9 \text{ ms}$  for AMPA synapses, the rate constants were chosen as  $\alpha=5 \text{ ms}$  and  $\beta=0.16 \text{ ms}$  for  $GABA_A$  synapses and  $\alpha=0.94 \text{ ms}$  and  $\beta=0.18 \text{ ms}$  for  $GLU$  synapses. The activation scheme of  $GABA_B$  receptors is more complex, as it involves the activation of  $K^+$  channels by  $G$  proteins (for details see [37]). The model used by Le Masson *et al.* [2] is a modified version of the  $GABA_B$  kinetic model introduced in [38]



PHYSICAL REVIEW E 73, 031908 (2006)



where the transmitter,  $T$ , binds to the receptor,  $R_0$ , leading to its activated form,  $R$ , and desensitized form,  $D$ . The  $G$  protein is transformed from an inactive ( $GDP$  bound) form,  $G_0$  to an activated form,  $G$ , catalyzed by  $R$ . Finally,  $G$  binds to open the  $K^+$  channel, with four independent binding sites. With some assumptions (see [3]) the kinetic model for this system reduces to

$$I_{GABA_B} = g_{GABA_B} \frac{[G]^4}{[G]^4 + K_d} [V(t) - E_k],$$

$$\frac{d[R]}{dt} = K_1(1 - [R])[T] - K_2[R],$$

$$\frac{d[G]}{dt} = K_3[R] - K_4[G], \quad (\text{A35})$$

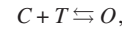
where  $[R]$  is the fraction of activated receptors and  $[G]$  is the concentration of  $G$  proteins. In these equations  $g_{GABA_B}$ ,  $K_1=0.52$ ,  $K_2=0.0013$ ,  $K_3, K_4=0.033$ , and  $K_d=100$ .

The strengths of the synaptic couplings  $g_{GABA_{A/B}}$  and  $g_{AMPA}$  are varied in different simulations.

## APPENDIX B: THE REDUCED MODEL

### 1. Synaptic currents

The simplest way to model synaptic currents is a two state scheme of the binding of a neurotransmitter  $T$  to postsynaptic receptors [3]. So the receptor mediated currents are both represented by a first order kinetic scheme



where the transition between closed ( $C$ ) and open ( $O$ ) states depend on the binding of the transmitter ( $T$ ) with forward and backward rates  $\alpha$  and  $\beta$  respectively. As in [39] we only consider voltage-independent rate constants. With this assumptions we get the following kinetic equation

$$\frac{d[O]}{dt} = \alpha(1 - [O])[T] - \beta[O] = \alpha[T] - [O]\alpha[T] - \beta[O]. \quad (\text{B1})$$

The synaptic current is given by

$$I_{syn} = g_{syn}[O](t)[V(t) - E_{syn}], \quad (\text{B2})$$

where  $g_{syn}$  is the maximal conductivity and  $E_{syn}$  is the reversal potential. For glutamate receptors  $E_{syn}=0 \text{ mV}$  and for  $GABA_A$  receptors  $E_{syn}=-50 \text{ mV}$ . The release and clearance of transmitter are extremely fast processes compared to the open/close kinetics, resulting in a very brief presence of transmitter in the synaptic cleft [40], which allows us to con-

MAYER, SCHUSTER, AND CLAUSSEN

PHYSICAL REVIEW E 73, 031908 (2006)

sider  $O$  to be constant during the transmitter release. For simplicity we assume the transmitter release time course to be a square pulse  $A\Theta(V_{pre})$  which occurs when the presynaptic neuron fires a spike, i.e., when the presynaptic potential  $V_{pre}$  gets depolarized towards positive potentials. If we assume that initially all synaptic channels are in the closed state, we get

$$\frac{d[O]}{dt} = \gamma\alpha A\Theta(V_{pre}) - \beta[O], \quad (\text{B3})$$

where  $\gamma = \alpha A$ . As  $GABA_B$  synapses contribute less than a tenth of the total inhibitory synaptic current, they are neglected here. The rate constants and amplitude were taken from the biophysical model A3. The constants for the  $GABA$  synapse were modified because of the absence of the  $GABA_B$  synapse:  $\alpha = 5 \text{ ms}^{-1}$  and  $\beta = 0.05 \text{ ms}^{-1}$ . For the GLU synapse we used the same constants as in the biophysical model:  $\alpha = 0.94 \text{ ms}^{-1}$  and  $\beta = 0.18 \text{ ms}^{-1}$ . We chose  $A = 0.5$ , and respectively,  $\gamma = 2.5$  for  $GABA$  synapses and  $\gamma = 0.47$  for glutamate synapses. The synaptic currents are governed by the following equations:

$$I_{GABA} = g_{GABA}[O]_{GABA}(v_{TC} - 2.5), \quad (\text{B4})$$

$$I_{GLU} = g_{GLU}[O]_{GLU}v_{RE}, \quad (\text{B5})$$

the reversal potential of the  $GABA_A$  synapse was rescaled by a factor of 30 to adapt it to the scale of the Hindmarsh-Rose model.

## 2. Transformation to a Lienard system

We begin with the autonomous  $(v, w)$  subsystem (6) and (7)

$$\dot{v}(t) = w - v^3 + 3v^2, \quad (\text{B6})$$

$$\dot{w}(t) = 1.8 - 5v^2 - w. \quad (\text{B7})$$

Then  $\ddot{v} = \dot{w} + (6v - 3v^2)\dot{v}$ ,  $\dot{w} = \ddot{v} - (6v - 3v^2)\dot{v}$ , and

$$w = -\ddot{v} + (6v - 3v^2)\dot{v} + 1.8 - 5v. \quad (\text{B8})$$

Inserting (B8) in (B6) yields

$$0 = \ddot{v} + (1.8 - 6v + 3v^2)\dot{v} + (v^3 + 2v^2 - 1.8),$$

$$0 = \ddot{v} + f(v)\dot{v} + g(v). \quad (\text{B9})$$

(B9) is the so-called Lienard form of Eqs. (B6) and (B7), where  $f(v) = 1.8 - 6v + 3v^2$  and  $g(v) = v^3 + 2v^2 - 1.8$ .

## 3. Stability of the equilibrium points

The stability of equilibrium points in the fast  $(v, w)$  subsystem is investigated by a linear approximation to the system (6) and (7). Suppose the equilibrium point has the  $v$  coordinate  $v_0$ , then the linear approximation is

TABLE I. Equilibrium points depending on  $v_0$  (see text). Only stable nodes and unstable spirals and saddle nodes occur.

Region	Values of $v_0$	Sign of $\text{Tr} A(v_0)$	Sign of $\text{Det} A(v_0)$	Type of node
I	$v_0 < -4/3$	-	+	stable
II	$-4/3 < v_0 < \text{Tr}_-$	-	-	saddle
III	$\text{Tr}_- < v_0 < 0$	+	-	saddle
IV	$0 < v_0 < \text{Tr}_+$	+	+	unstable spiral
V	$\text{Tr}_+ < v_0$	+	-	saddle

$$\begin{pmatrix} \dot{x} \\ \dot{y} \end{pmatrix} = A(v_0) \begin{pmatrix} x \\ y \end{pmatrix}, \quad (\text{B10})$$

where  $(x, y)$  are new coordinates whose origin is in the equilibrium point, and  $A(v_0)$  is the Jacobian in  $v_0$

$$A(v_0) = \begin{pmatrix} -3v_0^2 + 6v_0 & 1 \\ -10v_0 & -1 \end{pmatrix}. \quad (\text{B11})$$

The kind of equilibrium point may be determined by the signs of the trace  $\text{Tr}[A(v_0)] = -3v_0^2 + 6v_0 - 1$  and determinant  $\text{Det}[A(v_0)] = 3v_0^2 + 4v_0$  [12,41]. The eigenvalues  $\lambda_{1/2}$  of the Jacobian  $A(v_0)$  are expressed by

$$\lambda_{1/2} = \frac{1}{2} \{ \text{Tr}[A(v_0)] \pm \sqrt{ \{ \text{Tr}[A(v_0)] \}^2 - 4 \text{Det}[A(v_0)] } \}. \quad (\text{B12})$$

Table I gives the type of equilibrium point according to the region  $v_0$  belongs to; here  $\text{Tr}_- = (3 - \sqrt{6})/3$  and  $\text{Tr}_+ = (3 + \sqrt{6})/3$  are the negative and positive zeroes of  $\text{Tr}[A(v_0)]$ , respectively.

## 4. Periodic solutions for periodic forcing

The conditions for constants  $b, m, M > 0$  are

- (i) for  $|v| \geq b$ ,  $f(v) > m$ ,
- (ii)  $v \in \mathbb{R}$ ,  $f(v) > -M$ ,
- (iii) for  $|v| \geq b$ ,  $vg(v) > 0$ ,
- (iv)  $g(v)$  is monotone increasing in  $(-\infty, -b)$ ,
- (v)  $|g(v)| \rightarrow \infty$  for  $|v| \rightarrow \infty$ ,
- (vi)  $g(v)/G(v) \rightarrow 0$  for  $|v| \rightarrow \infty$ ,

where  $G(v) = \int_0^v g(u) du$ .

The proof can be sketched as follows:

(a) The existence of  $M$  is easy to establish as  $f(v)$  has a minimum at  $v = 1$ , further as  $f(v)$  is a convex function this minimum is the global one. If a  $M > |f(1) - (-2)|$  is chosen (ii) holds.

(b) Set  $M = m$ , then  $b_1$  may be chosen arbitrarily.

(c) Next  $vg(v)$  is a fourth degree polynomial where the coefficient of the  $v^4$  term is positive. So there exists a  $b_2$  with  $vg(v) > 0$  if  $v > b_2 > 0$ .

(d) As  $g(v)$  is a third degree polynomial, there is a  $b_3$ , such that  $g(v)$  is monotonously increasing in  $(-\infty, -b_3)$  and  $(b_3, \infty)$ .

Choose  $b = \max(b_1, b_2, b_3)$  then (i), (iii), and (iv) hold. Finally (v) and (vi) are obvious; so the proof is complete.



ROLE OF INHIBITORY FEEDBACK FOR INFORMATION

PHYSICAL REVIEW E **73**, 031908 (2006)

- [1] L. Marshall, M. Mölle, and J. Born, *Neuroscience* **121**, 1047 (2003).
- [2] G. Le Masson, S. Renaud-Le Masson, D. Debay, and T. Bal, *Nature (London)* **417**, 854 (2002).
- [3] A. Destexhe, T. Bal, D. A. McCormick, and T. J. Sejnowski, *Neuroscience* **76**, 2049 (1996).
- [4] A. Destexhe, D. A. McCormick, and T. J. Sejnowski, *Biophys. J.* **65**, 2473 (1993).
- [5] A. Amon, M. Nizette, M. Lefranc, and T. Erneux, *Phys. Rev. A* **68**, 023801 (2003).
- [6] R. Straube, S. C. Müller, and M. J. B. Hauser, *Semin. Hear.* **217**, 1427 (2003).
- [7] S. Raghavachari, and J. A. Glazier, *Phys. Rev. Lett.* **82**, 2991 (1999).
- [8] Eugene M. Izhikevich, *Int. J. Bifurcation Chaos Appl. Sci. Eng.* **10**, 1171 (2000).
- [9] S. M. Sherman and R. W. Guillery, *J. Neurophysiol.* **76**, 1367 (1996).
- [10] J. Pinell, *Biopsychologie, Spektrum Akademischer*, 4th edition, (Verlag, Berlin, 1997).
- [11] H. G. Schuster, *Complex Adaptive Systems* (Scator, Saarbrücken, 2001).
- [12] J. L. Hindmarsh and R. M. Rose, *Proc. R. Soc. London, Ser. B* **221**, 87 (1984).
- [13] M. Rabinovich, R. Huerta, M. Bazhenov, A. K. Kozlov, and H. D. I. Abarbanel, *Phys. Rev. E* **58**, 6418 (1998).
- [14] T. Bal, M. von Krosigk, and D. A. McCormick, *J. Physiol. (London)* **483**, 641 (1995).
- [15] A. Destexhe, A. Babloyantz, and T. J. Sejnowski, *Biophys. J.* **65**, 1538 (1993).
- [16] A. L. Hodgkin and A. F. Huxley, *J. Physiol. (London)* **117**, 500 (1952).
- [17] R. D. Traub and R. Miles, *Neuronal Networks of the Hippocampus* (Cambridge University Press, Cambridge, 1991).
- [18] X. J. Wang, J. Rinzl, and M. A. Rogawski, *J. Neurophysiol.* **66**, 850 (1991).
- [19] J. R. Huguenard, D. A. Prince, and T. J. Sejnowski, *J. Neurosci.* **12**, 3804 (1994).
- [20] T. Bal and D. A. McCormick, *J. Physiol. (London)* **468**, 669 (1993).
- [21] M. Dhamala, V. K. Jirsa, and M. Ding, *Phys. Rev. Lett.* **92**, 028101 (2004).
- [22] H. R. Wilson, *J. Theor. Biol.* **200**, 375 (1999).
- [23] L. S. Pontryagin, *Am. Math. Soc. Transl.* **18**, 275 (1967).
- [24] E. C. Zeeman, *Differential Equations for the Heart Beat and Nerve Impulse*, In *Dynamical Systems*, edited by M. Peixoto, (Academic Press, New York, 1973), p. 683.
- [25] H. Haken, *Synergetics, An Introduction* (Springer-Verlag, Berlin, 1977).
- [26] Jörg Mayer, Diploma thesis (University of Kiel, Kiel, 2004).
- [27] E. Doedel, *Congr. Numer.* **30**, 265 (1981).
- [28] B. Ermentrout, *Simulating, Analyzing, and Animating Dynamical Systems: A Guide to XPPAUT for Researchers and Students* (SIAM Books, Soc. for Industrial & Applied Math, 1st edition, 2002).
- [29] X.-J. Wang, *Physica D* **62**, 263 (1993).
- [30] Miklos Farkas, *Periodic Motions*, in *Applies Mathematical Sciences* (Springer-Verlag, Berlin, 1994), Vol. 104, p. 171.
- [31] M. G. Rosenblum and A. S. Pikovsky, *Phys. Rev. Lett.* **92**, 114102 (2004).
- [32] G. Ahlsen and S. Lindström, *Exp. Brain Res.* **58**, 134 (1985).
- [33] H. G. Schuster and W. Just, *Deterministic Chaos*, 4th edition, (Wiley-VCH, 2005).
- [34] A. Destexhe and A. Babloyantz, *NeuroReport* **4**, 223 (1993).
- [35] T. Otis and I. Mody, *Neuroscience* **49**, 13 (1992).
- [36] A. Destexhe, Z. F. Mainen, and T. J. Sejnowski, *J. Comput. Neurosci.* **1**, 195 (1994).
- [37] P. Dutar and R. A. Nicoll, *Nature (London)* **332**, 158 (1988).
- [38] A. Destexhe and T. J. Sejnowski, *Proc. Natl. Acad. Sci. U.S.A.* **92**, 9515 (1995).
- [39] A. Destexhe and M. Rudolph, *J. Comput. Neurosci.* **17**, 327 (2004).
- [40] J. D. Clements, *Trends Neurosci.* **19**, 163 (1996).
- [41] J. H. Argyris, G. Faust, and M. Haase, *Exploration of Chaos: An Introduction for Natural Scientists and Engineers* (Elsevier, Amsterdam, 1994).

## **3.2 Corticothalamic projections control synchronization in locally coupled bistable thalamic oscillators**

### Corticothalamic Projections Control Synchronization in Locally Coupled Bistable Thalamic Oscillators

Jörg Mayer,<sup>1</sup> Heinz Georg Schuster,<sup>1</sup> Jens Christian Claussen,<sup>1</sup> and Matthias Mölle<sup>2</sup>

<sup>1</sup>*Institute for Theoretical Physics and Astrophysics, University of Kiel, 24098 Kiel, Germany*

<sup>2</sup>*Department of Neuroendocrinology, University of Lübeck, 23538 Lübeck, Germany*

(Received 8 February 2007; published 8 August 2007)

Thalamic circuits are able to generate state-dependent oscillations of different frequencies and degrees of synchronization. However, little is known about how synchronous oscillations, such as spindle oscillations in the thalamus, are organized in the intact brain. Experimental findings suggest that the simultaneous occurrence of spindle oscillations over widespread territories of the thalamus is due to the corticothalamic projections, as the synchrony is lost in the decorticated thalamus. In this Letter we study the influence of corticothalamic projections on the synchrony in a thalamic network, and uncover the underlying control mechanism, leading to a control method which is applicable for several types of oscillations in the central nervous system.

DOI: 10.1103/PhysRevLett.99.068102

PACS numbers: 87.19.La, 05.45.-a, 84.35.+i, 87.19.Nn

Coupled oscillators are abundant in physics [1,2], chemistry [3], and biology [4–6]. Whenever large numbers of coupled oscillators are considered, the collective behavior of the ensemble is of great interest [2,7]. A widespread phenomenon in populations of periodic, noisy, and chaotic oscillators (or maps) is the appearance of synchronous collective oscillations, studied theoretically [7] as well as experimentally [3,8]. In neural systems the phenomenon of spike burst activity is widespread and of great importance [9,10]. This activity is characterized by a recurrent transition between a resting state and a firing state with a burst of multiple spikes. Bursting is a multiple time scale effect and appears due to a slow process which modulates a fast subsystem [9,11].

Neural cells in the thalamus are known to exhibit spike burst activity during periods of drowsiness, inattentiveness, and sleep [12,13]. Spindle oscillations, a hallmark of early sleep stages, observed in the electroencephalographic recordings of sleeping humans as oscillations in a 12–15 Hz frequency range, are considered to be the result of synchronized spike burst activity of millions of neurons in the thalamus [10,14]. Despite experimental findings in thalamic slices, where the spindle oscillations propagate like a traveling wave through the network [15], in the intact brain spindle oscillations occur almost synchronously over widespread territories of the thalamus [14,16]. These contrasting results between *in vitro* and *in vivo* experiments occur due to the absence of corticothalamic projections (synaptic connections from the cortex to the thalamus) in a thalamic slice as, after ablation of the cortex, synchrony is lost in the thalamus [14,16,17].

In a coupled system of oscillators, oscillations become more and more coherent when the coupling strength is increased [2,7]. In this Letter, we explore the possibility to induce the transition from the decoherent state to the coherent state—in which bursts occur synchronously—by external signals. For this reason, we investigate the mechanism by which corticothalamic projections control coher-

ence of thalamic spindle oscillations. The knowledge of control mechanisms for synchrony in neural systems may help to understand the origins and mechanisms of sleep and other processes in the mammalian brain, and—in the long run—to control them.

The Letter is organized as follows: We introduce our simplified model of the thalamocortical oscillator based on [13,18,19]. Then we study burst-synchronization quasianalytically for two coupled neurons. Finally, we study the collective behavior of thalamic oscillators, verify the experimental observation that corticothalamic projections control synchrony in the thalamus by using human slow wave electroencephalogram (EEG) data to control our computational thalamus model.

The dynamics of the system described in [19] is mainly determined by a slow change between a bistable state where a stable fixed point and a stable limit cycle coexist, and a monostable state where only a stable fixed point exists. This behavior can be described by a slowly modulated overdamped movement of a particle in a rotating symmetric time-dependent double well potential

$$U(r, t, \varphi) = \frac{1}{2}r^2 - \frac{1}{4}\alpha(t)r^4 + \frac{1}{6}r^6 \quad (1)$$

(see Fig. 1), where  $r = \sqrt{x^2 + y^2}$ , and  $\varphi(t) = \omega t$  captures the oscillation in phase (mod  $2\pi$ ); see Ref. [20] for a related model. Depending on the slow variable  $\alpha(t)$ , the system possesses either one stable fixed point, or it shows bistability with a stable fixed point and a stable limit cycle. As the relaxation within the wells is fast compared to  $\alpha(t)$ , so the quasiadiabatic approximation is applicable. We get an equation for the movement in the  $r$  direction for the single oscillator

$$\begin{aligned} \dot{r} &= -\partial U(r, \alpha)/\partial r + I^{\text{ext}} + F(t), \\ \dot{u} &= \mu[r(1-u) - 0.375u], \end{aligned} \quad (2)$$

where  $\alpha(t) = a(1-u)$ ,  $F(t)$  is a common control signal.

PRL 99, 068102 (2007)

PHYSICAL REVIEW LETTERS

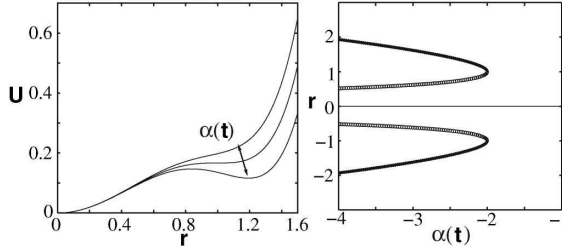
week ending  
10 AUGUST 2007

FIG. 1. Depending on  $\alpha$ , the system possesses either one stable fixed point or it shows bistability with a stable fixed point and a stable limit cycle. Left:  $U(r, t, \varphi)$  for different values of  $\alpha$ . Right: Bifurcation diagram of (2) with  $\alpha(t)$  considered as a bifurcation parameter. Solid lines indicate a stable fixed point, open circles an unstable limit cycle and filled circles a stable limit cycle.

Following [9], we first study synchrony in two bistable elements coupled linearly via  $r$ :

$$\begin{aligned} \dot{r}_i &= -r_i + a(1 - u_i)r_i^3 - r_i^5 + I_i^{\text{ext}} + \epsilon r_j, \\ \dot{u}_i &= \mu[r_i(1 - u_i) - 0.375u_i], \end{aligned} \quad (3)$$

where  $\epsilon > 0$  is the coupling strength,  $\mu = 0.0004$  scales the refractory period  $\tau \sim \mu^{-1}$ , and  $a = 2.5$  is chosen such that  $U(r, \alpha)$  is a double well potential for  $u < 0.2$ , and  $i \neq j$ , respectively, are the indices.  $I_i^{\text{ext}}$  is the external input, which is a Poisson distributed shot noise with a rate of 1/100 ms, refractory period of 30 ms, pulse duration of 2 ms, and an amplitude of 0.6. We emphasize that the  $I_i^{\text{ext}}$  are stochastically independent, so  $\langle I_i^{\text{ext}}, I_j^{\text{ext}} \rangle = \delta_{i,j}$ . Through the coupling the potentials of the bistable elements get deformed

$$U_i(r_i, \alpha_i, \epsilon) = \frac{1}{2}r_i^2 - \frac{1}{4}\alpha_i(t)r_i^4 + \frac{1}{6}r_i^6 - \epsilon r_j r_i, \quad (4)$$

where  $i \neq j$  respectively are the indices. If neuron 2 has just become excited, i.e., it stays in the right well in Fig. 1, then  $u_2 \approx 0.15$  and  $r_2 \approx 1.25$ . Further, we assume that neuron 1 is in the ground state and does not get an input spike. Mutual synchronization will occur if  $U_1(r_i, \alpha_i, \epsilon)$  gets so strongly deformed that the barrier between the two wells vanishes; i.e., only the external well persists. This is the case if  $\partial U / \partial r = 0$  is fulfilled in only one point for  $r \in (0, \infty)$ . The transition point can be calculated by applying Sturm's theorem [21], accordingly synchronization of interwell jumps should occur at  $\epsilon \approx 0.23$ . The estimation above only gives the values of  $\epsilon$  where  $r$  synchronizes, but however as  $u$  obeys a linear differential equation, which gets activated by  $r$ , we expect  $u$  to synchronize at the same value of  $\epsilon$  as  $r$ . The numerical simulation of (3) for different  $\epsilon$  in Fig. 2 verifies this argumentation. Our goal is to induce the transition to synchrony by external control signals. Having clinical applications in mind, desiring to achieve large effects with weak external triggers, we want the external control signal to support the internal

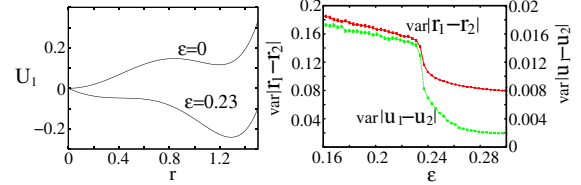


FIG. 2 (color online). Left: The potential  $U_1$  with no coupling and  $u = 0.15$  and for the case that neuron 2 is in the excited state and  $u_{1/2}$  are both 0.15 for a coupling strength of  $\epsilon = 0.23$ . See (4) and Fig. 1. Right: Variations of  $|r_1 - r_2|$  (red) and  $|u_1 - u_2|$  (green/light gray) as a function of  $\epsilon$ . As the interwell jumps synchronize at  $\epsilon \approx 0.23$ , the variations of  $|r_1 - r_2|$  and  $|u_1 - u_2|$  rapidly decrease at this point.

dynamics of the coupled system; i.e., both the open loop control signal and the internal coupling will be needed to induce the transition to synchrony. At this point we present a qualitative understanding of a control mechanism which is based on the dynamics of the reciprocal coupled oscillators presented above, but is also applicable in larger networks. We assume the slow process  $u_i(t)$  to be a relaxation oscillator with relaxation time  $\tau$ , which scales with  $\mu^{-1}$ ; this relaxation process gets activated by the variable  $r_i(t)$ , in turn  $u_i(t)$  inhibits excitation of  $r_i$  during the relaxation time  $\tau$ . So  $u_i(t)$  can be interpreted as a refractory process which leads to a dead time, in which the single oscillator is not excitable. So the maximum phase difference between any arbitrary chosen oscillators is at most of the magnitude of  $\tau$ . Another way to block excitation of the  $r_i$  is a common, sufficiently strong hyperpolarization [i.e.,  $F(t)$  is negative] of all oscillators. If the duration of this hyperpolarization exceeds  $\tau$ , the  $u_i(t)$  will decay back to the excitable ground state. That means they all have the same phase. Of course the phase of the  $u_i(t)$  can diffuse in time because of the highly stochastic input. But if the phase resetting is done repetitively, the variance of the phases of  $u_i$  can be confined. The amplitude of the hyperpolarization depends on the amplitude of the Poisson distributed input spikes, it has to be strong enough to suppress excitation of the  $r_i$ . Numerically, we find  $\tau \approx 4.96$  s and the system stays in the excited state for  $T_e = 0.45$  s. Just like the coupling, also an external control signal deforms the potential, and, if applied appropriately, interacts in a promotive way for synchronization with the intrinsic dynamics of the coupled oscillators. We choose  $F(t)$  to be a periodic train of square pulses with a pulse height  $F = 0.1$  and pulse duration  $T_e$ . The positive part of  $F(t)$  results in an amplification of the coupling strength  $\epsilon$ . Between the pulses there is an inactive phase where  $F = -0.1$  lasting  $\tau_s$  (see Fig. 3),

$$U(r_i, \alpha_i, \epsilon) = \frac{1}{2}r_i^2 - \frac{1}{4}\alpha_i(t)r_i^4 + \frac{1}{6}r_i^6 - [\epsilon r_j + F(t)]r_i. \quad (5)$$

If we further assume that the  $u_i$  have been reset to their ground state by the negative part of the control signal, the

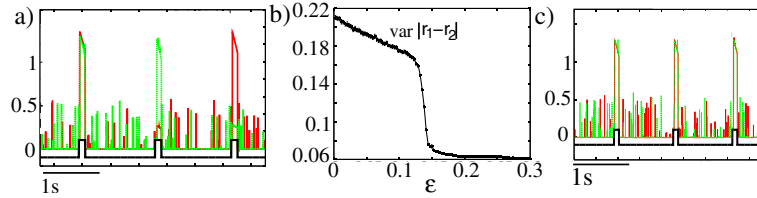


FIG. 3 (color online). (a) and (c)  $r_1$  (red),  $r_2$  (green/light gray) and  $F(t)$ . (a) For a coupling strength of  $\epsilon = 0.12$  the interwell jumps occur asynchronously. (b) Variations of  $|r_1 - r_2|$  as a function of  $\epsilon$ , both oscillators were modulated by  $F(t)$ . As the interwell jumps synchronize at  $\epsilon \approx 0.14$ , the variations of  $|r_1 - r_2|$  rapidly decrease. For the parameters chosen here, both control signal and internal coupling are needed. (c) For  $\epsilon = 0.15$  the interwell jumps occur synchronously, triggered by  $F(t)$ .

first well vanishes at  $\epsilon \approx 0.14$  resulting in synchronization of interwell jumps. The simulation of (5) for different  $\epsilon$  in Fig. 3 verifies this argumentation. In the remainder, we will use cortical slow wave EEG data as the control signal. Taken together, this common signal combined with an internal nearest neighbor coupling, should lead to synchronous network oscillations.

Now we model the thalamic network by a two-dimensional  $50 \times 50$  square lattice,

$$\begin{pmatrix} \dot{r}_{ij} \\ \dot{u}_{ij} \end{pmatrix} = \tilde{F}(r_{ij}, u_{ij}) + \epsilon \begin{pmatrix} \sum_{i'j'} G_{ij'i'j'} r_{i'j'} \\ 0 \end{pmatrix} + F^{\text{ext}}(t), \quad (6)$$

where the uncoupled dynamics of the  $i$ th node obeys  $\tilde{F}(r_{ij}, u_{ij})$  given by (2) and  $G$  determines the coupling between the neurons.  $F^{\text{ext}}(t) = \kappa \mathcal{E}(t)$  is the common external forcing which consists of human slow wave sleep EEG data  $\mathcal{E}(t)$ . Almost any coupling scheme can be cast into the form of (6) by choosing the right  $G$  matrix [22]; here we use a linear nearest neighbor coupling with radius 1 without self loops. In a first instance, we study the system without external control, such as  $F(t) = 0$ . Depending on  $\epsilon$ , we observe four different kinds of collective phenomena. For  $\epsilon < 0.029$  the oscillators are desynchronized. Because of the nearest neighbor coupling for  $0.029 < \epsilon < 0.057$  bursts propagate like traveling waves through the network. For  $\epsilon > 0.057$ , burst synchronization occurs (see Fig. 4). For even larger  $\epsilon$ , a trivial homogeneous state (not shown) occurs. Now we use the meanfield activity as a measure for the degree of synchrony in the system [2].

Here we are mainly interested in the transition of the traveling bursts to synchronous network bursts, and the possibility to induce this transition by an external control signal. As mentioned above, it was observed in thalamic slices that spindle oscillations propagate in a way similar to traveling waves in the absence of corticothalamic projections [14,16]. In [10] the authors examined whether a comparable temporal grouping of spindle activity, coinciding with cortical slow wave oscillations can be found during human slow wave sleep. The results clearly show that also in the human sleep the spindles become synchronized by corticothalamic projections. This phenomenon was part of several numerical and experimental investigations [17,23]; however, the dynamical mechanisms of how cortical slow waves lead to coherent spikes in the thalamus are still unknown.

Finally, we verify our approach computationally in comparison with experimental data. Consequently, we use a hybrid network consisting of a computational model of the thalamic slice, which gets real slow wave sleep EEG data as a common input, to investigate the control of coherence in the thalamic network. While one might argue that the architecture of this model does not reflect nature in detail, as the thalamocortical projections are completely neglected, one reason for this approximation is the fact that the corticothalamic projections outnumber the thalamocortical projections by an order of magnitude [14,24]; second it was shown that slow waves also occur with extensive destruction of the thalamus and transected corpus callosum; these facts indicate that the thalamus is not

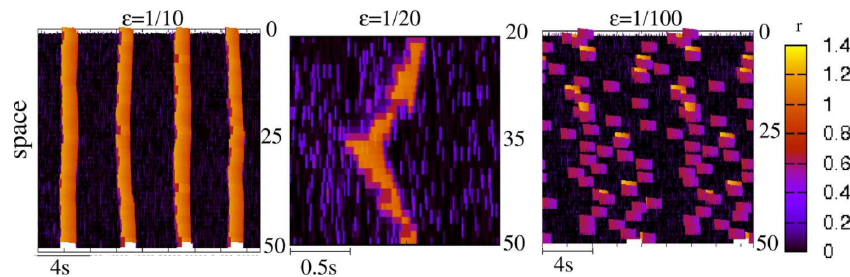


FIG. 4 (color online). Depending on  $\epsilon$  the network shows either asynchronous ( $\epsilon < 0.029$ ) or synchronous oscillations ( $\epsilon > 0.057$ ). Between these two states traveling waves occur.

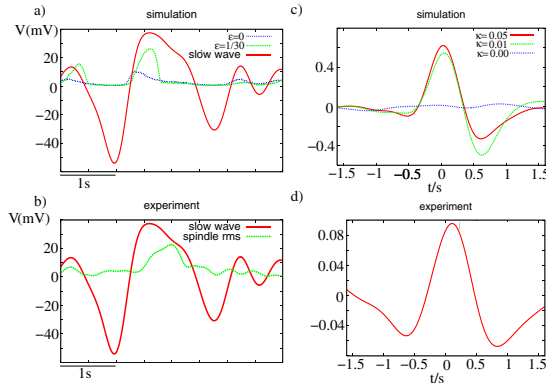


FIG. 5 (color online). Correlation of meanfield network activity  $V = \frac{1}{2500} \sum_i \sum_j r_{ij}$  with driving input signal depending on the driving parameter  $\kappa$  for  $\epsilon = 1/30$ . (a) and (b) Numerical simulation of the network driven by the same EEG spindle sleep data as measured in the experiment [10]. For  $\kappa = 0.0$  correlations vanish. (a) shows that the internal coupling is needed for proper synchronization as without it the meanfield only shows little variations, the reason for this effect is the same as described above for the two neuron network. (c) and (d) The corresponding experimentally obtained correlations between spindle rms which corresponds to the  $r_{ij}$  scaled by a factor of 30 and EEG activity.

essentially involved in the genesis of slow wave rhythm [6]. From both reasons and the results shown in Fig. 5(a) and 5(b) we post that synchronization in the thalamus mainly is controlled through open loop repetitive phase resetting by the cortex, in the same way as described above for the two neuron network. The results obtained by our hybrid network (see Fig. 5) provide a minimal model comparable with the experimental results in [10].

The effect described above was modeled by Steriade's group based on conductance based neuron models [25]. In this detailed biophysical neuron models the dead time or refractory period between two spindle oscillations is caused by the  $I_h$  [13] current, which corresponds to the slow variable  $u$  in our model. In both systems, coherence of thalamic spindles is established by a reset of the slow refractory variable. Our reduced model now allows to identify the dynamical mechanism of this control process by means of threshold modulation. Further, the synchronizing effect gets increased by the depolarizing part of the control signal. As the key mechanism is the reset of the slow refractory variable, this control mechanism should be applicable for a wide range of bistable systems with a slow refractory variable, as cortical slow waves and other neural systems.

To conclude, we have studied the synchronizing influence of corticothalamic projections in a thalamic network by a theoretical model and computationally reproduced the experiment. As the model equations (apart from parameter choices) do not rely specifically on a neural substrate, we anticipate the qualitative behavior to be generic also for

other stochastically driven systems composed of excitable units, like several types of oscillations in the central nervous system.

This research has been supported by the Deutsche Forschungsgemeinschaft (No. SFB 654 "Plasticity and Sleep"). We thank Jan Born and Lisa Marshall for intensive and fruitful discussions.

- [1] K. Wiesenfeld and J.W. Swift, Phys. Rev. E **51**, 1020 (1995); K. Wiesenfeld, C. Bracikowski, G. James, and R. Roy, Phys. Rev. Lett. **65**, 1749 (1990).
- [2] M. G. Rosenblum and A. S. Pikovsky, Phys. Rev. Lett. **92**, 114102 (2004).
- [3] I. Z. Kiss, Y. Zhai, and J.L. Hudson, Phys. Rev. Lett. **88**, 238301 (2002); Science **296**, 1676 (2002).
- [4] J. Buck and E. Buck, Science **159**, 1319 (1968).
- [5] T. J. Walker, Science **166**, 891 (1969).
- [6] M. Steriade, A. Nuñez, and F. Amzica, J. Neurosci. **13**, 3266 (1993).
- [7] Y. Kuramoto, *Chemical Oscillations, Waves & Turbulence* (Springer, New York, 1984); Physica (Amsterdam) **50D**, 15 (1991); A. S. Pikovsky, M. G. Rosenblum, and J. Kurths, Europhys. Lett. **34**, 165 (1996); N. F. Rulkov, Phys. Rev. Lett. **86**, 183 (2001).
- [8] Z. Neda, E. Ravasz, Y. Brechet, T. Vicsek, and A. L. Barabasi, Nature (London) **403**, 849 (2000).
- [9] M. Dhamala, V. K. Jirsa, and M. Ding, Phys. Rev. Lett. **92**, 028101 (2004).
- [10] M. Mölle, L. Marshall, S. Gais, and J. Born, J. Neurosci. **22**, 10941 (2002).
- [11] J. L. Hindmarsh and R. M. Rose, Proc. R. Soc. B **221**, 87 (1984).
- [12] M. Steriade, *The Intact and Sliced Brain* (MIT, Cambridge, MA, 2001).
- [13] A. Destexhe, A. Babloyantz, and T. J. Sejnowski, Biophys. J. **65**, 2473 (1993).
- [14] M. Steriade, Proc. Natl. Acad. Sci. U.S.A. **98**, 3625 (2001).
- [15] U. Kim, M. V. Sanchez-Vives, and D. A. McCormick, Science **278**, 130 (1997).
- [16] A. Destexhe, J. Physiol. (Paris) **94**, 391 (2000).
- [17] D. Contreras, A. Destexhe, T. J. Sejnowski, and M. Steriade, Science **274**, 771 (1996).
- [18] G. Le Masson, S. Renaud-Le Masson, D. Debay, and T. Debay, Nature (London) **417**, 854 (2002).
- [19] J. Mayer, H. G. Schuster, and J. C. Claussen, Phys. Rev. E **73**, 031908 (2006).
- [20] T. Aoyagi, Phys. Rev. Lett. **74**, 4075 (1995).
- [21] J. Ch. Sturm, Bull. Férussac **11**, 419 (1829).
- [22] L. M. Pecora and T. L. Carroll, Phys. Rev. Lett. **80**, 2109 (1998).
- [23] T. Bal, D. Debay, and A. Destexhe, J. Neurosci. **20**, 7478 (2000).
- [24] S. M. Sherman and R. W. Guillery, *Exploring the Thalamus* (Academic, Burlington, 2001).
- [25] A. Destexhe, D. Contreras, and M. Steriade, J. Neurophysiol. **79**, 999 (1998).

### **3.3 Excitation of coherent oscillations in a noisy medium**

PHYSICAL REVIEW E 77, 021916 (2008)

**Excitation of coherent oscillations in a noisy medium**

Jan Köhler, Jörg Mayer, and Heinz Georg Schuster

*Institut für Theoretische Physik und Astrophysik, Christian-Albrechts Universität, Olshausenstraße 40, 24098 Kiel, Germany*

(Received 5 November 2007; revised manuscript received 13 December 2007; published 27 February 2008)

We numerically study the influence of neuronal threshold modulation on the properties of cortical traveling waves. For that reason we simplify a Wilson-Cowan-type integrodifferential equation model of propagating neocortical activity to a spatially discrete version. Further we introduce a noisy threshold. Depending on the noise level we find different states of the network activity, ranging from asynchronous oscillations, traveling waves, to synchronous oscillations. Finally, we induce the transition between these different states by an external modulation.

DOI: [10.1103/PhysRevE.77.021916](https://doi.org/10.1103/PhysRevE.77.021916)

PACS number(s): 87.19.L-, 84.35.+i, 87.19.R-

**I. INTRODUCTION**

A common feature of locally coupled excitable media are traveling waves; accordingly they are observed in physical [1], chemical [2], and biological [3–5] systems. There are several mathematical models describing experimental observed dependence of traveling waves on the system parameters [6–8], like the threshold. A recent work verified the theoretical prediction that modulation of neuronal threshold with electrical fields can increase, decrease, and even block traveling waves in cortical slices [3,4].

A biological example for the occurrence of traveling waves is the deep sleep of mammals [5]. During most of non-REM (NREM) sleep, almost all cortical neurons undergo a slow oscillation in the membrane potential, switching between a silent hyperpolarized state, and active depolarized state of high frequency firing [5,9]. This repetitive change between a depolarized active state and a hyperpolarized silent state occurs, due to the interplay of intrinsic ion currents, in neocortical neurons and network interactions [5,10]. Further cortical slow waves can be generated and sustained by the cortex alone [5,11]. This allows us to study the mechanisms generating cortical slow waves and their excitation in an isolated model for cortical activity. Although slow waves, a striking feature of mammalian NREM sleep, are well studied, only little is known about how they are generated in the cortical network and how to enhance them by external signals.

As cortical slow waves contribute to the long-term consolidation of new memories [9,12], an enhancement of slow wave sleep should help to increase consolidation of previously learned tasks. In a recent study it was shown that transcranial application of slowly oscillating potentials (0.75 Hz), during emerging slow wave sleep, enhances declarative memory performance [9]. Studying open-loop control of cortical slow waves by threshold modulation, might lead to more efficient control signals, and finally improve efficiency of transcranial electric stimulations in clinical applications.

The paper is organized as follows: As numerical simulations of neural systems require spatial discrete networks, we will simplify a Wilson-Cowan-type integrodifferential equation model of propagating neocortical activity, introduced by Pinto and Pinto-Ermentrout, to a spatially discrete model. In

a second step we verify by a numerical simulation, that our simplified model reproduces the threshold dependence of the wave propagation speed in the Pinto-Ermentrout model. Additionally, we introduce a noisy threshold and study the influence of noise on the coherence of a single element and the activity in a one-dimensional (1D) ring. Further, we study wave propagation and coherent oscillation on a two-dimensional (2D) network. Finally, we modulate the threshold periodically and show how to induce synchronous oscillations in the 2D network.

**II. TRAVELING WAVES IN A SPATIAL DISCRETE MODEL**

Experimentally acquired electroencephalography (EEG) data of slow wave oscillations show only the average activity of populations of neurons and give no information about biophysical details such as the spike form or the kinetics of the intrinsic ion currents. Following Freeman [13] and Wilson and Cowan [14] we assume that the functional units of the single brain regions consist of populations of neurons and not of single neurons. The neurons in these populations possess a high connectivity and have a quite similar response to similar inputs. This redundancy allows one to study networks of neuron populations. Here the single variables do not describe membrane potentials of single neurons but rather the average activity of a population of neurons. A very important model of the averaged cortical activity was developed by Wilson and Cowan [14]. In a recent work by Pinto and Ermentrout [3] this model was modified to represent traveling pulse propagation in the disinhibited neocortex. The Pinto-Ermentrout model is given by

$$\begin{aligned} \dot{u}(x,t) + u(x,t) &= \int dx' w(x-x') \theta[u(x',t) - \vartheta] - v(x,t), \\ \dot{v}(x,t) &= \epsilon u(x,t), \end{aligned} \quad (1)$$

where  $w(x-x') = e^{-|x-x'|/2}$  and  $\theta$  is the Heaviside function. As all real neural networks consist of single elements, i.e., the neurons, a continuum model is only valid for very large neural populations. Therefore a natural way to describe the dynamics is a discretization of Eq. (1),



KÖHLER, MAYER, AND SCHUSTER

PHYSICAL REVIEW E 77, 021916 (2008)

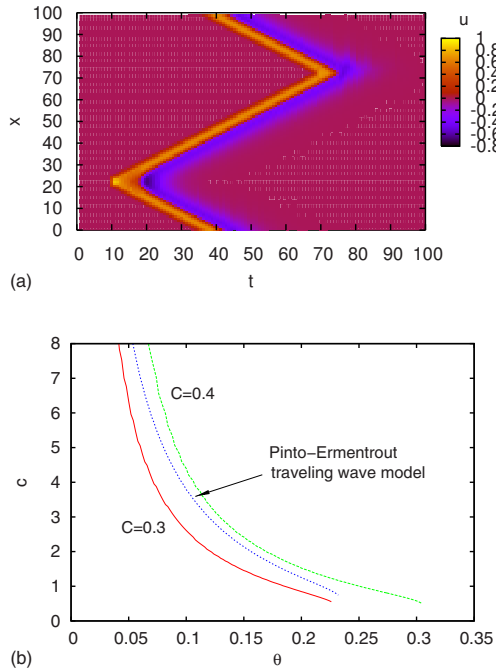


FIG. 1. (Color online) (a) Traveling wave in a 1D network with periodic boundaries. The wave propagates in both directions. Because of the periodic boundaries the wave fronts meet each other and eliminate themselves. (b) The threshold dependences of the velocity of wave propagation in a 1D network for the Pinto-Ermentrout model (blue/dotted) Eq. (1) for  $\epsilon=0.2$ , compared to the spatial discrete model, Eq. (2), with a nearest neighbor coupling, Eq. (3), for  $N=100$  elements with  $A=0.4$ ,  $\epsilon=0.2$ , and  $C=0.3$  (red/solid), respectively,  $C=0.4$  (green/dashed). The characteristic shape of  $c(\vartheta)$  stays qualitatively the same.

$$\begin{aligned} \dot{u}_i + u_i &= \sum_j W_{i,j} \theta[u_j - \vartheta] - v_i, \\ \dot{v}_i &= \epsilon u_i, \end{aligned} \quad (2)$$

where  $W_{i,j}$  is a normalized, towards periphery declining function. Now we go one step further and reduce the coupling function to a nearest neighbor coupling,

$$W_{i,j} := \begin{cases} A: & i=j \\ C: & |i-j|=1 \\ 0: & \text{else,} \end{cases} \quad (3)$$

where  $C$  represents the coupling strength. Figure 1 shows that our spatial discrete model qualitatively reproduces the dependence of the traveling wave's velocity of propagation  $c(\vartheta)$  on the threshold  $\vartheta$ .

### III. NOISY THRESHOLD

Each neuron is under the influence of multiple sources of noise, e.g., synaptic noise, channel noise, and Johnson noise

[15]. Mostly neuronal activity is described by stochastic differential equations with an internal noise in the form of a fluctuating input current. Here we will study the influence of a noisy threshold as done before in Refs. [16,17]. The threshold noise represents the probability that the population can fire even when the activity has not reached the threshold yet or stays quiescent even though the activity is above the threshold [18]. Contrary to what happens when the noise is added to the input current, fully white Gaussian noise cannot be applied. Moreover, the Gaussian distributed white noise term  $\xi_i(t)$  will be updated every  $\Delta t$  times, which leads to the random innovations  $D\xi_i(t_n)$ . Because of the discrete update the sequence  $\xi_i(t_n)$  is somehow colored [19]. But, for  $\Delta t=0.1$ , which is two orders of magnitude lower than the time constant of our model, the coloring of the  $\xi_i(t_n)$  can be neglected. The threshold  $\vartheta$  then becomes  $\vartheta_0 + \xi_i(t_n)$ , where  $\xi_i(t_n)$  are the Gaussian white noise innovations with zero mean and intensity  $D$ .

#### A. Dependence of the collective behavior in a 1D network on the noise intensity

In order to measure the influence of noise on the collective dynamics of the network, we observe the dependence of the squared fluctuation  $\sigma^2$  of the mean field on the noise intensity  $D$ .

$$\sigma^2 := \langle (u(t) - \langle u(t) \rangle)^2 \rangle, \quad (4)$$

$$u(t) := \frac{1}{N} \sum_i u_i(t). \quad (5)$$

Figure 2 shows the squared fluctuation over  $D$  for different values of  $\vartheta$ . We see a pronounced maximum at  $D \approx \vartheta$ , indicating that the network shows coherent oscillations.

Considering a single element, we find that for small and for large noise the spikes appear irregular while the system oscillates coherently for moderate noise  $\vartheta \approx D$ . This effect was first described in [20] for a single excitable system and is called coherence resonance. We will discuss this interesting case for a single element later.

#### B. Dependence of the collective behavior of a 2D network on the noise

In [4] it was shown that applying electrical fields on a neural tissue, leads to effects which can be described by a threshold modulation. For that reason we study the dependence of the collective behavior in a two-dimensional network with periodic boundaries on the noise intensity  $D$  and the threshold  $\vartheta$ . We display the different states in a phase diagram as shown in Fig. 3. We find three different states which can be walked through by tuning either the noise intensity or the threshold of the single element. In the *traveling waves possible* state, an external induced traveling wave can propagate through the network. Up to a certain intensity the noise supports the traveling wave; that means the wave propagates even for large values of  $\vartheta$  (solid line in Fig. 3).

In the traveling waves state the noise occasionally excites a single element, which starts a traveling wave that can

EXCITATION OF COHERENT OSCILLATIONS IN A...

PHYSICAL REVIEW E 77, 021916 (2008)

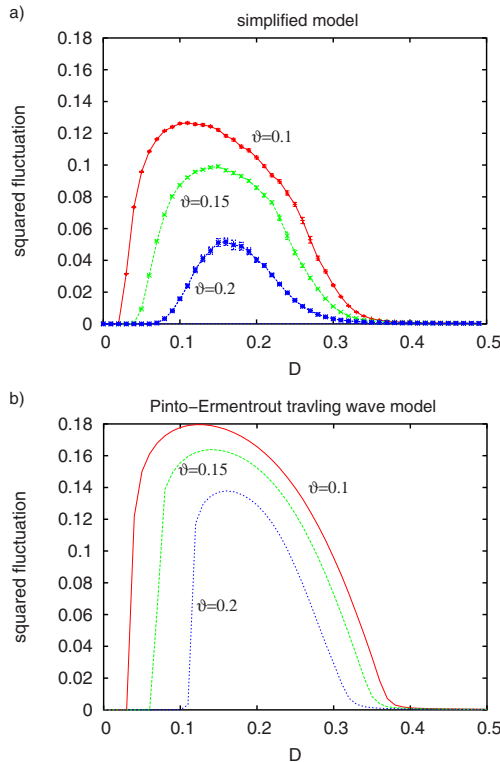


FIG. 2. (Color online) The squared fluctuations of the mean field of a 1D ring consisting of 100 units. (a) The simplified model with  $\epsilon=0.2$ ,  $A=0.4$ ,  $C=0.3$ . (b) The Pinto-Ermentrout traveling wave model with  $\epsilon=0.2$ . Both for  $\vartheta=0.1$  (red/solid),  $\vartheta=0.15$  (green/dashed), and  $\vartheta=0.2$  (blue/dotted). The mean-field fluctuations of both show a strong maximum at  $\vartheta \approx D$ , indicating a coherence resonance of the collective network dynamics.

propagate stably (dashed line in Fig. 3). In the *oscillatory* state the whole network oscillates synchronously. On the transition from the traveling waves state to the oscillatory state the frequency of the traveling wave occurrence rises until the traveling waves occur with resonance frequency where the whole network starts to oscillate synchronously.

### C. Influence of noise on the wave propagation

As seen in Fig. 3, with noise a wave can propagate even for values of the threshold where no traveling waves are observed in the deterministic case. A similar effect was observed experimentally in [21] in subexcitable chemical reactions. Here we are mainly interested if the influence of noise only increases the maximal threshold where waves can still propagate or if it also increases the wave propagation speed  $c(\vartheta)$ . At a first glance, this seems to be reasonable, as in our model the wave propagation speed  $c(\vartheta)$  depends sensitively on the threshold. The numerical simulation in Fig. 4 shows that the noise not only increases the maximal threshold where waves can still propagate, it also increases the wave

propagation speed. Physically the noise acts as a threshold reducer and as such enhances traveling waves.

### D. Noise-induced coherence

The phase diagram shows that coherent oscillations in the network can arise by tuning the noise intensity  $D$ . This behavior was studied in several works for global coupling [22,23]. Here we show numerically that it also occurs with local coupling. We advert that this order is achieved by increasing the intensity of the independent local noise and not by an external periodic forcing as in the case of stochastic resonance. Further, it does not depend on an additional constant drive or the oscillatory nature of the elements.

While the stochastically driven single elements of our network show coherence resonance, the deterministic system does not show self-sustained oscillations but noise of an optimal intensity generates a quasiregular signal. Such noise-driven excitable systems are often considered as coherence resonance oscillators [23]. To explain the influence of noise on the network we first study the influence of noise on the single element. For this purpose we use two different measures. As a measure for the temporal order in the single element we use the characteristic correlation time [20]

$$\tau_c := \int_0^T C^2(t) dt,$$

where  $C(t)$  is the normalized autocorrelation function. We integrate up to  $T=1000$  instead of  $T=\infty$  to prevent divergence in case of a periodic signal. A simple sine wave would have the correlation time  $\tau_c=500$ . As a measure for the spatial coherence in the network we use the squared fluctuation of the mean field. The simulation shows that the synchronization occurs at the same noise intensity as coherence resonance in the single element (Fig. 5). As in a previous work shown for Hodgkin-Huxley neurons, the coherence resonance (CR) is enhanced in two different ways depending on the coupling [24]. For weak coupling only the single element shows CR and no spatiotemporal order is observed. For strong enough coupling, as shown in Fig. 5, the maximum of the local and global coherence measure both jump to a maximum at almost the same noise intensity, indicating spatiotemporal coherence in the network. The reason for that observation is that by the coupling the noise-induced limit cycles stabilize and thus synchronize.

The application of homogenous noise on our network would lead to an identical behavior of all elements. Therefore a single uncoupled element (with an adjusted self-coupling) shows the same behavior as the mean field. As shown in Fig. 5(a), the correlation time of a single element is much less than the correlation time of a network with heterogeneous noise. The mutual stabilization of the noise-induced limit cycles cannot take place if all elements behave exactly the same. For that reason we expect a similar increase as the synchronization with rising noise heterogeneity as shown in [25]. This should also apply to the demonstrated increase of synchronization with rising parameter heterogeneity.

KÖHLER, MAYER, AND SCHUSTER

PHYSICAL REVIEW E 77, 021916 (2008)

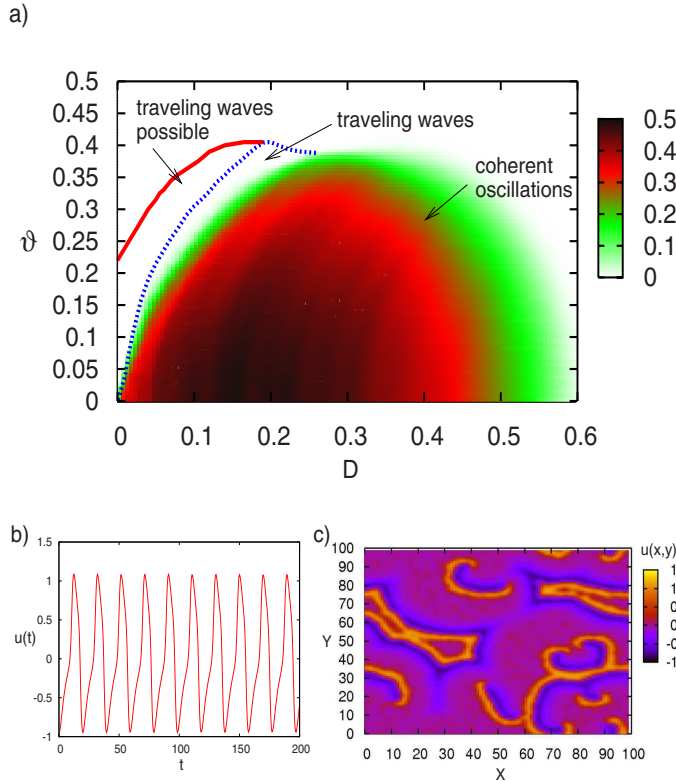


FIG. 3. (Color online) (a) The phase portrait for an  $100 \times 100$  network with  $\epsilon=0.2$ ,  $A=0.4$ ,  $C=0.3$ , and periodic boundary conditions. The color indicates the size of the squared fluctuation: below the red (solid) line traveling waves are possible (traveling waves possible state), and below the blue (dashed) line traveling waves are induced by noise automatically (traveling waves state). (b) The oscillation of the mean field for  $\vartheta=0.2$  and  $D=0.2$ . (c) Noise induces traveling waves for  $\vartheta=0.38$  and  $D=0.18$ .

#### IV. THRESHOLD MODULATION

We modulate the threshold with a square wave and observe the influence of the modulation  $\vartheta(t)$  for the different network states. With the modulation term the Heaviside function in Eq. (2) becomes

$$\theta[u_j(t) + \xi_j(t) + \vartheta(t) - \vartheta_0].$$

We find that the length of the positive and negative parts of the modulation are of minor importance while the resonance

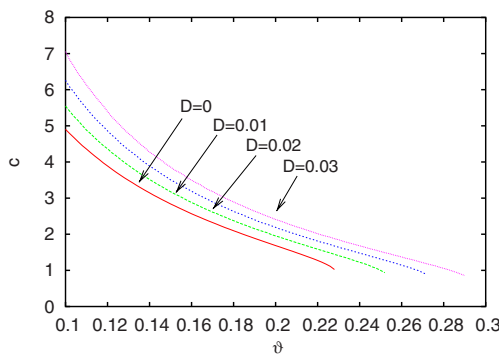


FIG. 4. (Color online)  $c(\vartheta)$  for a  $50 \times 50$  network with  $A=0.4$ ,  $C=0.3$ ,  $\epsilon=0.2$ , and periodic boundary conditions. The wave propagation speed and the maximal threshold where wave propagation is possible increase with the noise intensity  $D$ .

frequency always shows the most effect. Besides the square wave modulation we modulate with only the positive part—and only the negative part of the square wave (Fig. 6).

For small  $D$  (traveling wave and traveling wave possible state) the modulation barely increases the squared fluctuation more than a simple constant threshold modulation. Also the negative modulation has no influence on the oscillation; the positive and the symmetrical modulation show nearly the same effect.

For large noise, however, the squared fluctuation can be increased strongly by square wave modulation, while simple constant modulation has nearly no effect. The negative modulation is less important than the positive modulation, while the square wave has the largest effect.

#### V. CONCLUSION AND OUTLOOK

We showed that the Pinto-Ermentrout traveling wave model can be simplified to a spatially discrete network with nearest neighbor coupling, without losing the main feature—the characteristic shape of  $c(\vartheta)$ . Introducing a noisy threshold we found that the network shows pronounced coherence resonance. Extending the model to a two-dimensional network we showed in a phase diagram the dependence of different network states on the noise intensity and the threshold height. The transition from silent network to self-induced traveling wave to coherent oscillation state can be achieved by either tuning the threshold or the noise intensity. Further-

EXCITATION OF COHERENT OSCILLATIONS IN A...

PHYSICAL REVIEW E 77, 021916 (2008)

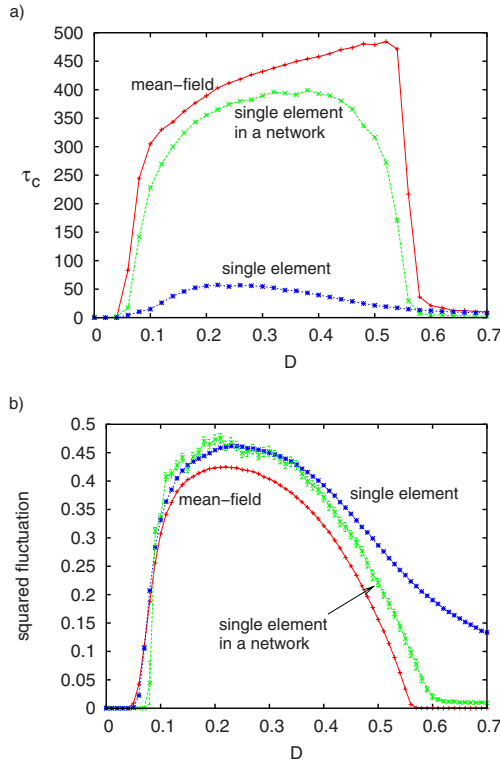


FIG. 5. (Color online) (a) The correlation time  $\tau_c$  for the mean field (red/solid), a single element (green/dashed) in the  $50 \times 50$  network  $A=0.4$ ,  $C=0.3$ , and for a single element (blue/dotted)  $A=1.6$ ,  $C=0$  with  $\vartheta=0.2$  and  $\epsilon=0.2$ . Note that  $\tau_c$  is only a measure for temporal coherence, not for the amplitude of the mean-field oscillations. (b) The associated squared fluctuation as a measure for spatial coherence in the network and a measure of activity for a single element.

more, the wave propagation speed and the maximal threshold where wave propagation is possible increase with the noise intensity. For small noise intensities a threshold modulation with a periodic signal has nearly the same effect as threshold modulation with a constant signal. For larger noise intensities, however, a constant threshold modulation has no effect, while symmetric, positive, and negative modulation increase the oscillation of the network.

In future we will investigate the influence of the coupling range, asymmetric coupling, and network architecture on the different network states. In future works the noise-induced phase transition—shown in our model—will be investigated in chemical and biological systems.

For instance, the threshold and noise level dependence of the network states and the wave propagation speed can be

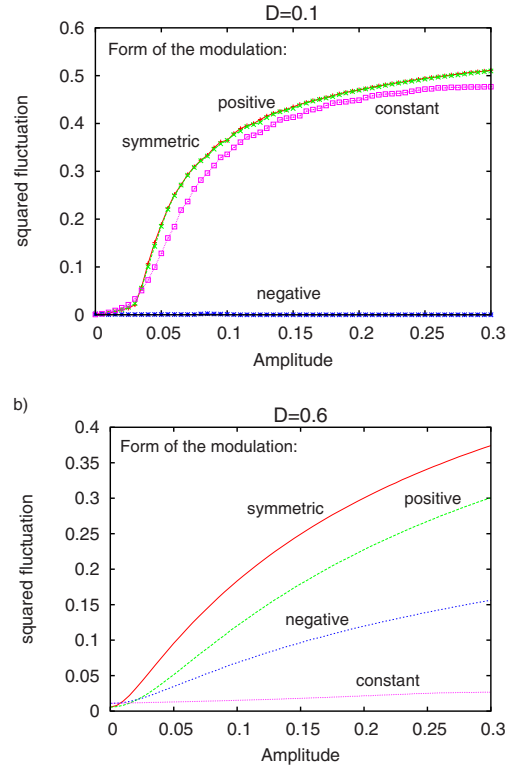


FIG. 6. (Color online) The squared fluctuation over the amplitude of the modulation for a  $50 \times 50$  network with  $\vartheta=0.3$ ,  $\epsilon=0.2$ ,  $A=0.4$ ,  $C=0.3$  and periodic boundary conditions for (a)  $D=0.1$  and (b)  $D=0.6$ . Both compare modulation with a square wave (red/solid), modulation with only the positive part of the square wave (green/dashed), modulation with only the negative part of the square wave (blue/dotted), and constant threshold modulation (purple).

examined with an experimental setup similar to that in [4]. With a high density electrode array [26], threshold height and noise intensity can be tuned individually. Another method to tune the noise intensity is to vary the temperature of the tissue [15,27], however, this is only possible in a certain range as the tissue will be damaged otherwise.

#### ACKNOWLEDGMENTS

The authors wish to thank Jan Born, Matthias Mölle, Lisa Marschal, and Jens Christian Claussen for many discussions. This research has been supported by the DFG financed SFB 654 "Plastizität und Schlaf".

KÖHLER, MAYER, AND SCHUSTER

PHYSICAL REVIEW E **77**, 021916 (2008)

- [1] L. S. Schulman and P. E. Seiden, *Science* **233**, 425 (1986).
- [2] A. N. Zaikin and A. M. Zhabotinsky, *Nature (London)* **225**, 535 (1970).
- [3] D. J. Pinto and G. Bard Ermentrout, *SIAM J. Appl. Math.* **62**, 206 (2001).
- [4] K. A. Richardson, S. J. Schiff, and Bruce J. Gluckman, *Phys. Rev. Lett.* **94**, 028103 (2005).
- [5] M. Massimini, R. Huber, F. Ferrarelli, S. Hill, and G. Tononi, *J. Neurosci.* **24**, 6862 (2004).
- [6] M. C. Cross and P. C. Hohenberg, *Rev. Mod. Phys.* **65**, 851 (1993).
- [7] J. Rinzel, D. Terman, X.-J. Wang, and B. Ermentrout, *Science* **279**, 1351 (1998).
- [8] J. J. Tyson and J. P. Keener, *Physica D* **32**, 327 (1988).
- [9] L. Marshall, H. Helgadóttir, M. Mölle, and J. Born, *Nature (London)* **444**, 610 (2006).
- [10] A. Destexhe, A. Babloyantz, and T. J. Sejnowski, *Biophys. J.* **65**, 1538 (1993).
- [11] M. Steriade, A. Nunez, and F. Amzica, *J. Neurosci.* **13**, 3266 (1993).
- [12] R. Stickgold, *Nature (London)* **437**, 1272 (2005).
- [13] W. Freeman, *Mass Action in the Nervous System* (Academic, New York, 1975).
- [14] H. R. Wilson and J. D. Cowan, *Biol. Cybern.* **13**, 55 (1973).
- [15] W. Gerstner and W. M. Kistler, *Spiking Neuron Models. Single Neurons, Populations, Plasticity* (Cambridge University Press, 2002).
- [16] A. V. Holden, *Models of the stochastic activity of neurones*, 1976.
- [17] B. Lindner, M. J. Chacron, and A. Longtin, *Phys. Rev. E* **72**, 021911 (2005).
- [18] W. Gerstner, *Neural Comput.* **12**, 43 (2000).
- [19] M. Barbi and L. Reale, *BioSystems* **79**, 61 (2004).
- [20] A. S. Pikovsky and J. Kurths, *Phys. Rev. Lett.* **78**, 775 (1997).
- [21] S. Kádár, J. Wang, and K. Showalter, *Nature* **391**, 770 (1998).
- [22] W.-J. Rappel and A. Karma, *Phys. Rev. Lett.* **77**, 3256 (1996).
- [23] S. K. Han, T. G. Yim, D. E. Postnov, and O. V. Sosnovtseva, *Phys. Rev. Lett.* **83**, 1771 (1999).
- [24] Y. Wang, D. T. W. Chik, and Z. D. Wang, *Phys. Rev. E* **61**, 740 (2000).
- [25] C. Zhou, J. Kurths, and B. Hu, *Phys. Rev. Lett.* **87**, 098101 (2001).
- [26] R. A. Malkin and B. D. Pendley, *Am. J. Physiol. Heart Circ. Physiol.* **279**, H437 (2000).
- [27] L. Yang and Y. Jia, *BioSystems* **81**, 267 (2005).

### **3.4 Dynamical mean-field equations for a neural network with spike-timing dependent plasticity**

## Dynamical mean-field equations for a neural network with spike timing dependent plasticity

Jörg Mayer and Heinz Georg Schuster  
*Institut für Theoretische Physik und Astrophysik,  
 Christian-Albrechts Universität, Olshausenstraße 40, 24098 Kiel, Germany*  
 (Dated: April 11, 2008)

We study the discrete dynamics of a fully connected network of threshold elements interacting via dynamically evolving synapses displaying spike timing dependent plasticity. We use dynamical mean-field equations, which become exact in the thermodynamical limit, to study the behavior of the system driven with uncorrelated and correlated Gaussian noise. We find that stochastic independent input leads to a noise dependent transition to the coherent state where all neurons fire together and observe coherence resonance. When correlated noise is used the results depend strongly on the correlation time of the input noise, suggesting a functional benefit of correlated noise for synaptic plasticity.

PACS numbers: PACS number

In neuroscience, the ability of the connections or synapses, between neurons to change in strength, is called plasticity. Half a century ago Donald Hebb [1] postulated that the change of synaptic weights depends on the correlation of pre and postsynaptic cell activity. Experimental evidence indicates that synaptic changes in cortical neurons depend on the precise temporal order between presynaptic and postsynaptic firing [2, 3]. Thus spike time dependent plasticity (STDP) means that presynaptic spikes preceding postsynaptic spikes lead to longterm synaptic potentiation (LTP) whereas reverse time ordering leads to longterm depression (LTD). A bi-directional model of synaptic plasticity, describing both LTP and LTD, has proved necessary for a number of different learning mechanisms in computational neuroscience [4], artificial neural networks [5], and biophysics [2, 6]. Whereas the time evolution of neural networks with either symmetric or asymmetric synapses have been widely investigated in detail and recently synaptic changes have been investigated for oscillator networks numerically [7–9], a mean field theory of dynamical evolving synapses is still missing.

It is well known that noise can play an important and constructive role in a resonant fashion for signal transmission [10], the spreading of traveling waves [12], the coherence of single oscillators [11] and the synchronization of coupled oscillators [12]. The aim of our work is to investigate, by using dynamical mean-field (DMF) equations, how uncorrelated and correlated stochastic input influences the collective behavior of neural networks. We use correlated noise, as noise in the brain is mostly correlated [13] and even changes its color in dependence different stages of consciousness [14]. Our numerical results show that threshold elements interacting via dynamically evolving synapses, detect temporal correlations and allow to draw conclusions on the correlation time of the stochastic input. Furthermore correlated noise clearly outperforms white noise with the same intensity in enhancement of synaptic couplings. Further a deeper understanding of neural plasticity might help to understand

the onset of cortical slow waves [15], which group most other neural rhythms during deep sleep [16, 17].

Our model consists of  $i = 1 \dots N$  neurons whose time dependent activities  $x_i^t$  are updated in parallel according to

$$x_i^t = g(h_i^t) \quad (1)$$

$$h_i^{t+1} = \frac{1}{N} \sum_j J_{ij}^t g(h_j^t) + \xi_i^t \quad (2)$$

Where  $g = \theta(h_i^t - \vartheta)$  is the Heaviside function and  $\vartheta$  the threshold. The variable  $\xi_i^t$  describes stationary uncorrelated or correlated external Gaussian noise

$$\langle \xi_i^t \xi_j^{t'} \rangle = \sigma^2 A(t, t') \delta_{ij} \quad (3)$$

where  $A(t, t') = \exp(-|t - t'|/\tau)$ ,  $\sigma^2$  is the noise intensity,  $\tau$  is the correlation time and the angular brackets denote the average over the noise.  $A(t, t') = \sigma^2 \delta_{tt'}$  describes uncorrelated Gaussian noise. Whereas  $\tau > 0$  describes correlated noise, generated by a first order autoregressive (Ar(1)) process [18, 19].  $J_{ij}^t$  obeys

$$J_{ij}^{t+1} = \lambda J_{ij}^t + (\alpha x_i^{t+1} x_j^t - \beta x_i^t x_j^{t+1}), \quad (4)$$

with the decay time

$$\tau_d = 1/|\ln \lambda|. \quad (5)$$

$J_{ij}^t$  measures the strength of a synapse that leads from neuron  $j$  to neuron  $i$ . We reduce the spike timing dependent plasticity rule to its bare bones by modeling the synaptic change via a temporal asymmetric update rule (4). For causal firing  $J_{ij}^t$  increases by  $\alpha$  whereas it decreases by  $\beta$  if neuron  $i$  fires before neuron  $j$ . The parameter  $\lambda = 0.95$  is introduced to prevent from unphysiological synaptic growth [7, 8]. The fixed point of (4) is given by  $J_{ij} = (\alpha - \beta)/(1 - \lambda)$ , and it is reached in the case where all neurons are in the excited state i.e.  $x_i^t = 1$  for all  $i$ . For given values of  $\sigma$  and  $\vartheta$  the stability of the

fully excited state is determined by the fixed point, accordingly the same results can be achieved for different values of  $\alpha - \beta$  if  $\lambda$  is chosen appropriately. Experimental results suggest that  $\alpha$  is larger than  $\beta$  [20]. Here we choose  $\alpha = 0.55$  and  $\beta = 0.3$  for the following studies. For  $J_{ij}^0 = 0$  we obtain from (4)

$$J_{ij}^t = \sum_{\tau=1}^{t-1} \lambda^{t-1-\tau} (\alpha x_i^{\tau+1} x_j^\tau - \beta x_i^\tau x_j^{\tau+1}) \quad (6)$$

and from (1) and (2)

$$h_i^{t+1} = \sum_{\tau=1}^{t-1} \frac{\lambda^{t-1-\tau}}{N} \left( \alpha x_i^{\tau+1} \sum_j x_j^\tau x_j^t - \beta x_i^\tau \sum_j x_j^{\tau+1} x_j^t \right) + \xi_i^t \quad (7)$$

To study the dynamical properties of the network we use the dynamical functional approach [21–24], which leads from (7) to the generating functional (8)

$$Z = \int_{-\infty}^{+\infty} \prod_{i,t} \frac{dh_i^t d\hat{h}_i^t}{2\pi} \exp \left\{ - \sum_{i,t,t'} \frac{\sigma^2}{2} \hat{h}_i^t R(t,t') \hat{h}_i^{t'} - \sum_{i,t} i \hat{h}_i^t \left[ h_i^{t+1} - \sum_{\tau=1}^{t-1} \frac{\lambda^{t-1-\tau}}{N} \left( \alpha x_i^{\tau+1} \sum_j x_j^\tau x_j^t - \beta x_i^\tau \sum_j x_j^{\tau+1} x_j^t \right) \right] \right\}, \quad (8)$$

where  $R(t,t')$  is the inverse of the correlation function  $A(t,t')$  [25]. After a Hubbard-Stratonovich transformation [26] we obtain in the saddle-point approximation, i.e. for  $N \rightarrow \infty$ , the following effective site independent functional (9)

$$Z^{eff} = \int_{-\infty}^{+\infty} \prod_t \frac{dh^t d\hat{h}^t}{2\pi} \exp[-f\{C^{t,\tau}, h^t, \hat{h}^t\}] \quad (9)$$

and  $f$  is given by

$$f = \sum_t \left\{ \sum_{t'} \frac{\sigma^2}{2} \hat{h}^t R(t,t') \hat{h}^{t'} - i \hat{h}^t \left[ h^{t+1} - \sum_{\tau=1}^{t-1} \lambda^{t-1-\tau} (\alpha C^{t,\tau} x^{\tau+1} - \beta C^{t,\tau+1} x^\tau) \right] \right\} \quad (10)$$

We can translate (9,10) back to an effective single neuron equation for the mean-field which depends only on time

$$h^{t+1} = \sum_{\tau=1}^{t-1} \lambda^{t-1-\tau} (\alpha C^{t,\tau} x^{\tau+1} - \beta C^{t,\tau+1} x^\tau) + \xi^t \quad (11)$$

where  $C^{t,\tau} = \langle x^t x^\tau \rangle$ ,  $x^t = g(h^t)$ , and  $\langle \xi^t \xi^{t'} \rangle = \sigma^2 A(t,t')$ . The correlation function  $C^{t,\tau}$  must be determined self consistently. Equ.(11) is our main result. In the numerical simulation of (11) every time step  $t$  is repeated for  $Q$  realizations, i.e.  $Q$  stochastic independent random numbers  $\xi^t$  are considered for every  $t$ .  $C^{t,\tau}$  is computed for  $\tau$  up to  $t-1$  and averaged over the noise. In this way Equ. (11) is simulated self consistently. Numerical simulations show, that it serves as a good approximation for the network model with large  $N$  ( $> 10000$ ).

We next compare the results obtained from Equ. (11) with a direct simulation of the system (1-4) involving

single neurons. We choose the averaged activity  $S^t$  as a measure for the order in the network

$$S^t = \frac{1}{N} \sum_{i=1}^N \langle x_i^t \rangle. \quad (12)$$

If it is 1 all neurons are in the excited state, if it is zero all neurons are silent. As mentioned above we are also interested in the case of correlated noise to test, whether our simple model of STDP is able to distinguish between correlated and uncorrelated input. Here we will study the influence temporal correlated noise, which is observed in the powerspectrum of the EEG during slow wave sleep [14], generated by an Ar(1) process [18, 19]

In Fig 1 we show the averaged activity  $S^t$  (12) of the system as a function of the noise amplitude  $\sigma$  and the neural threshold  $\vartheta$ . We see that for small noise amplitudes  $\sigma$  the system remains silent, simply because the neural activity is too low to generate synaptic strength



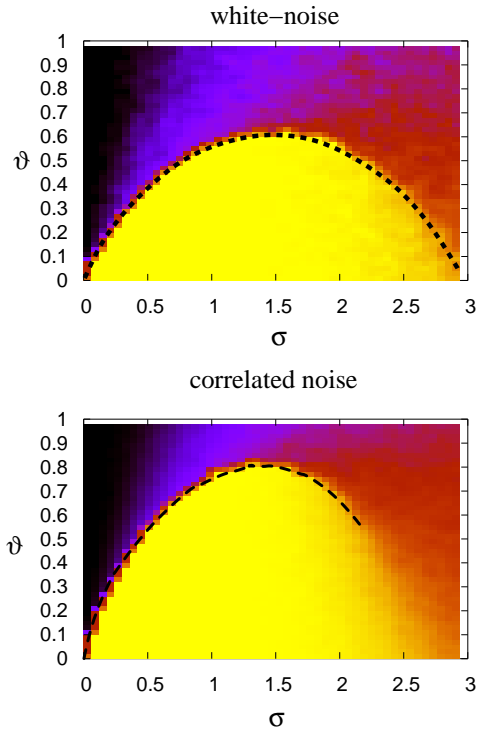


FIG. 1: (color online) Density plot of the averaged activity  $S^t$  for  $t = 1000$  as a function of the neural threshold  $\vartheta$  and the amplitude  $\sigma$  of the uncorrelated noise  $\langle \xi_i^t \xi_j^t \rangle = \sigma^2 \delta_{ij} \delta_{tt'}$  (top) and the correlated noise with correlation time  $\tau = 9.5$  [19] ( $\alpha = 0.55$ ,  $\beta = 0.3$ ,  $\lambda = 0.95$ ). The result for the direct simulation of the network with  $n = 1000$  neurons agrees very well with the mean-field equations (averaged over 1000 realizations) in both cases. The dashed line marks the boundary of the all excited state (yellow/grey) in the DMF model. With correlated noise (bottom) the all excited state reaches to larger thresholds  $\sigma$  than with white noise.

which will not decay via  $\lambda$ . Similarly if the neural threshold becomes too big the neurons cannot be excited, because of the same effect. If the noise amplitude increases the disordering effect of the noise takes over and the neurons will fire randomly with an average activity one half. For an intermediate noise level we observe coherence resonance. We emphasize that this important effect is present in both, the network and the dynamical mean-field model for uncorrelated and correlated noise. Further correlated noise induces the transition to the fully excited state ( $x_i^t = 1$  for all  $i$ ) for values of the threshold  $\sigma$  where it is not possible with white noise. So in our model correlated noise clearly outperforms white noise in enhancement of synaptic couplings.

Fig. 2 shows the averaged activity  $S^t$  (12) of the system as a function of the correlation time  $\tau$  of  $\xi_i^t$  and the

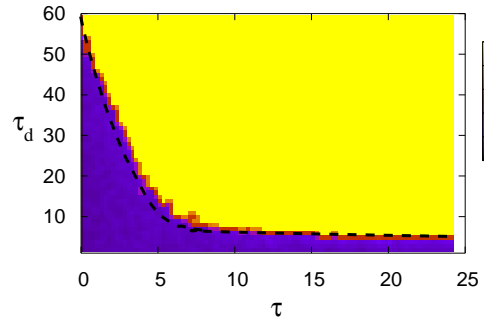


FIG. 2: (color online) Density plot of the averaged activity  $S^t$  for  $t = 1000$  as a function of the synaptic decay time  $\tau_d$  (5) and the correlation time  $\tau$  of the correlated noise  $\xi_i^t$  ([19]) generated as described in [19] ( $\alpha = 0.55$ ,  $\beta = 0.3$ ,  $\lambda = 0.95$ ). Also for correlated noise the result for the direct simulation of the network with  $n = 1000$  neurons agrees very well with the mean-field equations (averaged over 1000 realizations). The dashed line marks the boundary of the all excited state (yellow/grey) in the DMF model

decay time of the synapses  $\tau_d$  (5). In dependence of the correlation time  $\tau$  of the noise the transition to the state with  $x_i^t = 1$  for all  $i$  occurs at different values of the synaptic decay time  $\tau_d$  (5). This allows to discriminate between long and short term temporal correlations by tuning  $\lambda$  in (4).

In Fig. 3 we study the dynamical evolution of the average activity and show the influence of finite size effects. In both models we observe, that with increasing number of the neurons or the number of realizations the curves converge. In the network model the transition to the correlated state occurs always earlier than in the DMF. The reason for this effect is that in the DMF model spatial fluctuations are ignored, but spatial fluctuations accelerate the temporal evolution of the  $J_{ij}$  (4). Such in finite size networks the transition occurs always earlier than in the DMF model.

*To conclude:* We showed that dynamical functionals are an efficient way to reduce the spatiotemporal problem of STDP to site independent DMF-equations. We make the approximation of vanishing spatial fluctuations, which is only exact in the thermodynamic limit. However our simulations show, that the thermodynamic limit is a good approximation for finite populations, in a certain biological reasonable parameter space. Further our studies clearly show that correlated noise outperforms white noise in the generation of synaptic couplings. While stimulation by either periodic or constant electric or magnetic fields is widely known and applied [27], our studies on the noise level and correlation dependence of the behavior implicate that brain stimulation by correlated noise might lead to constructive effects, like for example an

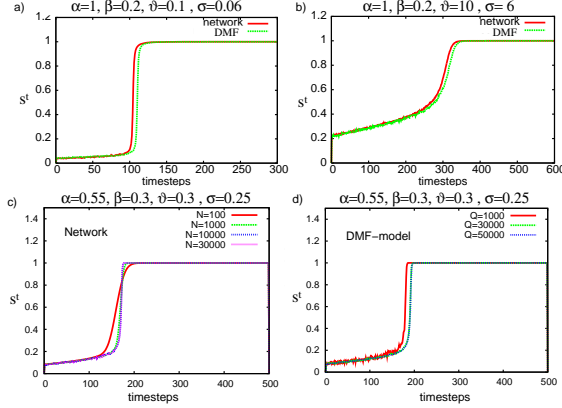


FIG. 3: (color online) Temporal evolution of the averaged activity  $S^t$  (12) for different values of the system parameters, for the network (red/solid) (with size  $N=300000$ ) and for the DMF model (green/dashed) (averaged over  $Q=50000$  realizations) with uncorrelated white noise  $\langle \xi_i^t \xi_j^{t'} \rangle = \sigma^2 \delta_{ij} \delta_{tt'}$ . a) and b): large difference between  $\alpha$  and  $\beta$ , for low noise level a sudden transition occurs where all neurons are in the excited state  $x_i^t = 1$  for all  $i$ , for high noise level  $\sigma$  combined with large  $\theta$  the transition occurs a lot smoother. c) and d) little difference between  $\alpha$  and  $\beta$ , here finite size effects play an important role, but also here in both models the curves coalesce if  $N$  and  $Q$  are getting larger

enhancement of spike timing dependent learning. In future works the evolution of initially imprinted activity-patterns will be in the focus of our work, further we want to study synchronization of threshold elements with a dead-time, coupled via synapses showing STDP.

This research has been supported by the Deutsche Forschungsgemeinschaft (DFG) within SFB 654 "Plasticity and Sleep". The authors thank Jan Born and Udo Erdmann for intensive and fruitful discussions.

[1] D. Hebb, *The Organization of Behavior: a neuropsychological approach*, New York: Wiley VCH, (1949)  
 [2] H. Markram, J. Lübke, M. Frotscher, and B. Sakmann, *Science* **275**, 213 (1997); G. Q. Bi and M. Poo, *J. Neurosci.* **18**, 10464 (1998); *Annu. Rev. Neurosci.* **24**, 139 (2001); G. M. Wittenberg and S. S.-H. Wang, *J. Neurosci.* **26**, 6610 (2006); J.-P. Pfister and W. Gerstner, *ibid.* **26**, 9673 (2006).  
 [3] G. M. Wittenberg, M.R. Sullivan and J.Z. Tsien, *Hippocampus* **12** 637 (2002)

[4] Gastone C. Castellani, Elizabeth M. Quinlan, Leon N Cooper, and Harel Z. Shouvalb, *PNAS*, **98**, 12772, (2001)  
 [5] Bienenstock, E. L., Cooper, L. N, and Munro, P. W., *J. o. Neurosci.* **2**, 32, (1982)  
 [6] S. Song, K. D. Miller, and L. F. Abbott, *Nat. Neurosci.* **3**, 919 (2000)  
 [7] P. Tass and M. Majtanik., *Biol. Cybern.*, **94**, 58 (2006)  
 [8] Yuri L. Maistrenko, Borys Lysyansky, Christian Hauptmann, Oleksandr Burylko, and Peter A. Tass, *Phys. Rev. E* **75**, 066207 (2007)  
 [9] J. Rubin, D.D. Lee and H. Sompolinsky. *Phys. Rev. Lett* **86**, 364 (2001)  
 [10] Benzi R., Sutera A., and Vulpiani A., *J. Phys. A* **14**, L453-L457 (1981)  
 [11] A. S. Pikovsky, J. Kurths, *Phys. Rev. Lett.* **78**, 775 - 778 (1997)  
 [12] J. Köhler, J. Mayer, H.G. Schuster, *Phys. Rev. E* **77**, 021916 (2008)  
 [13] R. Soma, D. Nozaki, S. Kwak, Y. Yamamoto, *Phys. Rev. Lett.* **91**, 078101 (2003)  
 [14] R. Ferri, F. Rundo, O. Bruni, M. G. Terzano, C. J. Stam, *Clinical Neurophysiology*, **116**, 2783, (2005)  
 [15] Huber R, Ghilardi MG, Massimini M, Ferrarelli F, Riedner BA, Peterson MJ, Tononi G., *Nat. Neuroscience*, **9** 1169 (2006)  
 [16] M. Mölle, L. Marshall, S. Gais and J. Born, *Journal of Neuroscience*, **22**, 10941, (2002)  
 [17] J. Mayer, H. G. Schuster, J. C. Claussen, M. Mölle, *Phys. Rev. Lett.* **99**, 068102 (2007)  
 [18] A. Kiraly, I. M. Janosi *Phys. Rev. E* **65**, 051102 (2002); C. Chatfield, *The Analysis of Time Series: An Introduction*, sixth edition, Chapman and Hall/CRC, (2003); S. Erland, P. E. Greenwood, *Phys. Rev. E* **76**, 031114 (2007)  
 [19] We generate the correlated noise by an Ar(1) process  $\tilde{\xi}_i^{t+1} = \gamma \tilde{\xi}_i^t + \eta_i^t$ , where  $\eta_i^t$  describes Gaussian white noise  $\langle \eta_i^t \eta_j^{t'} \rangle = \sigma^2 \delta_{ij} \delta_{tt'}$ . After a rescaling to obtain a noise-intensity independent of  $\gamma$  and with negligence of the initial conditions [18], the autocorrelation function obeys  $\langle \xi_i^t \xi_j^{t'} \rangle = \sigma^2 \exp(-|t-t'|/\tau)$  where  $\xi_i^t$  is the rescaled noise,  $\tau = 1/|\log \gamma|$  and  $0 < \gamma < 1$ .  
 [20] Zhang, L.I., Tao, H.-z.W., Holt, C.E., Harris, W.A. and Poo, M.-m. *Nature* **395**, 37 (1998)  
 [21] H. Sompolinsky and A. Zippelius. *Phys.Rev.* **B 25**, 6860 (1982)  
 [22] L. Molgedey, J. Schuchhardt and H. G. Schuster, *Phys. Rev. Lett.* **69**, 3717 (1992)  
 [23] H. Eissfeller, M. Oppen. *Phys. Rev. Lett.* **68**, 2094 (1992)  
 [24] H.G. Schuster, *Complex Adaptive Systems*, Scator Publ. Saarbruecken (2001) p. 207.  
 [25] H.S. Wio, P. Colet, M. SanMiguel, L. Pesquera, M.A. Rodriguez, *Phys. Rev. A* **40**, 7312 (1989)  
 [26] R.L. Stratonovich. *Dokl. Akad. Nauk SSSR* **115** (1957), J. Hubbard. *Phys. Rev. Lett.* **3** (1959)  
 [27] L. Marshall, H. Helgadottir, M. Mölle and Jan Born, *Nature* **444**, 610 (2006)

# 4 Discussion

## 4.1 Conclusions

In this thesis, thalamic oscillations are modeled and analyzed on different levels of description. The widely used conductance based neuron models form the motivation for several simplifications. One might argue that these simplifications do not resemble biological complexity of neuronal models, as the biophysical basis of neurons, the ion channels, is disregarded. If we consider the dynamical behavior of the thalamic circuit, modeled by conductance based neuron models and our extended Hindmarsh-Rose equations, both systems show qualitative similar effects. Our four-variable extension of the Hindmarsh-Rose model reproduces the spindle oscillations quite good. The extension was directly motivated from the biophysical model and necessary, because without it no waxing and waning oscillations are possible. One of the main insights won by these extensive studies on the thalamic circuit and the single neurons is the following: From the generation of an action potential, over the adaptive threshold, to the waxing and waning spindle oscillations, neural behavior depends critically on the existence of processes working on different time scales. Contrary to the often as constant considered threshold, the ability of the neural threshold to adapt to external forces plays a crucial role in thalamic relay neurons. The adaptive threshold allows the neurons to respond to a strong inhibition by a down regulation of the threshold. As this adaptive process is slow compared to the process responsible for the action potential, a sudden decrease in inhibition leads to an overshoot of the membrane potential resulting in a spike or even a burst of several spikes. In the presence of strong inhibition, this postinhibitory rebound leads to very robust metastable self-oscillations in the thalamic circuit, which are initiated by an input spike and terminated by an additional even slower process. During the oscillatory phase, the incoming signals are masked and thereby the information transfer reduces significantly. As during sleep, or by almost all anesthetics, inhibitory neurotransmitters are released, this multi time scale effect might be the mechanism responsible for the loss of sensory perception during sleep and anesthesia.

In the second part of this thesis, different types of network behavior are studied. For that reason, the insights won from the study of the elementary thalamic circuit are used to derive a canonical model for thalamic oscillations, which allows to study synchronization in large networks. Although this model incorporates only the most salient dynamical features of the thalamic circuit, it allows to reproduce several experimental results qualitatively. Spindle oscillations observed in the EEG are believed to be the result of millions of synchronously oscillating neurons. EEG studies show that the thalamic spindles are temporally grouped by cortical slow-wave activity (Möller *et al.*, 2002). It is assumed that this

temporal grouping is associated by a synchronization of thalamic oscillations. By using a network consisting of locally coupled bistable elements, we could reproduce the experimental observed grouping of thalamic spindles when slow-wave EEG-data were used as a control signal. The simplicity of our model allowed to identify the underlying dynamical mechanism, which can be described as a repetitive phase resetting of the process leading to the long silent periods between the spindles. One might argue that the architecture of this model does not reflect nature in detail, as the connections from the thalamus to the cortex are completely neglected, however several experiments figured in this thesis, indicate that the thalamus is not essentially involved in the genesis of slow-wave rhythm (Steriade *et al.*, 1993b).

As mentioned above, it is believed that the sleep slow oscillation is initiated maintained and terminated by the cortex alone (Tononi *et al.*, 2006). Probably the best-known model for the cortical activity is the Wilson Cowan model (Wilson and Cowan, 1973). Pinto and Ermentrout (Pinto and Ermentrout, 2001) modified this model to represent traveling pulse propagation in the disinhibited neocortex. However, the Pinto-Ermentrout traveling wave model assumes a continuous medium, as all real neural network consist of single elements, i.e. the neurons, a continuum model is only valid for very large neural populations. We derived a discretized version of this model and studied the behavior of a 2-dimensional network. As recent experiments indicate that cortical activity can be influenced by external electric signals (Marshall *et al.*, 2006), which are believed to modulate the threshold (Richardson *et al.*, 2005b) of the neurons, we investigated several kinds of threshold modulation. In our model, we showed that modulations of the threshold by Gaussian noise allow a precise tuning of the network behavior. It is well known that noise plays a constructive role in many complex systems, our results suggest that brain stimulation by noise might also have a beneficial role for slow-wave sleep. However, it is a technical challenge to verify our computational study on the noise dependence of cortical activity.

The hypothesis of synaptic sleep homeostasis posts that slow-wave sleep emerges by a total increase of the synaptic weights during waking, resembling an increase of the mean-field coupling strength. A possible mechanism responsible for this increase of connectivity is spike-timing dependent plasticity (STDP), a special form of Hebbian learning. We reduced spike-timing dependent plasticity to its bare bones, by using a time discrete update rule for synaptic strengths. We show that in a fully connected network of threshold elements, coupled by synapses displaying STDP, a transition to a stable coherent state occurs. Further we found that correlated noise increases synaptic growth compared to uncorrelated input, what reproduces experimental observations (Huber *et al.*, 2004) qualitatively. Besides these phenomenological observations to our best knowledge it is the first work in which a mean-field theory for spike-timing dependent plasticity is derived, allowing computational treatment without spatial finite size effects. Despite these interesting findings, it has to be mentioned that further studies are necessary to test whether our strongly simplified model resembles important features of synaptic plasticity like the strengthening of initially imprinted patterns.

Altogether, in this thesis several aspects of sleep in the thalamocortical system were treated, ranging from single cell dynamics over thalamic and cortical network activity to a

model of synaptic potentiation. A common feature of all models derived and used in this thesis is the description of neural activity on a phenomenological level of description, coarse graining out details but preserving the dynamical behavior. Besides this conclusion, our computational models allow some experimentally testable forecasts, which will be given in the outlook.

## 4.2 Outlook

Our simplified models allow to analyze the dynamic behavior of large networks. So far, synchronization in a thalamic network, cortical activity in cortical network and synaptic potentiation in a model for cortical synapses have been treated. The future plans can be divided into two directions, on the one hand further open questions in a theoretical manner of the observed phenomena is needed and on the other hand the models derived should be used to make experimentally verifiable forecasts. In this thesis synchronization of thalamic spindles has been modeled by open loop control, however, the thalamocortical system forms a closed feedback loop. Though the architecture used in this thesis is reasonable, in a next step the model for cortical and thalamic activity should be coupled. A long-term goal is to be able to reproduce the temporal grouping of thalamic spindles by the cortical slow-waves, observed in the EEG, in a computational model where this effect is selforganized in the thalamocortical feedback loop. This work will take place in close cooperation with the clinical research group of Jan Born at the medical university in Lübeck. It is planned to use experimental results to create a large-scale model of the thalamocortical system, which in turn should lead to improved protocols for clinical studies. Of particular interest is the connection between slow-wave oscillations and spindle oscillations at the onset of NREM sleep. Experimental results suggest that the slow-wave originates in the anterior cortex and travels to the posterior cortex (Massimini *et al.*, 2004a). A goal will be to model that effect and understand the underlying mechanisms. Further, a large-scale model of the thalamocortical system allows to study detailed influence of external control signals on cortical and thalamic activity.

A canonical model for the onset of slow-wave oscillations has already been studied in (Schuster *et al.*, 2008), it is found that in this model the onset to slow-wave oscillations occurs by a Hopf bifurcation and terminates by a saddle-node bifurcation. It is believed that the thalamus plays a decisive role for consciousness besides relaying incoming information. An unsolved question is how different areas of the cortex communicate during waking and why this communication comes to a breakdown during slow-wave sleep (Massimini *et al.*, 2005). A possible explanation for this effect is that the thalamus is also incorporated in the communication between different cortical areas, what was already shown for the visual system (Guillery and Sherman, 2002). A large-scale model of the thalamocortical system might help to gain insight in this exciting question.

From a theoretical point of view, synchronization of oscillators with different time scales is of great importance for the understanding of neural systems. However, in networks of coupled neurons only a few analytical results are possible. In (Schuster and Mayer, 2008)

the influence of inhibition of coupled oscillators working on different timescales is studied mathematical rigorous. It is found that with inhibitory coupling it is the slowest oscillator who dominates the fast one: In the synchronous case, the slowest oscillator determines the frequency of the mean field.

The complexity of the central nervous system requires several extensions of the systems considered here. A widely open field of research is the influence of the network architecture on the observed phenomena. Mostly only two extremes of couplings are considered, namely all to all or nearest neighbor coupling. In particular, the computational models of cortical activity have to be extended by a complex network architecture like small world networks. Computational results indicate that slow-wave oscillations critically depend on long-range connections in cortical slices (Compte *et al.*, 2003). As only little is known about the network architecture and large-scale connectivity in the cortex, a close cooperation with experimentalists is irreplaceable.

May be the most promising and exciting field for future work is the modeling of sleep homeostasis. In (Mayer and Schuster, 2008) a model for synaptic potentiation is suggested. This model allows in principle to reproduce the local sleep hypothesis in (Huber *et al.*, 2004), we will test our model for this feature within the next months in a network with spatial inhomogeneous correlated input. Further the evolution of initially imprinted patterns will be studied under the influence of noise. However probably the most important effect of downscaling and synaptic consolidation has not been understood up to now. Several experiments indicate that the down regulation and consolidation of synapses takes place during sleep. Here a close collaboration with experimentalists is necessary to make models which are biological reasonable and allow verifiable forecasts. A computational model reproducing this effect is a long time goal in computational neuroscience. Here first computational simulations show promising results by considering bursting neurons coupled via spike-timing dependent plasticity.

# Bibliography

- Abbott, L. F. and Gerstner, W. (2004). Homeostasis and learning through spike-timing dependent plasticity. *Methods and models in neurophysics*.
- Abbott, L. F. and Kepler, T. B. (1990). Model neurons: from hodgkin-huxley to hopfield. In L. Garrido, editor, *Statistical Mechanics of Neural Networks*, pages 5–18, Springer-Verlag, Berlin.
- Achermann, P. and Borbély, A. A. (1997). Low-frequency ( $\approx$  1Hz) oscillations in the human sleep electroencephalogram. *Neuroscience*, **81**:213.
- Achermann, P., Dijk, D. J., Brunner, D. P., and Borbely, A. A. (1993). A model of human sleep homeostasis based on EEG slow-wave activity: quantitative comparison of data and simulations. *Brain Res Bull*, **31**:97.
- Ahlsén, G., Lindström, S., and Lo, F. S. (1985). Interaction between inhibitory pathways to principal cells in the lateral geniculate nucleus of the cat. *Experimental Brain Research*, **58**:134.
- Amzica, F. and Steriade, M. (1995a). Disconnection of intracortical synaptic linkages disrupts synchronization of a slow oscillation. *Journal of Neuroscience*, **15**:4658.
- Amzica, F. and Steriade, M. (1995b). Short-and long-range neuronal synchronization of the slow ( $\approx$  1 Hz) cortical oscillation. *Journal of Neurophysiology*, **73**:20.
- Aoyagi, T. (1995). Network of Neural Oscillators for Retrieving Phase Information. *Physical Review Letters*, **74**:4075.
- Argyris, J., Haase, M., and Faust, G. (1994). *Die Erforschung des Chaos: Eine Einführung fuer Naturwissenschaftler und Ingenieure/John Argyris, Gunter Faust, Maria Haase*. Vieweg.
- Bair, W., Zohary, E., and Newsome, W. T. (2001). Correlated Firing in Macaque Visual Area MT: Time Scales and Relationship to Behavior. *Journal of Neuroscience*, **21**:1676.
- Bal, T., Debay, D., and Destexhe, A. (2000). Cortical Feedback Controls the Frequency and Synchrony of Oscillations in the Visual Thalamus. *Journal of Neuroscience*, **20**:7478.
- Bazhenov, M., Timofeev, I., Steriade, M., and Sejnowski, T. J. (2002). Model of Thalamocortical Slow-Wave Sleep Oscillations and Transitions to Activated States. *Journal of Neuroscience*, **22**:8691.

- Bennett, M. (2002). Huygens's clocks. *Proceedings: Mathematical, Physical and Engineering Sciences*, **458**:563.
- Beurrier, C., Congar, P., Bioulac, B., and Hammond, C. (1999). Subthalamic Nucleus Neurons Switch from Single-Spike Activity to Burst-Firing Mode. *Journal of Neuroscience*, **19**:599.
- Bi, G. and Poo, M. (1998). Synaptic Modifications in Cultured Hippocampal Neurons: Dependence on Spike Timing, Synaptic Strength, and Postsynaptic Cell Type. *Journal of Neuroscience*, **18**:10464.
- Birbaumer, N. and Schmidt, R. F. (1996). *Biologische Psychologie*. Springer New York.
- Borbely, A. A., Tobler, I., and Hanagasioglu, M. (1984). Effect of sleep deprivation on sleep and EEG power spectra in the rat. *Behav Brain Res*, **14**:171.
- Chen, R. (1997). Depression of motor cortex excitability by low-frequency transcranial magnetic stimulation. *Neurology*, **48**:1398.
- Chudler, H., Eric (2008). <http://fc.units.it/ppb/neurobiol/Neuroscienze>.
- Coenen, A. M. L. and Vendrik, A. J. H. (1972). Determination of the transfer ratio of cat's geniculate neurons through quasi-intracellular recordings and the relation with the level of alertness. *Experimental Brain Research*, **14**:227.
- Colet, P., Wio, H. S., and San Miguel, M. (1989). Colored noise: A perspective from a path-integral formalism. *Physical Review A*, **39**:6094.
- Compte, A., Sanchez-Vives, M. V., McCormick, D. A., and Wang, X. J. (2003). Cellular and Network Mechanisms of Slow Oscillatory Activity ( $\approx 1$  Hz) and Wave Propagations in a Cortical Network Model. *Journal of Neurophysiology*, **89**:2707.
- Contreras, D., Destexhe, A., Sejnowski, T. J., and Steriade, M. (1996). Control of Spatiotemporal Coherence of a Thalamic Oscillation by Corticothalamic Feedback. *Science*, **274**:771.
- Destexhe, A. (2000). Modelling corticothalamic feedback and the gating of the thalamus by the cerebral cortex. *Journal of Physiology-Paris*, **94**:391.
- Destexhe, A. and Babloyantz, A. (1993). A Model of the Inward Current  $I_h$  and its possible role in thalamocortical oscillations. *NeuroReport*, **4**:223.
- Destexhe, A., Babloyantz, A., and Sejnowski, T. J. (1993a). Ionic mechanisms for intrinsic slow oscillations in thalamic relay neurons. *Biophysical Journal*, **65**:1538.
- Destexhe, A., Contreras, D., and Steriade, M. (1998). Mechanisms Underlying the Synchronizing Action of Corticothalamic Feedback Through Inhibition of Thalamic Relay Cells. *Journal of Neurophysiology*, **79**:999.



- Destexhe, A., McCormick, D. A., and Sejnowski, T. J. (1993b). A model for 8-10 Hz spindling in interconnected thalamic relay and reticularis neurons. *Biophysical Journal*, **65**:2473.
- Diesmann, M., Gewaltig, M. O., and Aertsen, A. (1999). Stable propagation of synchronous spiking in cortical neural networks. *Nature*, **402**:529.
- Ermentrout, G. B. (1999). XPP-Aut: X-windows PhasePlane plus Auto.
- FitzHugh, R. (1961). Impulses and Physiological States in Theoretical Models of Nerve Membrane. *Biophysical Journal*, **1**:445.
- Freeman, W. (New York 1975). *Mass Action in the Nervous System*. Academic Press.
- Fuentealba, P., Timofeev, I., Bazhenov, M., Sejnowski, T. J., and Steriade, M. (2005). Membrane Bistability in Thalamic Reticular Neurons During Spindle Oscillations. *Journal of Neurophysiology*, **93**:294.
- Gais, S. and Born, J. (2004). Low acetylcholine during slow-wave sleep is critical for declarative memory consolidation. *Proceedings of the National Academy of Sciences*, **101**:2140.
- Gardiner, C. W. (1985). *Handbook of stochastic methods for physics, chemistry, and the natural sciences*. Springer.
- Gerstner, W. and Kistler, W. M. (2002a). *Spiking neuron models*. Cambridge University Press New York.
- Gerstner, W. and Kistler, W. M. (2002b). *Spiking Neuron Models. Single Neurons, Populations, Plasticity*. Cambridge University Press .
- Guillery, R. W. and Sherman, S. M. (2002). Thalamic Relay Functions and Their Role in Corticocortical Communication Generalizations from the Visual System. *Neuron*, **33**:163.
- Haken, H. (1983). Synergetics. an introduction. *Springer Series in Synergetics*.
- Hebb, D. O. (1949). *The organization of behavior*. MIT Press Cambridge, MA, USA.
- Hill, S. and Tononi, G. (2005). Modeling Sleep and Wakefulness in the Thalamocortical System. *Journal of Neurophysiology*, **93**:1671.
- Hindmarsh, J. L. and Rose, R. M. (1984). A Model of Neuronal Bursting Using Three Coupled First Order Differential Equations. *Proceedings of the Royal Society of London. Series B, Biological Sciences*, **221**:87.
- HMS (2008). <http://cdn.channel.aol.com/body/hv/101940>. Harvard Health Publications (Harvard Medical School).

- Hodgkin, A. L. and Huxley, A. F. (1952). A quantitative description of membrane current and its application to conduction and excitation in nerve. *The Journal of Physiology*, **117**:500.
- Holler, I., Siebner, H. R., Cunnington, R., and Gerschlagner, W. (2006). 5Hz repetitive TMS increases anticipatory motor activity in the human cortex. *Neuroscience Letters*, **392**:221.
- Hubbard, J. (1959). Calculation of Partition Functions. *Physical Review Letters*, **3**:77.
- Huber, R., Ghilardi, M. F., and Massimini, M. (2004). Local sleep and learning. *Nature*, **430**:78.
- Izhikevich, E. M. (2000). Neural excitability, spiking and bursting. *International Journal of Bifurcation and Chaos*, **10**:1171.
- Izhikevich, E. M. (2003). Simple models of spiking neurons. *IEEE Transactions on Neural Networks*, **14**:1569.
- Izhikevich, E. M. (2007). *Dynamical Systems in Neuroscience: The Geometry of Excitability and Bursting*. MIT Press.
- Kim, U., Bal, T., and McCormick, D. A. (1995). Spindle waves are propagating synchronized oscillations in the ferret LGNd in vitro. *Journal of Neurophysiology*, **74**:1301.
- Kiss, I. Z., Zhai, Y., and Hudson, J. L. (2002). Emerging Coherence in a Population of Chemical Oscillators. *Science*, **296**:1676.
- Köhler, J., Mayer, J., and Schuster, H. G. (2008). Excitation of coherent oscillations in a noisy medium. *Physical Review E*, **77**:21916.
- Kuramoto, Y. (1984). *Chemical oscillations, waves, and turbulence Springer series in synergetics*. Springer-Verlag.
- Le Masson, G., Renaud-Le Masson, S., Debay, D., and Bal, T. (2002). Feedback inhibition controls spike transfer in hybrid thalamic circuits. *Nature*, **417**:854.
- Livingstone, M. S., Hubel, D. H., and Recording, S. C. (2003). Effects of Sleep and Arousal on the Processing of Visual Information in the Cat. In *Essential Sources in the Scientific Study of Consciousness*, Mit Pr.
- Maistrenko, Y. L., Lysyansky, B., Hauptmann, C., Burylko, O., and Tass, P. A. (2007). Multistability in the Kuramoto model with synaptic plasticity. *Physical Review E*, **75**:66207.
- Markram, H., Lubke, J., Frotscher, M., and Sakmann, B. (1997). Regulation of Synaptic Efficacy by Coincidence of Postsynaptic APs and EPSPs. *Science*, **275**:213.

- Marshall, L., Helgadottir, H., Molle, M., and Born, J. (2006). Boosting slow oscillations during sleep potentiates memory. *Nature*, **444**:559.
- Marshall, L., Helgadóttir, H., Mölle, M., and Born, J. (2006). Boosting slow oscillations during sleep potentiates memory. *nature*, **444**:610.
- Marshall, L., Mölle, M., and Born, J. (2003). Spindle and slow-wave rhythms at slow-wave sleep transitions are linked to strong shifts in the cortical direct current potential. *Neuroscience*, **121**:1047.
- Massimini, M., Ferrarelli, F., Huber, R., Esser, S. K., Singh, H., and Tononi, G. (2005). Breakdown of Cortical Effective Connectivity During Sleep. *Science*, **309**:2228.
- Massimini, M., Huber, R., Ferrarelli, F., Hill, S., and Tononi, G. (2004a). The Sleep Slow Oscillation as a Traveling Wave. *Journal of Neuroscience*, **24**:6862.
- Massimini, M., Huber, R., Ferrarelli, F., Hill, S., and Tononi, G. (2004b). The Sleep Slow Oscillation as a Traveling Wave. *J. Neurosci.*, **24**:6862.
- Matthews, G. G. (2001). *Neurobiology: Molecules, Cells, and Systems*. Blackwell Publishing.
- Matthews, G. G. (2003). *Cellular Physiology of Nerve and Muscle*. Blackwell Publishing.
- Mayer, J. (2004). *Modellierung und analyse neuronaler dynamiken im thalamus, Diplomarbeit*. Master's thesis, Christian Albrechts Universität zu Kiel.
- Mayer, J. and Schuster, H. G. (2008). Dynamical mean-field equations for a neural network with spike timing dependent plasticity. *submitted to Physical Review Letters*.
- Mayer, J., Schuster, H. G., and Claussen, J. C. (2006). Role of inhibitory feedback for information processing in thalamocortical circuits. *Physical Review E*, **73**:31908.
- Mayer, J., Schuster, H. G., Claussen, J. C., and Mölle, M. (2007). Corticothalamic Projections Control Synchronization in Locally Coupled Bistable Thalamic Oscillators. *Physical Review Letters*, **99**:021916.
- McCulloch, W. S. and Pitts, W. (1943). A logical calculus of the ideas immanent in nervous activity. *Bulletin of Mathematical Biology*, **5**:115.
- Molgedey, L., Schuchhardt, J., and Schuster, H. G. (1992). Suppressing chaos in neural networks by noise. *Physical Review Letters*, **69**:3717.
- Mölle, M., Marshall, L., Gais, S., and Born, J. (2002). Grouping of Spindle Activity during Slow Oscillations in Human Non-Rapid Eye Movement Sleep. *Journal of Neuroscience*, **22**:10941.

- Montero, V. M. (1999). Amblyopia decreases activation of the corticogeniculate pathway and visual thalamic reticularis in attentive rats: afocal attention hypothesis. *Neuroscience*, **91**:805.
- Nagumo, J., Arimoto, S., and Yoshizawa, S. (1962). An Active Pulse Transmission Line Simulating Nerve Axon. *Proceedings of the IRE*, **50**:2061.
- Nernst, W. (1889). Die elektrische Wirksamkeit der Ionen. *Z Physik Chem*, **4**:129.
- Nernst, W. and Riesenfeld, E. H. (1902). Ueber elektrolytische Erscheinungen an der Grenzfläche zweier Lösungsmittel. *Annalen der Physik*, **313**:600.
- Nitsche, M. A., Fricke, K., Henschke, U., Schlitterlau, A., Liebetanz, D., Lang, N., Henning, S., Tergau, F., and Paulus, W. (2003). Pharmacological modulation of cortical excitability shifts induced by transcranial direct current stimulation in humans. *The Journal of Physiology*, **553**:293.
- Ohayon, M. M., Carskadon, M. A., Guilleminault, C., and Vitiello, M. V. (2004). Meta-analysis of quantitative sleep parameters from childhood to old age in healthy individuals: developing normative sleep values across the human lifespan. *Sleep*, **27**:1255.
- Pikovsky, A., Rosenblum, M., and Kurths, J. (2001). *Synchronization: A Universal Concept in Nonlinear Sciences*. Cambridge University Press.
- Pinel, J. P. J. (2007). *Basics of Biopsychology*. Pearson Allyn and Bacon.
- Pinto, D. J. and Ermentrout, G. B. (2001). Spatially structured activity in synaptically coupled neuronal networks: I. traveling fronts and pulses. *SIAM Journal on Applied Mathematics*, **62**:206.
- Pontryagin, L. S. (1957). Asymptotic behavior of solutions of systems of differential equations with a small parameter at higher derivatives. *Izv. Akad. Nauk. SSSR Ser. Math*, **21**:60.
- Rechtschaffen, A. and Kales, A. (1977). *A Manual of Standardized Terminology, Techniques and Scoring System for Sleep Stages of Human Subjects*. Brain Information Service/Brain Research Institute Los Angeles, CA.
- Richardson, K. A., Schiff, S. J., and Gluckman, B. J. (2005a). Control of Traveling Waves in the Mammalian Cortex. *Physical Review Letters*, **94**:28103.
- Richardson, K. A., Schiff, S. J., and Gluckman, B. J. (2005b). Control of traveling waves in the mammalian cortex. *Physical Review Letters*, **94**:028103.
- Rinzel, J. (1987). A formal classification of bursting mechanisms in excitable systems. *Lecture notes in biomathematics*, page 267.

- Rosenblum, M. G. and Pikovsky, A. S. (2004). Controlling synchronization in an ensemble of globally coupled oscillators. *Phys. Rev. Lett.*, **92**:114102.
- Rosenblum, M. G., Pikovsky, A. S., and Kurths, J. (1996). Phase synchronisation of chaotic attractors. *Phys. Rev. Lett.*, **76**:1804.
- Rubin, J., Lee, D. D., and Sompolinsky, H. (2001). Equilibrium Properties of Temporally Asymmetric Hebbian Plasticity. *Physical Review Letters*, **86**:364.
- Sah, P. and McLachlan, E. M. (1992). Potassium currents contributing to action potential repolarization and the afterhyperpolarization in rat vagal motoneurons. *Journal of Neurophysiology*, **68**:1834.
- Schuster, H. G. (2001). *Complex Adaptive Systems*. Scator Verlag.
- Schuster, H. G. and Just, W. (2006). *Deterministic Chaos*. Wiley-VCH.
- Schuster, H. G., Le Van Quyen, M., Chavez, M., Köhler, J., and Mayer, J. (2008). Dynamical Behavior and Control of Coupled Threshold Elements with Selfinhibition. *in preparation*.
- Schuster, H. G. and Mayer, J. (2008). Influence of external and internal inhibition on coupled neurons. *in preparation*.
- Shen, Y., Olbrich, E., Achermann, P., and Meier, P. (2003). Dimensional complexity and spectral properties of the human sleep EEG. *Clinical Neurophysiology*, **114**:199.
- Sherman, S. M. and Guillery, R. W. (1996). Functional organization of thalamocortical relays. *Journal of Neurophysiology*, **76**:1367.
- Sherman, S. M. and Guillery, R. W. (2001). *Exploring the Thalamus*. Oxford Univ Press.
- Sherman, S. M. and Guillery, R. W. (2006). *Exploring the Thalamus and Its Role in Cortical Function*. MIT Press.
- Singer, W. (1993). Synchronization of Cortical Activity and its Putative Role in Information Processing and Learning. *Annual Review of Physiology*, **55**:349.
- Singer, W. and Gray, C. M. (1995). Visual Feature Integration and the Temporal Correlation Hypothesis. *Annual Review of Neuroscience*, **18**:555.
- Sompolinsky, H. (1981). Time-Dependent Order Parameters in Spin-Glasses. *Physical Review Letters*, **47**:935.
- Sompolinsky, H. and Zippelius, A. (1981). Dynamic Theory of the Spin-Glass Phase. *Physical Review Letters*, **47**:359.

- Song, S., Miller, K. D., and Abbott, L. F. (2000). Competitive Hebbian learning through spike-timing-dependent synaptic plasticity. *Nature Neuroscience*, **3**:919.
- Steriade, M. (2001a). The GABAergic reticular nucleus: a preferential target of corticothalamic projections. *Proc Natl Acad Sci US A*, **98**:3625.
- Steriade, M. (2001b). *The Intact and Sliced Brain*. MIT Press.
- Steriade, M. (2003). The corticothalamic system in sleep. *Front Biosci*, **8**:d878.
- Steriade, M., Dossi, R. C., and Nunez, A. (1991). Network modulation of a slow intrinsic oscillation of cat thalamocortical neurons implicated in sleep delta waves: cortically induced synchronization and brainstem cholinergic suppression. *Journal of Neuroscience*, **11**:3200.
- Steriade, M., McCormick, D. A., and Sejnowski, T. J. (1993a). Thalamocortical oscillations in the sleeping and aroused brain. *Science*, **262**:679.
- Steriade, M., Nunez, A., and Amzica, F. (1993b). Intracellular analysis of relations between the slow ( $\approx 1$  Hz) neocortical oscillation and other sleep rhythms of the electroencephalogram. *J Neurosci*, **13**:3266.
- Stickgold, R., Hobson, J. A., Fosse, R., and Fosse, M. (2001). Sleep, Learning, and Dreams: Off-line Memory Reprocessing. *Science*, **294**:1052.
- Stratonovich, R. L. (1957). On a Method of Calculating Quantum Distribution Functions. *Soviet Physics Doklady*, **2**:416.
- Tass, P. A. and Majtanik, M. (2006). Long-term anti-kindling effects of desynchronizing brain stimulation: a theoretical study. *Biological Cybernetics*, **94**:58.
- Tononi, G. and Cirelli, C. (2003). Sleep and synaptic homeostasis: a hypothesis. *Brain Research Bulletin*, **62**:143.
- Tononi, G. and Cirelli, C. (2006). Sleep function and synaptic homeostasis. *Sleep Medicine Reviews*, **10**:49.
- Tononi, G., Massimini, M., and Riedner, B. A. (2006). Sleepy Dialogues between Cortex and Hippocampus: Who Talks to Whom? *Neuron*, **52**:748.
- Traub, R. D. and Miles, R. (1991). *Neuronal Networks of the Hippocampus*. Cambridge University Press.
- Tuckwell, H. C. (1988). *Introduction to Theoretical Neurobiology*. Cambridge University Press New York.

- Volgushev, M., Chauvette, S., Mukovski, M., and Timofeev, I. (2006). Precise Long-Range Synchronization of Activity and Silence in Neocortical Neurons during Slow-Wave Sleep. *Journal of Neuroscience*, **26**:5665.
- Wagner, U., Gais, S., Haider, H., Verleger, R., and Born, J. (2004). Sleep inspires insight. *Nature*, **427**:352.
- Walker, M. P. and Stickgold, R. (2004). Sleep-Dependent Learning and Memory Consolidation. *Neuron*, **44**:121.
- Wang, X. J. (1993). Genesis of bursting oscillations in the Hindmarsh-Rose model and homoclinicity to a chaotic saddle. *Physica D*, **62**:263.
- Wilson, H. R. (1999). *Spikes, Decisions, and Actions: The Dynamical Foundations of Neuroscience*. Oxford University Press.
- Wilson, H. R. and Cowan, J. D. (1973). A mathematical theory of the functional dynamics of cortical and thalamic nervous tissue. *Biological Cybernetics*, **13**:55.
- Wio, H. S., Colet, P., San Miguel, M., Pesquera, L., and Rodríguez, M. A. (1989). Path-integral formulation for stochastic processes driven by colored noise. *Physical Review A*, **40**:7312.
- Wittenberg, G. M. and Wang, S. S. H. (2006). Malleability of Spike-Timing-Dependent Plasticity at the CA3-CA1 Synapse. *Journal of Neuroscience*, **26**:6610.
- Xia, X. M., Fakler, B., Rivard, A., Wayman, G., Johnson-Pais, T., Keen, J. E., Ishii, T., Hirschberg, B., Bond, C. T., Lutsenko, S., *et al.* (1997). Mechanism of calcium gating in small-conductance calcium-activated potassium channels. *Nature*, **386**:167.
- Yingling, C. D. and Skinner, J. E. (1977). Gating of thalamic input to cerebral cortex by nucleus reticularis laminaris. *Attention, Voluntary Contraction and Event-Related Cerebral Potentials. Prog Clin Neurophysiol. Basel, Karger*, pages 70–96.
- Zeeman, E. C. (1972). Differential equations for the heartbeat and nerve impulse. *Towards a Theoretical Biology*, **4**:8.
- Zhang, L. I., Tao, H. W., Holt, C. E., Harris, W. A., and Poo, M. (1998). A critical window for cooperation and competition among developing retinotectal synapses. *Nature*, **395**:37.





# Acknowledgements

First, I would like to thank my advisor, Prof. Dr. Heinz Georg Schuster, for giving me the opportunity to work on this interesting topic. Without his ideas and motivation, this thesis would not have been possible. I am especially grateful that he gave me the opportunity to plan and realize research projects as independently as possible.

Further, I want to express my gratitude to the “Deutsche Forschungsgesellschaft” for financial support during my graduate studies within SFB 654. I would also like to thank the Wilhelm und Else Heraeus-Stiftung and the The Max-Planck-Institut für Physik komplexer Systeme for financial support. Special thanks go to the people at the Institute of Theoretical Physics and Astrophysics in Kiel, in particular to Jan Köhler, Dr. Jens Christian Claussen, Andreas Franke and Norbert Lüthje. And at the Institute for neuroendocrinology in Lübeck in particular Matthias Mölle, Jan Born and Lisa Marshall. Last but not least, I would like to thank my family for their support during my studies.

April 2008



# Curriculum Vitae

Name: Jörg Mayer  
Geburtstag: 6. Oktober 1978  
Geburtsort: Freising  
Wohnort: 24118 Kiel  
Familienstand: ledig  
Staatsangehörigkeit: deutsch  
Anschrift: Gutenbergstr. 22  
24118 Kiel  
email: mayer@theo-physik.uni-kiel.de

1985 - 1989 St. Korbibinian Grundschule Freising  
1989 - 1998 Josef-Hofmiller-Gymnasium Freising  
26. Juni 1998 Allgemeine Hochschulreife  
1998 - 1999 Zivildienst im Krankenhaus Fehmarn (Pflegedienst)  
1999 - 2004 Physikstudium an der Christian-Albrechts-Universität zu Kiel  
16.10.2001 Vordiplom in Physik  
2001 - 2004 Physikstudium an der Christian-Albrechts-Universität zu Kiel  
12.11.2004 Hauptdiplom in Physik  
Ab 3.2005 Doktorand bei Prof. Dr. Heinz Georg Schuster  
am Institut für Theoretische Physik und  
Astrophysik der Christian-Albrechts Universität  
Kiel im Rahmen des Sonderforschungsbereiches 654

Semester and der CAU: 18



# Selbstständigkeitserklärung

Ich erkläre, dass ich die vorgelegte Arbeit - abgesehen von der Beratung durch meinen Betreuer Prof. Dr. Heinz Georg Schuster - selbständig und nur unter Benutzung der angegebenen Literatur angefertigt habe. Die den Veröffentlichungen zugrunde liegende Forschungsarbeit wurde - abgesehen von der Beratung und Hilfe durch Prof. Dr. Heinz Georg Schuster - ausschließlich von mir selbst durchgeführt. Ausnahmen sind die folgenden Veröffentlichungen:

- Bei den Artikeln „The Role of Inhibitory Feedback for Informationtransfer in the Thalamus“ und „Corticothalamic projections control synchrony in locally coupled bistable“ oscillators hat Dr. Jens Christian Claussen zur quantitativen Analyse beigetragen.
- Bei dem Artikel „Corticothalamic projections control synchrony in locally coupled bistable oscillators“ hat Dr. Matthias Mölle die verwendeten Experimentellen Daten geliefert.
- Bei dem Artikel „Excitation of Coherent Oscillations in a noisy Medium“ hat Jan Köhler sämtliche numerischen simulationen durchgeführt und wesentlich zur Modellbildung beigetragen.

Weiterhin versichere ich, dass die vorliegende Dissertation weder ganz noch zum Teil bei einer anderen Stelle im Rahmen eines Prüfungsverfahrens vorgelegt worden ist. Die Arbeit ist unter Einhaltung der Regeln guter wissenschaftlicher Praxis entstanden. Ich habe keine früheren Promotionsversuche unternommen.

Kiel, den 22.04.2008